ARC-AUGMENTED LASER WELDING OF ALUMINUM

Edmund Joseph Haas
B.S., University of Oregon, 1979

A thesis submitted to the faculty
of the Oregon Graduate Center
in partial fulfillment of the
requirements for the degree
Master of Science
in
Materials Science and Engineering

December 18, 1986

The thesis "Arc-augmented Laser Welding of Aluminum" by Edmund J. Haas has been examined and approved by the following Examination Commitee:

Jack H. Devletian
Associate Professor
Thesis Research Advisor

William E. Wood
Professor

Lawrence E. Murr
Professor

Richard A. Elliott
Professor

ACKNOWLEDGEMENTS

The author would like to acknowledge the sponsorship of the Welding

Research Council for this work. He would also like to offer his sincere

appreciation to his Thesis Research Advisor, Dr. Jack H. Devletian

and the other members of his Thesis Committee: Drs. William E. Wood,

Lawrence E. Murr and Richard A. Elliott.

There are many other individuals the author would also like to thank:

Dr. John Dash of Portland State University who encouraged the author

to pursue an advanced degree at OGC; Bob Turpin and Dan Danks who

made significant contributions throughout the course of this study,

specifically during the set-up and operation of the experimental apparatus;

the Support Staff at OGC who offered their expertise and made much of

this work possible; the Students and Faculty of the Oregon Graduate

Center for making this such an outstanding learning experience; the

author's parents, Mr. and Mrs. William J. Haas who offered continual

encouragement and support; and lastly the author's wife Chris, who

among other things, brought two wonderful daughters into this world.

DEDICATION

This Thesis is dedicated to the memory of my Sister Cathy and our Uncle Ron. Unable to resist the temptation to philosophize in print, please allow me the following excursion: These two people, each filled with a unique love of live and with various strengths and weaknesses as have all who lived, had a very strong influence on the person I am. Being agnostic relative to metaphysical matters, I find it difficult to accept the idea that I may never "see" them again. I do know, however, that one thing cannot be taken away – they lived and were a part of life ..... and there seems to me something eternal about that. I am content with both the knowledge that I loved them very much and that they would be proud of what I've done with my life thus far. If only to be with them again.

TABLE OF CONTENTS

LIST OF TABLES

LIST OF FIGURES

ABSTRACT

Arc-augmented Laser Welding of Aluminum

Edmund J. Haas
Oregon Graduate Center, 1986

Supervising Professor: Jack H. Devletian

Aluminum alloys, while readily weldable with other techniques,
are very difficult to weld using the laser beam welding (LBW) process.
The purpose of this investigation was to examine the use of the arc
-augmented LBW process as a possible technique for successful LBW
of structural aluminum alloys.

LBW parameters were examined using an industrial type 1200 watt
continuous wave CO_2 laser. Because of the high surface reflectivity
and thermal diffusivity of aluminum, power densities of greater than
10^6 W/cm^2 were necessary to initiate and continue deep-penetration
mode welding. Beam focusing optics capable of producing this high
power density were limited by short depth of field which makes thick
section welding impossible. Surface preparations including anodizing
and grit blasting proved helpful while using longer focal length
lenses.

Synergy resulting from the combined action of the laser beam
and the gas tungsten arc produced a far greater volume of molten
metal than the individual contributions of each process added separately.
This synergistic effect was seen when the laser beam was augmented
with an arc produced by a conventional gas tungsten arc welding (GTAW)
electrode. Evidence was obtained showing this increase in melted
volume to be related to an increase in the efficiency of the gas

tungsten arc. Measured changes in arc column resistance and current coupled with high speed videography results showing the arc rooting to the laser induced hot-spot confirm an overall increase in applied power density (mainly from the GTAW arc).

Weld preheating temperatures close to the melting point of aluminum was found to promote thermal coupling of laser energy. The increase in absorption of the laser beam by aluminum was proposed as a possible mechanism of the observed arc-laser synergism in the combined process.

Results from arc-augmented LBW of mild steel are provided which show the increase in melted volume to be similar to that obtained for aluminum, and based on this, the dominant mechanism of arc-laser synergism was proposed to be an increase in the GTAW efficiency.

Relative to the engineering significance of this work, possible benefits from the arc-augmented LBW technique (on aluminum) would include coupling a GTAW torch to an already existing LBW application with increased quality or productivity as an aim. It would not make economical sense to do the reverse because of the high cost of a LBW system relative to the increase in welding velocity or penetration depth one might gain from a GTAW system.

I. Introduction

Lasers have seen remarkable development since their discovery early in the 1960's[1]. Originally nothing more than a laboratory curiosity, these first lasers gave way to newer and better sources of coherent, monochromatic radiation, both in terms of stability and power. Indeed, these are the outstanding features of the laser as a usable tool, since extremely high power densities of fixed wavelength light can be focused on a workpiece surface. Industrially important lasers of either the pulsed wave (PW) or contiuous wave (CW) variety have found many applications involving several classes of materials. Plastic, rubber, glass, green ceramic, nylon, wood, paper, and many metals are just some of the types of engineering materials that have been laser processed[2,3]. Most of the early applications involved drilling, trimming or spot welding since industrially availble lasers were of the solid state PW variety[4]. The pulsed ruby laser beam welding (LBW) system developed by the Air Force Materials Laboratory (AFML) was used by Grumman Aerospace Corp. to evaluate welding of titanium, stainless steel, low-alloy steel, and nickel base alloys[5]. The practical penetration limit for through-thickness welding of these materials was determined to be approximately 1.0 mm, and they characterized the PW LBW capabilities to be essentially for thin section, microelectronics and instrumentation applications.

In order to produce thick section weldments in engineering materials, high power lasers were necessary and to this end a CW CO_2 laser with an output power of greater than 10 kW was developed by the AFML to enable continuous welding of aerospace alloys of thicknesses up to 2.0

cm. Aluminum, included in the list of materials investigated, proved very difficult to weld due to several causes[6], the most important being the very high initial surface reflectivity of aluminum for the 10.6 micron wavelength radiation produced by the CO_2 laser.

The objective of this thesis was to study the important problems related to the LBW of aluminum, and once an initial "reference point" of critical parameters was established, explore the effects of several engineering modifications to the standard welding conditions used. The next and most important step was to examine the use of an innovative technique developed by The Welding Institute[7] whereby the laser is augmented by an arc produced by a conventional gas tungsten arc welding (GTAW) electrode. Arc-augmentation of the CW CO_2 laser used for this study was considered to be an exciting possibility towards furthering aluminum weldability, and the main emphasis of the study concerned itself with the physical interactions of the two welding sources, and their as yet unexplained synergistic effect on one another.

II. Literature Review

The reduction of significant thermal distortion or heat—affected

zone (HAZ) in deep—penetration laser welding makes it especially

attractive for producing structural weldments[8,9]. High—strength

structural alloys for use in the aerospace and defense industries are

some of the more noteworthy applications where the laser has had

significant impact[10,11]. These contrast the already prevalent applications

involving thin section welding[12-14], however, and are therefore in

competition with electron beam welding (EBW) which has been an established

means of the thick section welding of these structural weldments.

Both EBW and deep—penetration mode LBW (in contrast to conduction mode

LBW) operate via the formation of a "keyhole" as shown in Figure 1. The

keyhole is a column of vaporized metal which can be traversed along

the weld joint to produce a through-thickness weld with one pass. As

the keyhole is translated, molten metal moves along the sides to the

back of the column and solidifies, thus forming the weld. Since one

could avoid the problems associated with welding in vacuum (necessary

for the transmission of an electron beam) the laser has been seen as a

means of attaining the quality of EBW without the problems involved

with creating and sustaining a vacuum in a suitably sized workstation.

Indeed, the laser has done just that in many cases[15-17] and has emerged

as a valuable metalworking tool[18,19] with even further growth expect-

ed[20,21].

Many different engineering materials have been successfully

welded with the LBW process. Titanium, nickel and cobalt base superalloys,

stainless steel, as well as many of the plain carbon, low alloy and

ultra-high strength steels have been successfully welded. In some cases, aluminum weldments have been made[22-26].

In relation to what materials could be welded with the LBW process, qualitative predictions are possible based on the thermo-physical properties of the material in question. An important thermo-physical property that presents itself as a problem in the LBW of aluminum is its very high thermal diffusivity. This is why most existing applications of laser welding aluminum are those involving thin sections[27]. In this way, heat will remain in the target zone long enough for the necessary specific heat input for melting to amass.

The very high initial surface reflectivity of aluminum for 10.6 micron wavelength laser light is the single most important thermo-physical property particularly troublesome with respect to LBW. The conversion of laser light energy to thermal energy within a metal target is a very complex process with the important events being electron-phonon collisions which convert laser photons to lattice vibrational energy. The electronic structure of aluminum produces a high free electron density within the solid which in turn results in poor thermal coupling (due to low phonon generation). The reflectivity is wavelength-specific, as shown in Figure 2, where the relationship between the normal spectral reflectance and light wavelength is seen to be nonlinear[28]. Absorption of laser energy is usually less than 10% when welding aluminum with a carbon dioxide laser due to the high initial surface reflectivity of aluminum. Given aluminum's high thermal diffusivity, the problem of high reflectivity is compounded by the fact that absorbed energy leaves the target area so rapidly.

Successful methods of welding aluminum involve techniques to overcome the influence of the high thermal diffusivity and initial surface reflectivity. One such method involves preheating the weld samples. The reflectivity of aluminum for 10.6 micron wavelength light diminishes with increasing temperature. The thermal diffusivity of aluminum also decreases with increasing temperature and so the absorption of beam energy would be expected to increase in an amount great enough to cause thermal coupling between the aluminum weldment and the incident CO_2 laser energy. This increase in absorption is even greater once welding begins and is thought by some to be due to the onset of melting[29-32] and by others to be due to the onset of vaporization[33,34]. In any case, preheating the workpiece should have a significant effect on laser welding aluminum.

The condition of the surface has been shown to be very important with respect to initial reflectivity. Surface roughness induced by wire brushing or grit blasting can have a positive effect on thermal coupling[35]. Special coatings to "blacken" the surface have been used to promote absorption[36]. The effect of the surface oxide layer on aluminum with respect to beam absorption remains somewhat controversial. Some workers have claimed an improvement from anodizing aluminum[35,38] while others have thought either the opposite[37] or no effect[6]. Regardless of degree, there is sufficient evidence to indicate surface preparation of the weldment has a significant engineering impact on the LBW of aluminum.

Alloying elements have been shown to affect the thermal coupling between laser light and aluminum weldments. Mazumder has shown that

magnesium lessened the criticality of irradiation parameters on aluminum alloy 5182 weldability, but pronounced loss of this element (due to evaporation during LBW) was noted[39].

An innovative idea that could provide a major step towards the succesful laser welding of aluminum is the application of an arc along with the laser as done by Steen and coworkers[7] in the welding of steel. Their work has uncovered an as yet unexplained synergistic effect when using the arc-augmented laser technique. An increase in both penetration and welding speed beyond that expected by the addition of each effect separately occurred while LBW steel which involved a complex phenomena due to the interaction of both sources. A mechanism was proposed by Steen et al[7] for this synergistic effect that related to the laser's ability to constrict the arc to a higher power density and therefore provide greater efficiency overall.

Diebold and Albright[40] have found improved arc stability at high rates of travel (welding velocity) for the combined LBW/GTAW process during the welding of aluminum alloy 5052. The GTAW process was considered the major influence when combined with the 600 watts of CW laser power used for their study based on the resulting LBW/GTAW weld bead dimensions, which were more representative of the GTAW process than the LBW process. They related the synergistic effect observed during the combined process to GTAW anode spot stabilization by the impinging laser beam.

III. Experimental Procedure

A. Materials

The materials used in this investigation were 3003 and 5052 aluminum alloys and cold rolled mild steel (AISI 1018). Typical chemical compositions are given in Table I. The aluminum specimens were taken from 0.32 cm (0.125") plate while the 1018 steel specimens were taken from 0.48 cm X 15.2 cm (0.188" X 6.0") strapping. Initial weld samples were 3.8 cm X 7.6 cm (1.5" X 3.0") coupons, while for later welding 7.6 cm X 15.2 cm (3.0" X 6.0") plates were used. An alloy of titanium (Ti-6Al-4V) was used for part of the weld preheating section.

B. Surface Preparation

The weld specimens were cut to size, degreased with acetone, and then grit blasted with #24 mesh Al_2O_3 to provide a roughened surface prior to LBW and/or GTAW. Figure 3 shows a scanning electron micrograph of the resulting surface condition typical of such preparations. All specimens were either used immediately or re-prepared before welding to minimize the growth of oxide films.

C. LBW System

A GTE Sylvania Model 971 CO_2 Gas Transport Laser was used in this investigation (Figure 4). Due to the coherent nature of the laser output beam, the 1200 watts of continuous laser radiation at a wavelength of 10.6 microns could be focused to a very small area to achieve energy densities of up to 10^8 w/cm^2. Power densities necessary to heat,

melt, or vaporize most materials were therefore easily attained. The specifications of this industrial type laser are shown in Table II.

A helium-neon alignment laser, colinear with the CO_2 laser, was used to produce a visible beam coincident with the invisible infrared laser beam. The use of the HeNe laser facilitated two operations; alignment of the external optics, and positioning of the workpiece with respect to the point of impingement of the focussed beam. A numerically controlled X-Y table was used to scan specimens across the stationary laser beam.

D. Laser Beam Parameters

A GTE Sylvania Model 491 Power Meter was used to measure the total laser beam output power. Its utilization provided a practical way to check the operational stability of the laser. If the equilibrium of the system was in question, one needed to simply check the measured power at a particular applied current and compare this to the power vs. current graph. If the readings did not match, the system was not functioning properly. This could be due to any of several possible causes; misalignment of the mirrors in the laser head (rear mirror and output coupler), improper lasing gas mixture, high cooling water temperature which could cause distortion of the internal beam generating components (folding mirrors), or improper alignment of the beam through the external optics housing. When the laser was operating properly, the power vs. current graph allowed an output power level to be set simply by applying the current indicated by the graph. This made the tedious task of measuring the power with the power meter unnecessary except

occasionally to insure proper operation.

The raw beam was characterized by using thick plexiglass sheet, which allowed alignment of the beam through the focussing lens and examination of the beam diameter or power distribution. Wedge-shaped plexiglass specimens were used to accurately determine the focal lengths of the lenses used for this investigation. After scanning the 30 degree angled wedge under the focused beam, the distance between the narrowest point of the resulting burn and the lens (corresponding to the focal length) was then measured with a height gauge. Once the focal point was found, the focused spot size could be calculated (based on the appropriate optical relationships) and using the measured results of the power meter, the power densities could then be determined.

E. Power Supply For GTAW

An ESAB Model DTU 300 GTAW Power Supply was used for this investigation. The rated output was 300 amperes at 32 volts with a 60% duty cycle. An important part of this unit was the high frequency start which greatly helped arc initiation.

F. Current and Voltage Monitoring for GTAW

A 300 Amp shunt was connected in line with the electrode cable to measure welding output amperage, which was found using a digital voltmeter. Welding Voltage was measured using an analog voltmeter connected in parallel with the electrodes during GTAW.

G. Preheat Power Supply

A furnace control power supply was used in conjuntion with a quartz filament lamp to provide weld preheating for this investigation. The power supply/quartz lamp was controlled using a thermocouple connected to the weld specimen. In this way, one could set the controller for a particular temperature and the quartz lamp would radiate the necessary heat to a copper plate with the sample mounted on its top side. Welding began once the lamp extinguished, signaling that the sample was at the desired temperature.

H. Welding Procedure

The welding set-up is shown in Figure 5. A 7.6 cm (3.0") ceramic cup without a gas lens was used with an air cooled GTAW torch. Because of physical limitations involved with producing a combined plasma between the laser and the GTAW arc, the electrode was positioned at a 30 degree angle with respect to the base plate. The cup was modified to accommodate this welding arrangement and provide adequate shielding. The shielding gas used was 100% argon in all cases both through the GTAW torch and the laser assembly (lens shielding and plasma control cross jet). A standard 0.24 cm (0.09") diameter, 2% thoriated tungsten electrode was used in all cases.

Actual welding began with a high frequency start of the GTAW unit and DC straight polarity. A set pattern of welding was used to generate the welds made for comparison (Figure 6). First, a backhand (BH) GTAW weld, then a forehand (FH) GTAW weld was made. A BH LBW weld followed by a BH LBW/GTAW weld and lastly a FH LBW/GTAW weld was then made.

Since in reality there is no difference between BH and FH LBW (with the beam impinging normal to the specimen surface), only one welding pass was needed. This pattern was followed for each scan rate investigated, while all other welding parameters were held constant.

I. High Speed Videography

A Spin Physics Model SP 2000 High Speed Motion Analysis System was used in this investigation (Figure 7). This system was capable of providing up to 12,000 partial frames per second, which could be played back on the veiwing screen at variable rates. A VHS format video tape was recorded off the system master tapes for inspection on a VCR and individual still photographs were taken from the display screen with a 35mm camera. The phenomena of arc-rooting and the effects of plasma interactions associated with arc-augmented laser welding were the main areas of investigation while using this system.

J. Microscopy

A Carl Zeiss Research Metallograph was used for both microscopic and macroscopic analyses in this study. A JEOL Model JSM-35 Scanning Electron Microscope with Energy Dispersive X-ray Analysis was also used for this project. Accurate values of weld metal cross sectional areas, depths, and widths were found using this tool.

After welding, the samples were photographed with a 35mm camera to provide a record of the weld bead surface appearance. These macrographs display such things as soot generated during welding, weld pool turbulence, or welding stability in general.

Weld beads were sectioned, cleaned and then electroplated with nickel prior to mounting in a conductive compound. The nickel plating was done for one specific reason; edge preservation to insure accurate measurments of weld depth, width, and cross sectional area. After standard metallographic grinding and polishing (up to and including .05 micron alumina) the aluminum samples were etched with a solution of 85 parts H_2O, 10 parts H_2SO_4, and 5 parts HF, while the mild steel samples were etched with 10% nital. These heavily etched sections were then photographed at approximately 10 magnifications in the SEM. The SEM was used because it had a lower magnification capability than the optical metallograph and because of this the weld bead and the entire base plate could be photographed together. Negatives from the SEM were then blown up to provide a 22.0 cm (8.5") X 28.0 cm (11.0") print. These large photographs were used in conjunction with a PLANIX 5 digital planimeter to accurately determine the weld metal A_w. The base plate thickness was used to calibrate the true magnification of the photograph and provide an accurate measure of the real A_w. In this way the differences between GTAW and LBW/GTAW welding could be quantified.

Weld metal cross sectional area estimates were made for most LBW welds based on measurements of weld width. These measurements were done on the projection screen of the Zeiss metallograph at 50 magnifications.

IV.   Results

A. Laser Beam Parameters

The total laser beam output power was measured with the power
meter and the relationship between the applied current and the resulting
output was characterized. As can be seen from Figure 8, the output
power was a linear function of applied current in the range used
in this investigation.

A thick plexiglass sheet was used to examine the raw beam character
(Figure 9), which allowed alignment of the beam through the external
optics housing to the 90 degree bending mirror and focusing lens.
Examination of the raw beam diameter and symmetry along with the
resulting power distribution was also accomplished. Wedge shaped
plexiglass samples were used to accurately determine the focal lengths
of the lenses used for this study. Figure 10 displays these plexiglass
samples. The measured focal lengths, spot sizes (calculated using the
relationships shown in Figure 11) and resulting power densities associated
with the lenses used for this study, along with other laser operating
parameters are listed in Table III.

B. Surface Modifications

The condition of a surface was found to greatly effect the metal's
reflectivity to laser light. In this part of the investigation,
various surface preparations on aluminum specimens were assessed for
their abilty to increase absorption of 10.6 micron wavelength laser light.

The list of suface modifications with possible benefit towards

increased laser beam absorption include (a) thermal sprayed aluminum powder coatings, (b) grit blasting for a roughened surface, and (c) anodizing to produce a thick oxide layer.

In order to avoid the potentially damaging occurence of a specular reflection back into the lens assembly, a specimen stage with a small amount of tilt was fabricated to study the basic laser welding capability for aluminum (Figure 12). A green plexiglass shield attached to this "stage" was used to absorb any reflected beam energy. A 6.02 cm (2.37") focal length lens was used for preliminary investigation of the ability to couple laser energy with aluminum. Figure 13 shows a scanning electron micrograph of a weld made on polished aluminum (mill finish) with the tilted stage. Since beam absorption did occur (and hence no specular reflection), further welding was not done with the tilted stage, but with samples positioned normal to the beam axis.

Welds shown in Figure 14 demonstrate further that the necessary power density for deep-penetration laser welding of aluminum was attained while using the 6.02 cm focal length lens. These SEM photographs also show both the explosive nature of the weld pool and the lack of repeatability from weld to weld. Evidence of the fragile nature of coupling was seen where the deep-penetration mode was abruptly lost as shown in the welds of Figure 15. Cross sectional views of these welds are shown in Figure 16.

The effect of a thermally sprayed aluminum powder coating as a surface preparation technique was compared to grit blasting and the differences in LBW response were noted. No measurable difference between these two surface conditions could be found, however, and so a

program of welding was implemented to find measurable differences
between polished, grit blasted and anodized aluminum on a comparative
basis. Using a 13.01 cm (5.12") focal length lens and scanning across
the interface from one surface preparation to another, grit blasting
with #24 mesh Al_2O_3 and black anodizing were compared to polished aluminum
(Figure 17) and the results (weld metal A_w) are contrasted in Figure
18. The polished sample was ground on 600 grit abrasive paper for
this comparison. It can be seen that both grit blasting and anodizing
had a positive effect on laser beam absorption. Even though there was
an increase in melting, the important feature noted was that true thermal
coupling of the laser energy with any of the samples was not observed
for this power density and sample thickness.

For comparison purposes, a thinner sheet (0.8 mm) was welded to
assess the effect of the high thermal diffusivity on the LBW of aluminum.
The result (Figure 19) demonstrated that even with the problem of high
reflectivity the coupling threshold could be overcome by going to
thinner materials and limiting the amount of heat lost by conduction
to the surrounding area, as seen where the weld pool was essentially
lost with laser "cutting" the outcome (exposing the backing plate).

Another weld was made with an aluminum backing plate under the
thin sheet of aluminum rather than the steel plate as used above. The
weld bead surface appearence of the resulting joint is shown in Figure
20. As can be seen from this SEM photograph, weld pool turbulence was
not excessively large as is usually the case. Figure 21 shows an
optical micrograph of the weld cross section with some porosity visible.

C. GTAW Current and Voltage

The GTAW current and voltage were measured during both GTAW alone and LBW/GTAW operation. It was found that a slight increase in current along with a decrease in voltage occurred when the laser shutter was opened and the two processes operated simultaneously, for the welding current setting of 60.6 amps. The GTAW current value of 81.0 amps showed an even larger difference during LBW/GTAW. No change was measured for the highest current setting (171.6 amps) case. Table IV shows the results of the current and voltage measurments during the GTAW and LBW/GTAW of aluminum.

D. Melting Efficiency

Three values of arc current where investigated in this study: 60.6 amps, 81.0 amps, and 171.6 amps. For the lowest current value case, the arc energy input was set just high enough to permit the high frequency start to initiate welding without moving the electrode closer to the sample or using other techniques aimed at arc startup. In this way the process could be run automatically without the need for changing any of the preset parameters. Stable operation and repeatability were necessary in order to make reliable comparisons between LBW, GTAW, and LBW/GTAW.

Figure 22 displays a plot of weld metal area (A_w) vs. scan rate obtained for the GTAW current setting of 60.6 amps. As shown in Figure 22, weld metal A_w for LBW was almost nonexistant at any scan rate. The values for LBW weld metal A_w were estimated by measuring weld width and assuming a hemispherically shaped fusion zone. GTAW

weld metal A_w decreased with increasing scan rate in typical fashion.

When the two processes were run simultaneously the resulting weld metal A_w indicated a synergistic effect had occurred. The values of Figure 22 indicated that 77% more weld metal A_w resulted with LBW/GTAW than the sum of LBW and GTAW values added seperatly, for the scan rate of 4.2 mm/sec. The influence of the laser decreased with increasing welding velocity as could be seen where the synergy at 67.7 mm/sec was 8% (this value was felt to be close to the range of error for these results).

The GTAW current setting of 81.0 amps yielded the plot of weld metal A_w vs. scan rate presented in Figure 23. The scan rate did not include a speed of 67.7 mm/sec since the influence of the laser was shown to become ambiguous with respect to GTAW at higher welding velocity. LBW results were similar to those in Figure 22 since nothing was changed with respect to LBW parameters. These data points were almost off the scale at the bottom of the graph. They were included here, however, for comparison with LBW/GTAW.

Arc-augmented laser welding results in Figure 23 showed a trend similar to that from Figure 22. The values of weld metal A_w for LBW/GTAW indicated a synergistic effect of 84% over the values of LBW and GTAW added together seperatly, for the scan rate of 4.2 mm/sec. As can be seen, the influence of the laser decreased with increasing welding velocity where the synergy became 33% for the scan rate of 34.0 mm/sec. Figures 24 and 25 display cross sectional optical micrographs comparing GTAW to LBW/GTAW during BH and FH welding at two scan rates for this welding current value. Increases in weld metal A_w from the

LBW influence on GTAW were associated with increased penetration depth and proportionately less increased weld width, as shown in these figures.

A difference in results for BH vs. FH welding was noted in the data of Figure 23. The difference between GTAW and LBW/GTAW, in terms of arc-laser synergy, was seen to be constant, however, reflecting only a carryover of directional effects from GTAW onto LBW/GTAW.

A high GTAW current setting of 171.6 amps was investigated to assess the influence of a large arc energy input on the arc-augmented laser synergy. LBW parameters were held constant as they were for the GTAW current setting cases of 60.6 amps and 81.0 amps presented above. A plot of weld metal A_w as a function of scan rate is presented in Figure 26. The weld metal A_w for LBW was not included in Figure 26 because the large magnitude of the GTAW and LBW/GTAW data dwarfed this inconsequential amount of melting. The weld metal A_w values (average of BH & FH) for GTAW and LBW/GTAW indicated a synergistic effect of 28% for the 8.5 mm/sec scan rate, which is ambiguous since the synergy at the 17.0 mm/sec scan rate was 45%. The synergy at the 34.0 mm/sec scan rate was 17%, following the trend of decreasing synergism with increasing welding velocity. There was no useful data generated for the 4.2 mm/sec scan rate because melting was too pronounced to permit useful comparisons between GTAW and LBW/GTAW.

As was the trend for the 81.0 amp GTAW case, less weld metal A_w was measured for BH than FH welding. In relation to the differences in synergy between pushing and pulling the weld, however, no new information was found.

E. Preheating

As a preliminary study of the effect of preheating on the ability
to couple laser beam energy with aluminum, a weld sample was made
whereby the laser beam could be run off from a progressing weld in
another material onto an aluminum susbtrate. Titanium, which is very
absorptive of 10.6 micron wavelength laser light due to both a lower
reflectivity and very low thermal diffusivity, was chosen to start the
weld pool which would be moved on to a sample of 5052 aluminum. The
resulting weld bead surface appearance is shown in Figure 27. Longitudinal
cross sections of the weld centerline are shown in Figure 28. Based
on the gradual decrease in penetration depth to the steady value
in the aluminum side shown in Figure 28, preheating from the advancing
titanium weld pool had a positive effect on laser beam thermal coupling.
Even though the ability to sustain the weld pool size on the aluminum
sample was not found (through "self preheating"), it was felt that
the preheating approach warranted further investigation.

Using the experimental set-up shown in Figure 29, the influence
of preheating the workpiece prior to LBW was examined. The equipment
used, with the exception of the shielding arrangment, was detailed in
the experimental procedure. The sheilding arrangment was basically a
box with a slightly positive pressure of argon gas to exclude oxygen
from the atmosphere. Figure 30 shows the weld bead surface appearance
while Figure 31 shows the resulting curve of weld metal A_w as a function
of preheating temperature. These values were based on estmates made
by measuring the weld width and assuming a hemispherical fusion zone
shape. The slope of the curve gradualy increased as the temperature

increased, indicating increasing beam absorption with temperature, yet the important feature noted was that thermal coupling between the aluminum sample and the impinging laser beam did not occur. Melting of the sample was very slight and in no way near what one would obtain with a sample of mild steel, for example.

It was felt that the effect of preheating on LBW could be defined further with comparison to its effect on GTAW and LBW/GTAW. The enclosed shroud for atmospheric protection was not used for this section of the preheating study. The set-up used is shown in Figure 32. The welding sequence went from GTAW for 5.0 cm to LBW/GTAW for 5.0 cm to LBW for 5.0 cm at each preheating temperature. All welding was done in the BH direction at a scan rate of 17.0 mm/sec, with the GTAW current set at 60.6 amps. Weld metal A_w measurments are presented in Figure 33 as a function of preheating temperature. The weld metal A_w increased from 0.51 mm^2 at $93^{\circ}C$ to 11.88 mm^2 at $524^{\circ}C$ for GTAW. For the arc-augmented laser welding case the weld metal A_w increased from approximately 0.85 mm^2 at $93^{\circ}C$ to 17.78 mm^2 at $524^{\circ}C$. Interesting results were obtained for the laser alone welding case. The weld metal A_w went from essentially nothing (.012 mm^2, estimated) at $93^{\circ}C$ to roughly 4.16 mm^2 (planimeter value) at $524^{\circ}C$, where thermal coupling took place. Figure 34 shows the $524^{\circ}C$ weld (LBW only) in process, with vaporization of magnesium the most likely cause of sparking, while the optical micrograph of Figure 35 displays a typical weld metal cross sectional view. The weld of Figure 35 shows both a high aspect ratio (high depth to width) and also a slight amount of porosity.

The most important feature of Figure 33 was the change in arc-laser

synergy. Ignoring the first preheating temperature results (63%
synergy), the trend showed steadily increasing synergy from 24% to 41%
with increasing temperature, up to the temperature where thermal
coupling took place and the synergistic effect was only 11%, based on
the weld metal A_w. This indicated a strong effect of the substrate
temperature on the absorption of laser beam energy, and, if one compared
this result with the increased weld metal A_w for LBW, the reason for
low synergy became evident. The value of synergy was found by dividing
the weld metal A_w for LBW/GTAW by the sum of the individual values of
weld metal A_w for LBW and GTAW. Since the value for LBW at 524°C was
high, the resulting value of synergy was low. Experimentily, this
demonstrated that the increased weld metal A_w for LBW/GTAW correlated
with the laser beam impinging on an already molten weld pool as a
basic mechanism of arc-laser synergy.

F. Materials Selection – Steel vs. Aluminum

Alloy 3003 aluminum was welded for comparison with the 5052
aluminum alloy used for the majority of this investigation. Other
than a difference in the soot generated for each alloy (Figure 36), no
welding distinction could be made between the two alloys. Figure 37
shows the amount of weld metal A_w generated for LBW, GTAW, and LBW/GTAW
for each alloy welded in the FH direction at a scan rate of 17.0
mm/sec with a GTAW current value of 60.6 amps. The amount of LBW weld
metal A_w is slightly exaggerated as shown in Figure 37 but the main
point here was that true thermal coupling was not attained for either
case. For the 3003 alloy, the arc-laser synergy was 21% and for

the 5052 alloy, the arc-laser synergy was 30%. This small difference between these alloys was felt to be close to the accuracy of the experimental measurements and therefore shed no real light on the question of alloy element effects, if there are any, on arc-augmented laser welding of aluminum.

An iron-based alloy was welded for comparison to the aluminum welding results. Figure 38 shows the weld bead surface appearance of representative welds. Immediatly obvious was the substantial thermal coupling of the laser beam energy with the mild steel sample, as shown in Figure 39 of the weld metal A_w vs. scan rate. From this figure, the amount of LBW deposited weld metal was comparable to the amount of GTAW weld metal, in sharp contrast to welding aluminum. The average weld metal A_w for LBW, GTAW, and LBW/GTAW revealed synergistic effects of 41% at the scan rate of 8.5 mm/sec decreasing to approximately 25% at the scan rate of 17.0 mm/sec and 11% at the 34.0 mm/sec scan rate. The optical micrographs of Figure 40 compare the cross sections of LBW, GTAW, and LBW/GTAW welds for BH and FH welding at the two higher scan rates refered to. This figure showed that increased weld metal A_w due to arc-laser synergy was linked to greater increases in penetration depth rather than broadening of weld widths, which suggested improved welding efficiency overall.

G. Arc Rooting

Bead on plate welds were made at high welding velocity to examine the lasers ability to stabilize the arc. The GTAW current setting of 60.6 amps was used at scan rates of 67.7, 84.7, and 101.6 mm/sec to

compare FH GTAW with FH LBW/GTAW. The results plotted for weld metal
A_w vs. scan rate in Figure 41 indicated a lack of consistency with
the usual trend of decreasing weld metal A_w at increasing scan rate.
This outcome made more sense when micrographs of the weld cross sections
in Figure 42 were examined, showing the presence of two seperate weld
pools (one for LBW and one for GTAW) and, hence, basically no interaction.
An interesting outcome was the large laser welds found in this figure,
which revealed that a combined plasma between the laser and arc had
not formed, and hence no synergy, while also pointing to a preheating
effect on laser beam absorption from the progressing GTAW weld.

Square groove autogenous welds were made with the 0.32 cm (0.125")
thick 5052 aluminum alloy to assess both the ability to make arc-augmented
laser weld joints in aluminum, and to see if the phenomenon of arc-rooting
was strong enough to permit high-speed welding of real weldments.
Groove faces were milled flat to permit extremely close joint fit-up.
Both halves of the intended weld were clamped securely as shown in
Figure 43. All welds were made in the FH direction so that the laser
could "aim" the arc. A weld joint was made with a GTAW current setting
of 60.6 amps and 4.2 mm/sec scan rate which followed a welding sequence
of GTAW for 5.0 cm, LBW/GTAW for 5.0 cm, and then LBW for 5.0 cm.
This same procedure was followed for the weld joint made with an 81.0
amp GTAW current value and 4.2 mm/sec scan rate, shown in Figure 44.
High speed welds at the 81.0 amp GTAW current setting were made at 42.3
and 84.7 mm/sec with a welding sequence of GTAW for 7.0 cm followed by
LBW/GTAW for 7.0 cm. Figure 45 shows the weld bead surface appearance
of the weld joint made at 84.7 mm/sec. Only the weld joint made with

a GTAW current value of 81.0 amps and scan rate of 4.2 mm/sec showed enough

promise to warrant microscopic examination, however. Cross sections

of the GTAW and LBW/GTAW portions of this weld joint are displayed in

Figure 46. The LBW portion missed the weld groove on this particular

sample but results from the other samples showed that no substantial

welding occurred.

High speed videography was used to investigate arc-rooting in

arc-augmented laser welding. Figure 47 shows the set-up used to

gather the information. The camera recorded the welding at a rate of

1000 frames per second. Although this was at the low end of the

capability of this high speed motion analysis system, the information

gained was indeed valuable. The frame sequence shown in Figure 48

contains information related to the arc-rooting phenomena. Frame

number 1 showed the GTAW plasma along with the plasma generated from

the impinging laser beam. The arc from the tungsten electrode began

to jump to the laser induced plasma in frame number 2, followed by an

interaction with the laser energy that outlined the converging beam in

frame number 3. Frames 4 and 5 showed a pulsating effect while in

frame number 6 the plasma detached from the substrate and vanished by

frame 7. No laser generated plasma was visible in frame number 7.

H. Plasma Interactions

It was found during preliminary welding tests that the cross jet

of argon gas used initially to disperse the laser generated plasma

also had an impact on the combined plasma formed in arc-augmented

laser welding of aluminum. Figure 49 exibits a plot of weld metal A_w

vs. scan rate for the resulting welds made with and without the gas cross jet. The amount of weld metal A_w exhibited somewhat less than conclusive evidence of a trend whereby the gas cross jet decreased the amount of melting. One could envision an effect at the lower welding velocities, however the result at the 8.5 mm/sec scan rate did not completly confirm that trend. Three still photographs from the high speed videography work compare this gas cross jet outcome in Figure 50, showing the shape of each plasma plume. The optical micrographs of Figure 51 display cross sectional views of the resulting welds, which showed weld width broadening, among other features, due to the gas cross jet.

Interactions between the GTAW and LBW induced plasmas were investigated with the high speed motion analysis system. Still photographs of a sequence of frames shot at 1000 frames per second showed the interaction of the impinging laser beam with the arc (Figure 52). Frame number 1 showed the general appearance of the GTAW plasma. Frame number 2 showed the general appearance of the combined plasma, while the evaporation of the laser induced plasma was caught in the detached stage in frame number 3. Frame number 4 depicted the basic veiw of the GTAW plasma without the influence of the laser beam.

The plasma generation differences between GTAW and LBW/GTAW are compared in Figure 53. These reprsentative still photographs contrast BH and FH welding at two different scan rates. As shown in Figure 53, the outstanding feature of the GTAW process was the appearance of pushing and pulling the arc column, while for the LBW/GTAW combination the arc column extension was noted.

Plasma interactions for arc-augmented laser welding of steel were

documented with high speed motion analysis for comparison with aluminum welding results. The photographs of Figure 54 show the laser induced plasma. An interesting point was seen in the second photograph of Figure 54 where the GTAW electrode glows from high heat. This was due either to absorption of the laser beam or radiated heat from the molten weld pool. The still photographs of Figure 55 exhibit the differences between GTAW and LBW/GTAW in the BH and FH directions, in terms of plasma interactions, and shows them to be basically the same as for aluminum.

An interesting result was obtained while aligning the laser beam coaxially with the arc at the beginning of the high speed videography work. As the GTAW torch was moved closer to the laser interaction zone, a sequence occurred where the arc became unstable. The second photograph of Figure 56 showed stable arcing while the third photograph of this figure showed arc instability. The "double" arc in the third photograph is responsible for the "double" weld shown in cross section in Figure 57.

I. Synergy for Aluminum and Steel Compared

Figure 58 summarizes the results of the Melting Efficiency and Materials Selection (1018 steel) sections, in terms of arc-laser synergism. An ambiguous data point was seen where the synergy at the 8.5 mm/sec scan rate for the 171.6 amp case was low. This outcome was due to the fact that BH and FH results were averaged for this graph and the value for the FH case was very low (10%) even though the backhand value (54%) was consistant with the overall trend as shown in

Figure 58. Aside from this minor detail, the important features of
Figure 58 were clear; synergy decreased with increasing scan rate in
all cases, and results for steel were in line with that for aluminum.

.

IV. Discussion

A. Laser Beam Parameters

Knowledge of beam operating parameters is critical to guarantee
successful laser processing of materials. For LBW, the total output
power, unfocused beam diameter, lens focal length (and corresponding
focussed spot size), determine the power density and the associated
depth of focus for the specific system. Once these parameters are
precisely set, the response of materials will be in relation to their
thermal and physical properties. Breinan and Banas[41] conducted research
on the response of elemental metals under varied laser beam parameters
to determine the fundamental aspects of laser/materials interactions.
An important finding in their work was the correlation of LBW parameters
with the material properties on welding performance. By combining the
important variables into two dimensionless parameters, a linear rela-
tionship was found on a log-log plot (Figure 59). The dimensionless
parameters (originally developed by Hablanian[42] for EBW), Vd/a (speed)
and hkT_m/P (penetration-power), were as follows:

V = welding speed

d = focal spot diameter

a = average thermal diffusivity = K/pC_p (298 K to M.P.)   where

 K = average thermal conductivity (298 K to M.P.)

        p = density

        C_p = average heat capacity (298 K to M.P.)

P = laser power

h = depth of penetration

$$T_m = \frac{H_L - H_{298}}{C_p} \qquad \text{where} \quad \begin{array}{l} H_L = \text{enthalpy of liq. at M.P.} \\ H_{298} = \text{enthalpy of sol. at 298 K} \end{array}$$

As shown in Figure 59, aluminum was at the "difficult to weld" end of the scale, while iron and titanium were at the "easy to weld" end. The data point for 304 stainless steel showed that the correlation was indeed correct for alloys as well as elemental metals.

The beam operating parameters were found in the present investigation by a combination of direct and indirect measurements. Since the resulting power density for a given beam/lens combination was extremely high ($>10^6$ w/cm^2 for this study), no direct measurement was feasible. Because of this, the power density of the focused spot was calculated based on the measured lens focal length (which enables one to calculate the spot size) and total output power. Once the focused spot size for a lens is known, the power density can be adjusted to produce heating, melting or vaporization of most engineering materials. The main problem with welding aluminum is that the power density necessary to initiate thermal coupling is within the range for vaporization once welding begins. The result is an overbalance where the weld pool is propelled out of the material with laser "cutting" produced. This "expulsion" of the weld pool (which is caused by rapid evaporation) is a very complex problem although the solution requires a reduction in the power density to the lowest acceptable value[43]. The main task necessary to solve this problem then would be to find a way to reduce this "threshhold" power density so that vaporization is minimized, while still welding in the deep-penetration mode. Snow et al[37] reported that aluminum was very sensitive to the input power

density, while Mazumder[44] concluded that the composition of individual aluminum alloys determined whether the irradiation parameters were critical. The LBW done with the 6.02 cm focal length lens in the present study demonstrated that aluminum was indeed sensitive to the power density, as shown in the welds of Figure 15, where the deep-penetration mode is abruptly lost after apparently stable operation. Although a reduction in output power was a possible cause, movement of the sample out of the focal plane was more likely the reason for the lowered power density which lead to this loss of coupling.

Many workers report that a minimum threshold power density of 10^{5-7} W/cm^2 exists for thermal coupling with aluminum[45-47]. This parameter is controlled largly through beam focusing optics, which for a given output power will shorten the depth of field as the power density is increased. The total power of the laser is the parameter which specifies the thickness of possible weldments (depth of field) once the power density is set. It can be seen that the ability to weld aluminum is not based on output power, per se, but the maximum power density obtainable. Low power lasers can be focused to weld aluminum, but the resulting depth of field limits their application to thin weldments. Moon and Metzbower[48] welded aluminum with an 8 kW laser focussed to a 10^6 w/cm^2 power density. The main impact of the higher total output power was related to weldment size (1.27 cm thick plate), rather than power density capabilities.

An important consideration left out of the discussion above related to high power lasers is that since a longer focal length lens can be used to produce the required power density, along with the

greater depth of field (larger weldments) comes the benefit of greater tolerance with respect to joint fitup and working distance. Welding with low power lasers requires precise lens to workpiece tolerances in order to attain the power density necessary to initiate and continue welding in aluminum. In applications requiring short focal length lenses, variations in weldment to lens distance caused by fixturing (or other causes) can mean the difference between thermal coupling and a specular reflection of the laser beam, as was clearly illustrated in Figure 15. Changes as small as 0.25 mm in lens to workpiece length can be ruinous to LBW with the 6.02 cm focal length lens used in this study.

By way of summary, the beam operating parameters have been shown to be of overriding importance with respect to LBW aluminum, in this study, and elswhere. The power density must be high enough to overcome the initial surface reflectivity, and the output power great enough to produce the required depth of penetration for a given weldment.

B. Surface Modifications

The surface condition of an aluminum substrate has much to do with its initial reflectivity of 10.6 micron wavelength laser light[49]. The surface preparations investigated in this study consisted of grit blasting, anodizing and thermal spraying aluminum powder coatings. Grit blasting and anodizing were found to promote laser melting of aluminum (Figure 18), which is in agreement with other workers[35,44,47]. The important part of this work was in relation to true thermal coupling, though, and it was here that information was lacking. The problem is

that welding differences are not by degree but by rather sharp changes, as shown earlier (Figure 15) where coupling is either attained or not (i.e. the threshhold power density requirement is overcome or not). This problem aggravates any attempt to measure the effect of surface modifications in a quantitative way. A detailed study of near threshold power density welding would be necessary to reach firm conclusions about the LBW of aluminum. It would be safe to assume, however, that surface preparations could reduce substantially the threshold power density for the deep-penetration mode as noted by Houldcroft[50], where keyhole welding was attained with the low power of 750 W in 1.5 mm stainless steel by using a special surface preparation technique. Since the present investigation primarily covered LBW/GTAW, further work on surface preparation effects was considered unnecessary because the beam would essentially impinge on a molten weld pool in the combined process, making any surface preparations superfluous.

Huntington and Eager[35] performed detailed studies on the aluminum surface absorption of laser light for a variety of surface conditions and joint geometries. Their aim was to quantify the differences between different weldment preparations on beam absorption, and to this end a special cone and holder assembly was made for absorption studies with both 200 W and 1300 W pulsed CO_2 lasers. Aluminum weldments were made with a 5.0 kW CW CO_2 laser. Based on their results, it was concluded that both grit blasting (-300 mesh glass beads) and anodizing had a positive effect on LBW aluminum. The high absorption of the grit blasted samples was attributed to absorption by glass beads imbedded in the surface[35], rather than an effect due to the roughening itself.

The results of the present investigation contradicts this conclusion since comparable enhanced absorption occurred for the roughened surface with no embedded particles found, as shown in the SEM micrograph of Figure 3. The increased absorption of the anodized surface was attributed to a lower free electron density in the oxide layer by Huntington and Eagar[35]. No evidence in the present study was found to either support or deny this conlusion. It is well known that oxide coatings are used to promote conductive heating when CW laser heat treating or transformation hardening steel[36]. There may be a similar effect with anodized aluminum surfaces. Other workers[37] have felt the oxide layer to be a hinderence to LBW aluminum, and so this complex area remains somewhat controversial.

C. GTAW Current and Voltage

The GTAW current and voltage was measured during both GTAW alone and LBW/GTAW. The work done by Steen et al[7] on iron base alloys included measurements of this type where they showed that the arc column resistance decreased and the current increased while the laser beam was on. The electrical efficiency of the combined process was therefore greater than that of GTAW alone. This was postulated as a basic mechanism of the arc-laser synergism phenomena[17]. The results from the present study on aluminum was consistant with the earlier work of Steen and co-workers for steel and it is postulated here that the resulting arc "stiffness" allows greater arc constriction and higher resulting power density at the weld pool. These convictions are strengthened by the chapters of this thesis on arc rooting and plasma interactions associated with arc-augmented LBW and will be

discussed further later.

D. Melting Efficiency

The work done under the broad heading of "Melting Efficiency" was an important part of the overall study of arc-augmented laser welding of aluminum. The data generated in this section allowed basic examination of the fundamental differences between the LBW, GTAW and LBW/GTAW of aluminum. The main approach used to make sense of the results was one of an energy required for melting relative to the energy supplied by the welding processes, and hence the term "efficiency" arose. Weld metal A_w provided a good check of the melting efficiency since "energy" could be related to unit volume of melted material. Depth of penetration measurements of welds made with the LBW process are the usual mode of comparison when citing changes in "efficiency" but for the case of LBW/GTAW the method used by Breinan et al[41] to measure weld metal A_w for LBW was adopted. Comparing weld metal A_w seemed logical when evaluating GTAW and LBW individually along with LBW/GTAW.

The energy input in J/mm (based on the ratio of the total input power to the welding velocity) divided by the amount of energy required to melt a given volume of metal, to a first approximation, should be equal to the weld metal A_w divided by an efficiency constant[51,52]. The efficiency constant incorporates both the heat transfer from the welding source to the weldment (f_1) and the melting efficiency of this heat source once it is absorbed (f_2). One can then use the following equations to evaluate the energy efficiency for welding :

$$A_w/f_1f_2 = H/Q$$

where,

H = P/V

P = power

V = welding velocity

$Q = C_p*T + *H$

C_p = average specific heat

*T = temperature change

*H = heat of fusion

For aluminum, $Q = 2.84$ J/mm^3 and given the measured values of weld

metal A_w and the process parameters, the product of the efficiencies

f_1 and f_2 can be found. For example, the GTAW welds (BH&FH) of 60.6

amps current setting, 12 volts, 8.5 mm/sec scan rate, and average weld

metal A_w of 0.86 mm^2 had an overall efficiency of 0.03. Now if it is

assumed that the efficiency remained the same for LBW/GTAW, the energy

input would have to be 120.4 J/mm to attain the weld metal A_w which

resulted (1.21 mm^2). This would mean a total input power of approximately

1020 watts, and subtracting the input power of the GTAW arc (which can

be taken as 618 since the arc parameters changed) the laser would

contribute approximately 400 W of power. Since 920 W of laser energy

was available, this figure would be possible (44% efficiency). The

main problem with this approach is the assumption of constant efficiency,

however, and it is for this reason that no definitive conclusions can

be made based on this analysis alone. The combined efficiency of

LBW/GTAW was shown to be significantly greater than the sum of the two

processes separaly, which could be the major cause of the arc-laser synergism. The overall efficiency of the combined process was found to be 0.02, based on weld metal A_w measurements, and the efficiency of LBW can be taken as 10^{-5}, which is so small as to be hardly worth considering. Whether the molten weld pool absorbes most of the laser beam or none at all then would only be speculative, based on this analysis alone.

In GTAW of steel, $Q = 10.42$ J/mm^3, and for the welds made with the same arc energy input as above, the average weld metal A_w (BH&FH) was 1.99 mm^2. The overall efficiency for these welds was then 0.24, which was typical for the GTAW process. Holding this value constant as before, the LBW/GTAW energy input would need to be approximately 2200 W. Since only 730 W was available from the GTAW and only 920 W was available from the LBW process, an increase in efficiency would necessarily have had to occur.

Following the method of Houldcraft[53], the melting efficiency can be estimated to a first order approximation based on the following equation:

$$VD/a = \text{"weld characteristic"}$$

where,

    V = weld velocity

    D = melted width

    a = thermal diffusivity

Any weld can be characterized using this relationship since efficiency is measured by comparing the amount of heat lost (thermal diffusivity) to the heat used for melting (based on a two dimensional heat flow

model). As the weld velocity is increased the efficiency should increase since the thermal diffusivity remains constant and less heat is lost to the surrounding material. For typical high energy density or high heat input rate welds, VD/a will be greater than 1, while for low heat input rate welds, the weld characteristic will be less than 0.1. Most welds made in practice have a weld characteristic of between 0.25 and 1. For the aluminum welds made with GTAW from above, the average weld characteristic was 0.05, while the LBW/GTAW welds had an average characteristic of 0.07. This is a 44% increase in weld characteristic. If the efficiency (based on weld characteristic) for LBW/GTAW was 44% greater than GTAW, the overall efficiency (f_1f_2) was also found to be 0.041. Putting this value back into the equation to find the energy input necessary to produce the amount of weld metal A_w measured for LBW/GTAW, and subtracting the arc energy input of the GTAW, the contribution of the laser would need to be as follows:

$$(Q)(A_w)/f_1f_2 = H = (2.84 \text{ J/mm}^2)(1.21 \text{ mm}^2)/(0.041) = 83.6 \text{ W/mm}$$

and,

$$P = (83.6 \text{ W/mm})(8.5 \text{ mm/s}) = 711 \text{ W}$$

The GTAW provided 618 W leaving 93 W necessarily added by the laser. This would mean an absorption of approximately 10% of the laser light, meaning that no significant improvement in thermal coupling occurred and the entire mechanism of arc-laser synergism was one of improving the efficiency of the GTAW by rooting the arc to a stable position.

Applying the method used above for aluminum, the results on steel could be compared. For GTAW, f_1f_2 was shown to be 0.24 for the welds

in question (60.6 amps, 8.5 mm/sec). The overall efficiency of LBW on steel at an 8.5 mm/sec scan rate is seen to be 0.22, which is very close to the value of GTAW from above. The LBW/GTAW welds show an overall efficiency of 0.34, reflecting an improvement in the combined process. Now using the weld characteristics in the same manner as before, the efficiency of the LBW/GTAW process can be found. For the GTAW, LBW, and LBW/GTAW welds the average weld characteristics are 0.703, 0.589, and 1.034 respectivly, showing again that an improvment in efficiency could account for the increased weld metal A_w.

E. Preheating

A topic of great controversy is the effect of preheating on the absorption of laser light. Several researchers[29-32] claim that the reflectivity goes down as one approaches the melting point of aluminum. Others[33,34] feel that the reflectivity does not decrease until one is very close to the boiling point.

The specular reflectivity of aluminum for 10.6 micron wavelength laser light was shown by Walters et al[29-31], Ujihara[32], and Walter and co-workers[33,34] to be temperature dependent. These researchers agree that anomalous reflectivity changes are observed during intense laser pulses. Specifically, a sharp decrease occurs midway through a pulse which reaches a plateau level prior to either partial or total recovery of reflectance. Ujihara used the Drude free electron model coupled with electron-phonon collision theory as a basis for his explanation of this phenomena. Walter asserted that Ujihara used incorrect values of the physical constants in his calculations, however, and went on to

show that experimental results left in considerable doubt the idea
that the melting point rather than the boiling point was the mark for
a considerable reduction in reflectance. Walters based his explanation
on numerical heat transfer calculations and microscopic examination of
samples subjected to laser pulses to show that the peak power-density
threshhold agreed with the intrinsic surface melt threshold. Indeed,
the treatment required to resolve this problem is beyond the scope of
this thesis. The important element, though, is that in terms of its
engineering import, preheating would provide a benefit since not only
does the reflectance decrease with temperature, but the thermal diffusivity
diminishes as well. What is important about this complex phenomenon
is that the LBW of aluminum is most difficult at lower temperatures and
with any increase in temperature a corresponding decrease in the
thermal coupling threshold must necessarily occur. Simply put, preheating
should work, based on theory, and does work, as shown experimentaly in
this project. Whether the mechanism for lowering the required power
density threshold is due to lower reflectivity or lower thermal diffusivity
is not resolved by the work on which this thesis is based. It is most
likely a combination of the two in varying degrees.

The in process LBW at 524°C in Figure 34 was considered a noteworthy
event. Not only did it demonstrate the validity of the preheating
approach, but it also revealed other inportant features as well. The
sparking or "burning" seen in Figure 34 was most likely due to the
fusion zone purification phenomena where magnesium is vaporized and
lost to the atmosphere. Moon et al[48] report that such welds have
lower strength than the work hardened material with a corresponding

increase in toughness due to lower inclusion contents. A possible solution to this problem could be to laser shock harden the weldments in a subsequent opperation[54].

An important benefit of the preheating approach was also noted where the lower solidification rate resulted from the higher heat input. This results in more time for gas bubbles, which would normally be trapped as porosity, to float to the surface of the molten weld pool by the method described by Stokes law[55].

F. Materials Selection - Steel vs. Aluminum

The welding done on steel provided a comparison between the work on aluminum and also the work done by other workers. The original discovery of arc-laser synergism was made by Steen and coworkers[56] in 1975, with a patent subsequently granted in 1976. Since that initial study, others have investigated aluminum as well as steel[40,57]. Arc-laser cutting was developed also at The Welding Institute[58].

Comparisons between the results on steel and aluminum show some interesting features. The first striking point noted was the great difference in thermal coupling ability for the two materials. The power density threshold required to initiate thermal coupling in steel is obviously much lower than that for aluminum. No effort was made to accurately quantify these values, however, since other workers have explored this area[41,59]. The results of this project offer convincing proof of this difference where for aluminum essentially no LBW occurred while for steel substantial absorption of beam energy resulted. The

discussion of melting efficiency from above pointed out the great differences in energy usage for the LBW of aluminum and steel.

The important aspects of LBW/GTAW differences in aluminum and steel were seen in Figure 58 where basically no difference in synergy was found. This, it is felt, offers strong evidence that the basic mechanism of arc-laser synergy is an improvement in GTAW efficiency by the laser rather than any change in the thermal coupling of the laser. If one expected a large contribution of the arc-laser synergy to be due to enhanced thermal coupling of the laser, the synergy values should be lower for steel than for aluminum since substantial thermal coupling occurs for steel with the LBW process alone (there is little room for improvement).

G. Arc Rooting

The phenomena of arc rooting which occurs in LBW/GTAW is well documented[60,61]. As seen throughout this thesis, it is felt that this is a dominant mechanism of the well recognized arc-laser synergism. High speed photography performed by Barth and Albright[57] confirmed initial ideas that the interactions were indeed complex. Their work was with 4330 alloy steel, though, and differences for aluminum were therfore unexplored. The work done in the present study did uncover some features peculiar to aluminum as opposed to steel in the LBW/GTAW process, even though the synergy values were basically the same.

An important ingredient in the arc rooting explanation is the hot spot created by the laser which the arc roots to. For steel this process is not hard to envision while for aluminum the converse is

true. Since there is no hot spot created for LBW aluminum (thermal coupling is lacking), there should be a significant loss of rooting ability. The work of Steen showed that the work function changes enough with temperature that a spot of only 300°C temperature would produce the ability to root the arc strongly in steel[56,61],. A similar effect would be expected for aluminuim, and the sequence of frames shown in Figure 48 exhibit convincing proof of arc rooting in aluminum. There is a combined influence, which was postulated by Steen et al[56], where the laser "roots" to the spot created by the arc and then the arc roots to this combined spot. It could be possible that the laser begins to couple once the arc "preheats" the interaction zone and then the arc roots to this spot. Both the effect of preheating and of increased efficiency by constricting the arc would then be operating

in this combined mode.

H. Plasma Interactions

High speed videography was used to investigate the interactions between the laser generated plasma and the plasma of the gas tungsten arc. It has been known since very early in the development of laser metal working that the plasma generated during deep-penetration welding or cutting could absorb the beam and cause sporadic thermal coupling. This beam attenuation can be avoided by suppling a jet of suitable inert gas which serves to blow the vapor out of the way of the impinging beam. In most laser welding applications the cross jet of gas provides a dual service: (1) shielding of the weld pool from the atmosphere and (2) plasma suppression[62]. Helium and argon are the two most

commonly used gases, each with their own advantages and disadvantages.
Argon tends to form a plasma at the beam interaction spot, however it
is used as a weld shielding gas more often since its density keeps it
in the target area while for the case of helium (which tends to float
away) one would be assured of maximum beam coupling. In any event,
compromises must be made to optimize the desired effects, etc., with
economic factors sometimes outweighing metallurgical factors. For the
present study, argon was soley used for shielding, plasma dispersal,
focusing lens shielding, and GTAW shielding.

The pressure developed over the weld pool by the plasma dispersal/weld
shielding gas cross jet has a great effect on weld pool formation.
Weld bead shape can be changed dramatically by varying the gas flow,
as shown by Arata et al[63]. Their work demonstated that the deepest
penetration occurred when the cross jet gas pressure was equal to or
slightly greater than the pressure of the vapor column within the
keyhole. It can be easily seen that the properties of the material
being welded would then dictate the proper cross jet gas pressure
during LBW.

Even though beam attenuation by the laser generated plasma plume
occurs in most cases, under suitable conditions, the plasma can be
desirable to promote thermal coupling. Donati et al[64] claim that for
surfaces highly reflective at the particular laser wavelength being
used this is exactly the case. They go on to assert that the plasma
absorbs the laser radiation and reradiates absorbed energy at much
shorter wavelength which can then be coupled with the target. Thus we
have another piece of evidence showing that the response of materials

to fixed LBW conditions will be in relation to the thermal and physical properties of the material. This interesting phenomenon could go a long way towards explaning the results shown in Figure 49 where penetration was increased by turning off the gas cross jet. Another possible explanation might be that the combined plasma was simply cooled by the jet making it less efficient.

I. Synergy Mechanisms

There are two important considerations towards a model of the basic mechanism of the arc-laser synergism documented in this thesis. The first involves the effects of weld preheating while the second concerns the phenomenon of arc rooting or constriction of the arc. From an efficiency standpoint, weld preheating by the GTAW arc should increase the absorption of the laser beam, while arc rooting (due to the lowered work function at the LBW hot spot) should increase the efficiency of the GTAW. Thus we have a situation where each process influences the other in a positive way when they are run in combination.

Arc rooting, as shown explicitly in this study, very definitely results in an increase in the overall efficiency of the GTAW process. Even though the GTAW process was extremely inefficient (due predominantly to the very inclined angle of the electrode), a small increase in efficiency could account for the total increase in weld metal A_w in the combined process, without any necessary increase in absorption of the laser beam. These convictions were strengthened by the comparisons made between the results found for steel with aluminum, where the amount of synergy was essentially the same for each material. This

points to the increase in GTAW efficiency as the dominant mechanism
for synergy.

The effects of weld preheating related directly to an increase
in absorption of laser beam energy due to the presence of a molten
weld pool (supplied by the GTAW process). There is basically no
direct evidence that could be offered as proof of this mechanism which
was derived from this investigation. It was seen that thermal coupling
was attained at a preheating temperature very near the melting point
of aluminum, which shows, albeit indirectly, that increased absorption
of the laser beam should occur when impinging on the molten weld
pool supplied by the GTAW process. An important feature concerning
this proposed mechanism, is the influence of the GTAW plasma on the
laser beam. Beam attenuation must to some extent necessarily occur as
seen where a laser induced plasma results when the beam penetrates the
GTAW plasma. Even though the GTAW plasma is not as absorptive of the
beam as that of the LBW, high speed videography showed the generation
of a laser extended "plume" on the GTAW plasma. Energy must be used
to create this plume and so must in some way attenuate the beam. The
end result could then be that the threshold power density never is
attained on the surface of the molten pool for thermal coupling to
occur. From the weld cross sectional macrographs, no evidence of
increased LBW influence was seen in the combined process, with only
the appearance of a larger GTAW weld resulting. It is therefore
concluded that the mechanism of arc-laser synergy is predominantly an
improvement in GTAW efficiency due to arc rooting induced by the LBW process.

VI. Conclusions

In the study of arc-augmented laser welding of aluminum the following can be concluded:

1. Synergy resulting from the combined action of the laser beam and the gas tungsten arc produced a far greater volume of molten metal than the individual contributions of each process added separately.

2. It was shown that this synergistic effect could be due to an improvement in the melting efficiency of both the LBW and GTAW contributions to the weld pool. This conclusion was strengthened by the measured increase in electrical efficiency in the combined LBW/GTAW process and the observed arc-rooting from the GTAW to the laser induced hot spot.

3. Weld preheating was found to enable thermal coupling of laser energy at a temperature very close to the melting point of aluminum. The increased absorption of the laser beam could be a mechanism of the observed arc-laser synergism since the laser beam would impinge on an already molten pool (supplied by the GTAW torch) in the combined process.

4. The synergistic effect of the LBW/GTAW process in aluminum alloys was found to be very close to the same value for steel. Because the melted volume from LBW was much greater for steel than aluminum, one would expect greater synergy for aluminum than steel if a significant improvement in LBW occured as a mechanism of this synergistic effect. This was felt to be strong evidence of the dominant role of increased

GTAW efficiency as a mechanism of the arc-laser synergy, particularly at low travel speeds.

5. The properties of aluminum (initial surface reflectivity and thermal diffusivity being the most important) are such that the response due to the impingement of a CO_2 laser beam (10.6 μm wavelength) will be minimal relative to other engineering materials. The power density necessary to initiate and continue welding in the deep-penetration mode is very high ($>10^6$ W/cm^2 in this study) and results in weld defects such as porosity and weld pool splashing due to gas evolution/ entrapment and low surface tension of the molten weld pool.

6. The surface oxide on aluminum appears beneficial to LBW while detrimental to GTAW, and so for the combined process grit blasting offered the greatest benefit.

REFERENCES

1. E. M. Breinan and C. M. Banas, "Welding with High Power Lasers", Advances in Metal Processing, Sagamore Army Materials Research Conference Proceedings, vol. 25, 1981, pp. 111-131.

2. E. B. Bruening, "Lets Look at Lasers", SME Technical Paper MR70-521, 1970.

3. W. M. Steen and C. M. Sharp, "Lasers in Production", Engineering Materials and Design, Feb. 1982, pp. 32-36.

4. B. H. Kear, E. M. Breinan, and E. R. Thompson, "Laser Processing of Materials", Advances in Metal Processing, Sagamore Army Materials Research Conference Proceedings, vol. 25, 1981, pp. 45-78.

5. F. R. Miller, "Air Force Materials Laboratory/Industry Interface for a Total Metals Joining Capability", SME Technical Paper MF73-713, 1973.

6. F. R. Miller, "Advanced Joining Processes", SAMPE Quarterly, Oct. 1976, pp. 46-54.

7. W. M. Steen and M Eboo, "Arc Augmented Laser Welding", Metal Construction, July 1979, pp. 332-335.

8. E. J. Morgan-Warren, "The Application of Laser Welding to Overcome Joint Asymmetry", Welding Journal, March 1979, pp. 76s-82s.

9. T. H. Malim, "More Power to New Breed of Lasers", Iron Age, April 1970, pp. 99-106.

10. S. Wesson, "Navy Finds Laser Key to Welding Alloy Hulls", American Metal Market/Metalworking News, April 1978, p. 12.

11. L. P. Earvolino and J. R. Kennedy, "Laser Welding Aerospace Structural Alloys", Welding Journal, March 1966, pp. 127s-134s.

12. W. G. Alwang, L. A. Cavanaugh, and E. Sammartino, "Continuous Butt Welding Using a Carbon Dioxide Laser", Welding Journal, March 1969, pp. 110s-115s.

13. R. Barber, "Laser Welding Applications", SME Technical Paper AD74-405, 1974.

14. "Army Finds $4 Million Savings with Laser Welding", Lasers & Applications, Sept. 1982, pp. 34-35.

15. R. R. Irving, "Laser Welding Becomes Competitive Welding System", Iron Age Metalworking Int., Dec. 1976, pp. 21-22.

16. B. D. Wakefield, "Lasers Challenge Electron Beam Welding in Speed, Quality", Iron Age, Dec. 1972, pp.88–89.

17. R. R. Irving, "Laser Welds Focus on Steel Plate Structures", Iron Age, May 1976, pp. 43–45.

18. G. E. Overstreet, "Heavy-Duty Light", Industrial Research, May 1974, pp. 40–44.

19. R. R. Irving, "Metalworking Lasers: Their Time Has Come", Iron Age, Sept. 1974, pp. 51–60.

20. "Autos", Welding Design & Fabrication, Nov. 1980, pp. 94–97.

21. D. F. Baxter, "Survey Report: Welding in The 80's", Metal Progress, March 1980, pp. 28–35.

22. R. C. Crafer, "Improved Welding Performance from a 2kw Axial Flow CO_2 Laser Welding Machine", Advances in Welding Processes, Fourth International Conference, vol. 1, 1978, Paper 46, pp. 267–278.

23. C. M. Banas, "High Power Laser Welding", A paperfrom 'Proceedings of The Symposium on Welding, Bonding and Fastening,' NASA, 1972, 22 p.

24. E. A. Metzbower and D. W. Moon, "Fractography of Laser Welds", Fractography and Materials Science, ASTM STP 733, 1981, pp. 131–149.

25. E. A. Metzbower and D. W. Moon, "Properties and Structures of Laser Welds of High Strength Alloys", Weldments: Physical Metallurgy and Failure Phenomena, Proceedings of The Fifth Bolton Landing Conference, 1978, pp. 245–256.

26. E. A. Metzbower and D. W. Moon, "Mechanical Properties, Fracture Toughnesses and Microstructures of Laser Welds of High Strength Alloys", Applications of Lasers in Materials Processing, Proceedings of a Conference, ASM, 1979, pp. 83–100.

27. P. F. Avramchenko, et al., "The Laser Welding of Wires Made of Super-High Purity Aluminum", Avt. Svarka, 1974, No. 11, pp. 69–70.

28. Y. S. Touloukian and D. P. DeWitt, Eds., "Thermophysical Properties of Matter", Thermal Radiative Properties-Metallic Elements and Alloys, Vol. 7, New York: IFI/Plenum, 1970, (Ref. from Aluminum: Properties and Physical Metallurgy, ASM, 1984, p.14, J. E. Hatch, Ed.)

29. C. T. Walters and A. H. Clauer, "Transient Reflectivity Behavior of Pure Aluminum at 10.6 micrometers", Applied Physics Letters, 33 (8), Oct. 1978, pp. 713–715.

30. C. T. Walters, "Anomalous Behavior of the Reflectivity of Metals Irradiated with 10.6 micrometer Pulses", Laser Applications in Materials Processing, SPIE Vol. 198, 1979, pp. 98–108.

31.   C. T. Walters, T. R. Tucker, S. L. Ream, A. H. Clauer, and
D. J. Gallant, "Thermal Coupling of CO_2 Laser Radiation to Metals",
Lasers in Metallurgy, Proceedings of a Conference, 1981, pp. 195-206.

32.   K. Ujihara, "Reflectivity of Metals at High Temperatures", Journal
of Applied Physics, Vol. 43, No. 5, May 1972, pp. 2376-2383.

33.   W. T. Walter, "Reflectance Changes of Metals During Laser Irrad-
iation", Laser Applications in Materials Processing, SPIE Vol. 198,
1979, pp. 109-117.

34.   W. T. Walter, N. Solimene, K. Park, T. H. Kim and K. Mukherjee,
"Optical Properties of Metal Surfaces During Laser Irradiation",
Lasers in Metallurgy, Proceedings of a Conference, 1981, pp. 179-195.

35.   C. A. Huntington and T. W. Eager, "Laser Welding of Aluminum and
Aluminum Alloys", Welding Journal, April 1983, pp. 105s-107s.

36.   K. H. Miska, "The Focus is on Lasers for Fabricating Metal Products",
Materials Engineering, Nov. 1977, pp. 50-52.

37.   D. B. Snow, M. J. Kaufman, C. M. Banas, and E. M. Breinan, "Evaluation
of Basic Laser Welding Capabilities-Final Report", R79-911989-17,
United Technologies Research Center, May 1979.

38.   J. Mazumder, "Laser Welding: State of the Art Review", Lasers in
Metallurgy, [Proc. Conf.], Chicago, Ill., 22-26 Feb., 1981, Met. Soc./AIME,
pp. 221-245.

39.   J. Mazumder, "Laser Welding: The Present State-Of-The Art",
Proc. of 1st Int. Laser Processing Conf., Anaheim, CA, 1981, Publ: Laser
Inst. of America, 1981.

40.   T. P. Diebold and C. E. Albright, "'Laser-GTA' Welding of Aluminum
Alloy 5052", Welding Journal, June 1984, pp. 18-24.

41.   E. M. Breinan and C. M. Banas, "Evaluation of Basic Laser Welding
Capabilities",R75-911989-4, United Technologies Research Center,
Oct. 1975, pp. 1-29.

42.   M. H. Hablanian, "A Correlation of Welding Variables", Proceedings
of the 5th Symposium Electron Beam Technology, 1963.

43.   N. N. Rykalin and Y. L. Krasulin, "Evaluation of Energy Parameters
in the Laser Welding of Metals", Soviet Physics-Doklady, Vol. 10,
No.7, Jan. 1966, pp. 659-661.

44.   J. Mazumder, "Laser Welding: State of the Art Review", Journal of
Metals, July 1982, pp. 16-24.

45.   K. Shinda, T. Ohmae, Y. Yoshida, S. Suzuki and M. Tamura, "Basic

Study on Laser Welding", Conf. Proc., Publ: Laser Institute of America, 1981, Paper 3, 9 p.

46. Y. Arata and I. Miyamoto, "Laser Welding", Technocrat, Vol. 11, No. 5, May 1978, pp. 33-42.

47. J. R. Shewell, "Design for Laser Beam Welding", Welding Design & Fabrication, June 1977, pp. 106-110.

48. D. W. Moon and E. A. Metzbower, "Laser Beam Welding of Aluminum Alloy 5456", Welding Journal, Feb. 1983, pp. 53s-58s.

49. S. T. Picraux and D. M. Follstaedt, "Surface Modification and Alloying: Aluminum", Surface Modification and Alloying, Edt. by J. M. Poate, G. Foti and D. C. Jacobson, Plenum Publishing Corp., 1983, pp. 287-321.

50. P. T. Houldcroft, "Laser and Electron Beam for Welding Engineering Components", Metal Construction, Oct. 1975, pp. 498-502.

51. C. Weisman, Ed., Welding Handbook, 7th ed., Vol. 1, Fundamentals of Welding, AWS, 1976, pp. 36-37.

52. E. F. Nippes, Coord., Metals Handbook, 9th ed., Vol. 6, Welding, Brazing and Soldering, ASM, 1983, pp. 31-32.

53. P. T. Houldcroft, Welding Process Technology, Cambridge Univ. Press, 1977.

54. A. H. Clauer, B. P. Fairand and B. A. Wilcox, "Laser Shock Hardening of Weld Zones in Aluminum Alloys", Met. Trans. A, Vol. 8A, Dec. 1977, pp. 1871-1876.

55. M. C. Flemings, Solidification Processing, McGraw-Hill, Inc., 1974.

56. W. M. Steen, "Arc Augmented Laser Processing of Materials", J. Appl. Phys., Vol. 51, No. 11, Nov. 1980, pp. 5636-5641.

57. J. S. Barth and C. E. Albright, Center for Welding Research Annual Report, The Ohio State University, June 1982.

58. J. Clarke and W. M. Steen, "Arc Augmented Laser Cutting", Proceedings of the Laser 1979 Conference, Munich, 1979, pp. 247-253.

59. P. G. Moore, "Surface Alloying Using Continuous Lasers", U.S. Naval Research Laboratory, Washington, D.C., reprint.

60. J. Alexander and W. M. Steen, "Penetration Studies on Arc Augmented Laser Welding", Welding Research in the 1980's, Conf. Proc., pp. 121-125.

61. M. Eboo, W. M. Steen and J. Clarke, "Arc-augmented Laser Welding", Advances in Welding Processes, Proc. of 4th Int. Conf., May 1978,

pp. 257–265.

62. F. D. Seaman, "An Evaluation of a High Power CO_2 (CW) Laser as a Welding Source", Advanced Welding Technology, Japan Welding Society, Tokyo, 1975, pp. 119–124.

63. Y. Arata, T. Oda and R. Nishio, "Effect of Assist Gas on Bead Formation in High Power Laser Welding", Trans. of JWRI, Vol. 12, No. 2, 1983, pp. 161–166.

64. V. Donati, L. Garifo, R. Menin, F. Pandarese, M. Onorato and P. Savorelli, "Analysis of High Power CO_2 Laser-Material Interaction. Results with High Speed Photography and 10.6 μ Absorption Measurements", Lasers in Materials Processing, Conf. Proc., ASM, 1983, pp. 1–5.

Table I. Chemical composition of materials.

ALUMINUM ALLOYS	Cu	Mn	Mg	Cr
3003	.05-.20	1.0-1.5	——	——
5052	----	----	2.2-2.8	.15-.35

IRON ALLOY	C	Mn	P_{max}	S_{max}
1018	.15-.20	.60-.90	.040	.050

Table II. CO_2 Laser Specifications.

LASER:

Wavelength	10.6 Micrometers (infrared)
Power Output	Nominal 1000 watts TEM_{00} (95% Gaussian) Operating Range: 1500 watts multimode, 1200 watts TEM_{00}
Beam Diameter	Approximately 13 millimeters at the TEM_{00} $1/e^2$ intensity limits.
Beam Divergence	1.4 milliradians
Beam Jitter	Less than ± 0.2 milliradian
Power Output Stability	Less than $\pm 5\%$ variation

GENERAL:

Power Requirements	460 volts ac (nominal) 3-phase, 60 Hz, 40 kW (50 Hz or 230 volts ac optional)
Gas Requirements	Separate Helium, Nitrogen, and Carbon Dioxide regulated to 15 PSIG or premixed bottles of these gases in the proper proportions
Water Cooling	8 Gallons per minute, 40 PSIG
Laser Head Size	4 feet high by 5 feet wide by 5 feet long
Laser Head Weight	2850 pounds
Power Supply Size	6 1/2 feet high by 5 feet wide by 2 feet deep
Power Supply Weight	2300 pounds
Vacuum Pump	Frame-mounted on anti-vibration pads with independent on-off switch
Auxiliary Vacuum Port	2-inch standard flange with blocking port for coupling to an external pump
Gas Consumption	CO_2 - 0.08 SCFH He - 1.8 SCFH N_2 - 0.4 SCFH

Table III. Laser operating parameters.

LASER: Continuous Wave CO_2 Gas Transport Type
(10.6 Micron Wavelength)

POWER: 1500 Watts (Multimode)
1200 Watts (TEM_{00} mode)

FOCUSSING OPTICS: ZnSe Lens 6.02 cm (2.37 in) F.L.
ZnSe Lens 13.01 cm (5.12 in) F.L.

UNFOCUSSED BEAM DIAMETER: 1.30 cm (0.5120 in)

FOCUSSED SPOT SIZE: 0.0063 cm (0.0025 in)
0.0135 cm (0.0053 in)

OPERATING POWER: 920 Watts

POWER DENSITY: 3.0×10^7 Watts/cm^2 (1.9×10^8 Watts/in^2)
6.4×10^6 Watts/cm^2 (4.2×10^7 Watts/in^2)

SCAN RATE: 0.42-10.16 cm/sec (10.0-240.0 in/min)

SHIELDING GAS: 100% Argon

Table IV. Effect of laser on GTAW parameters during combined Process.

PROCESS	CURRENT (AMPS)	DC VOLTAGE (VOLTS)
GTAW	60.6	12.0
LBW/GTAW	61.8	10.0
GTAW	81.0	13.0
LBW/GTAW	84.0	10.0
GTAW	171.6	16.0
LBW/GTAW	171.6	16.0
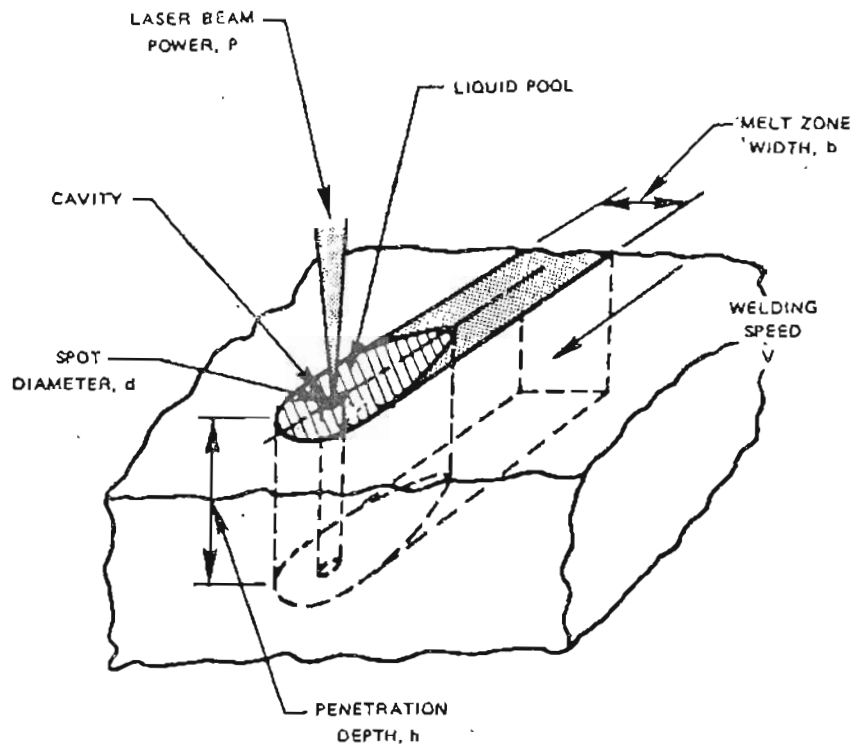
Figure 1. Schematic of Deep-Penetration Mode LBW through formation of a "Keyhole".
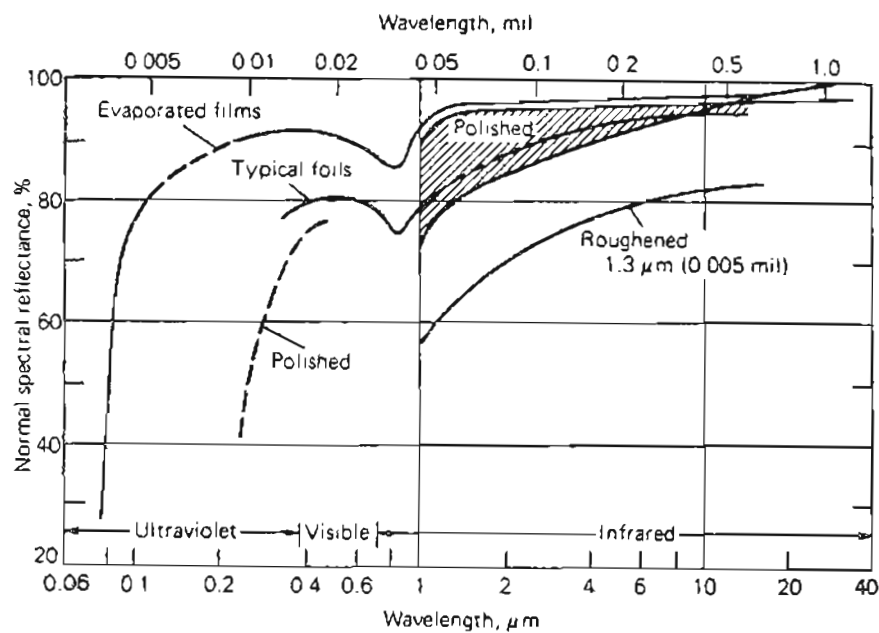
Figure 2. Reflectivity of light as a function of wavelength for various surface conditions of aluminum (after Ref. 28).
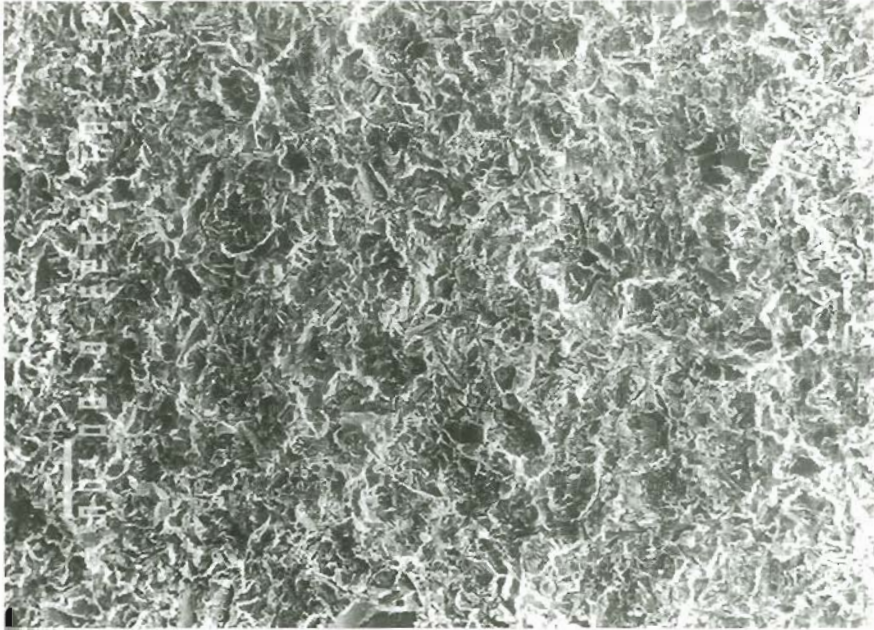
Figure 3. Scanning electron micrograph of surface condition resulting from grit blasting of aluminum (100X).
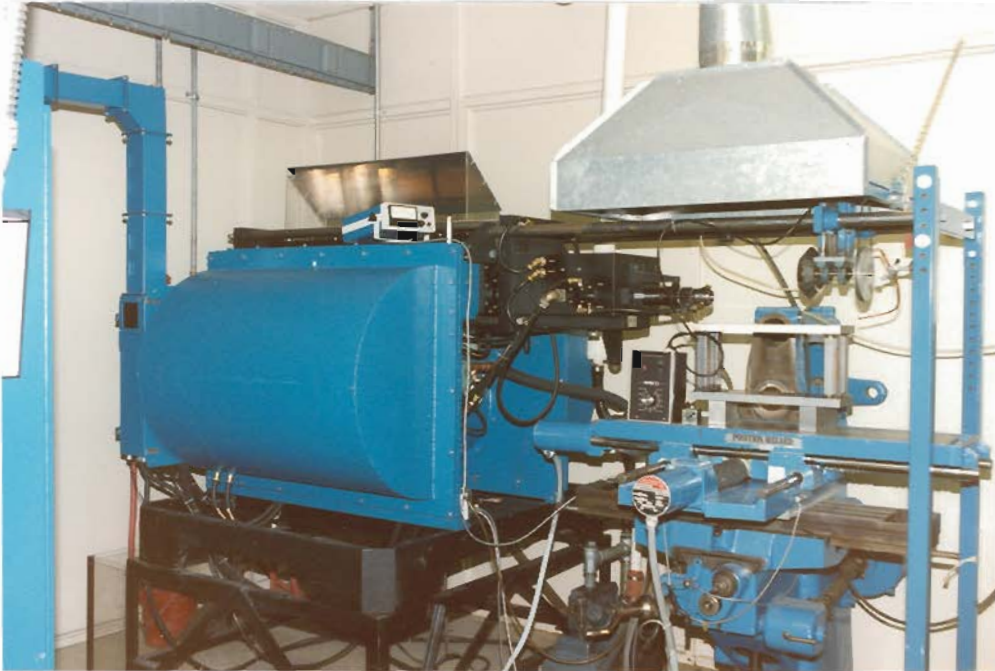
Figure 4. GTE Sylvania Model 971 CO_2 Gas Transport Laser (power supply not shown).
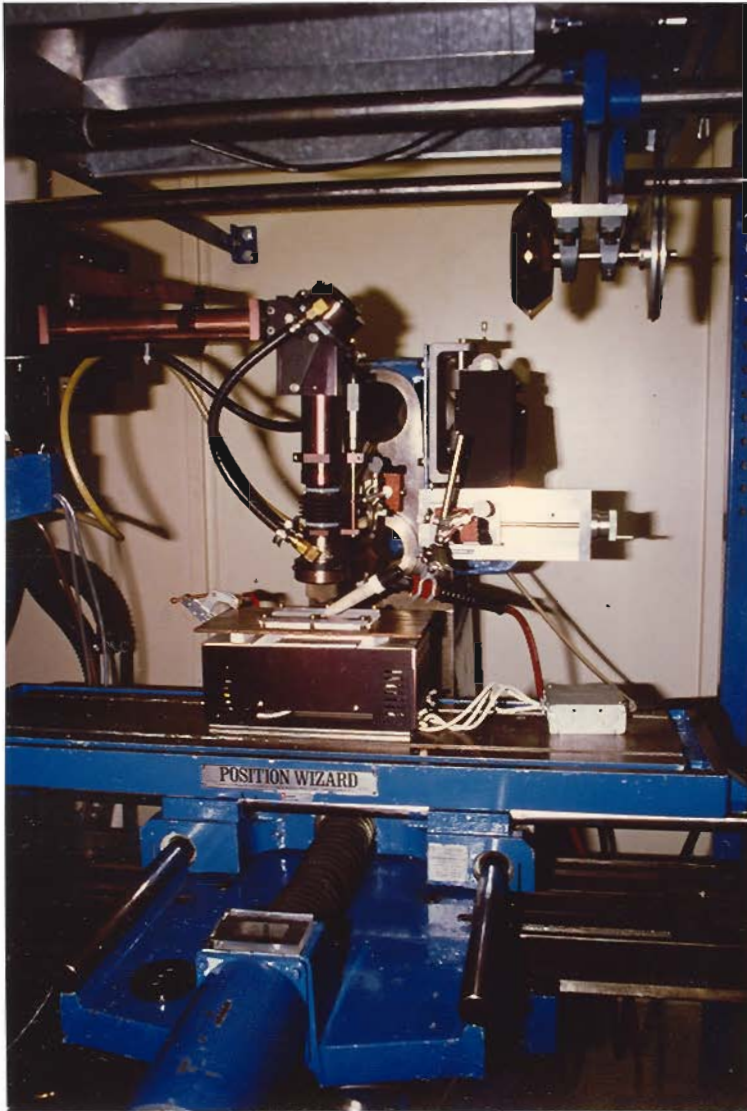
Figure 5. Welding set-up showing positioning of GTAW torch with respect to LBW system.
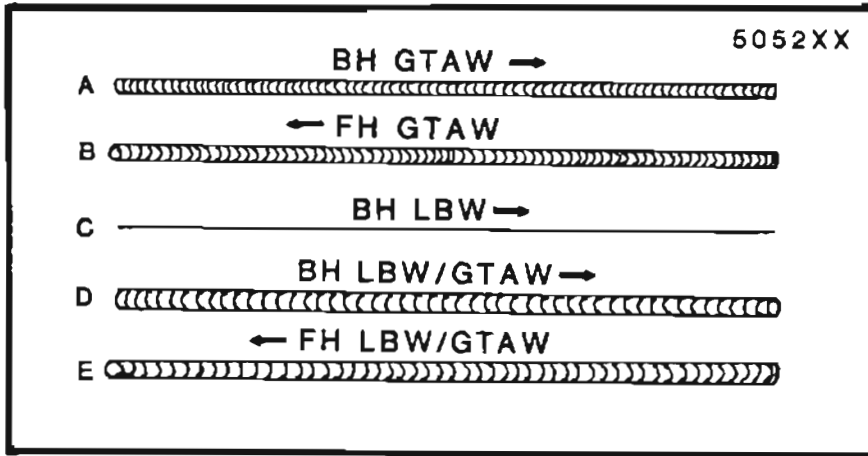
Figure 6. Schematic of welding sequence for each test specimen (upper right hand corner label refers to alloy type and specimen number).

Figure 7. Spin Physics High Speed Motion Analysis System.
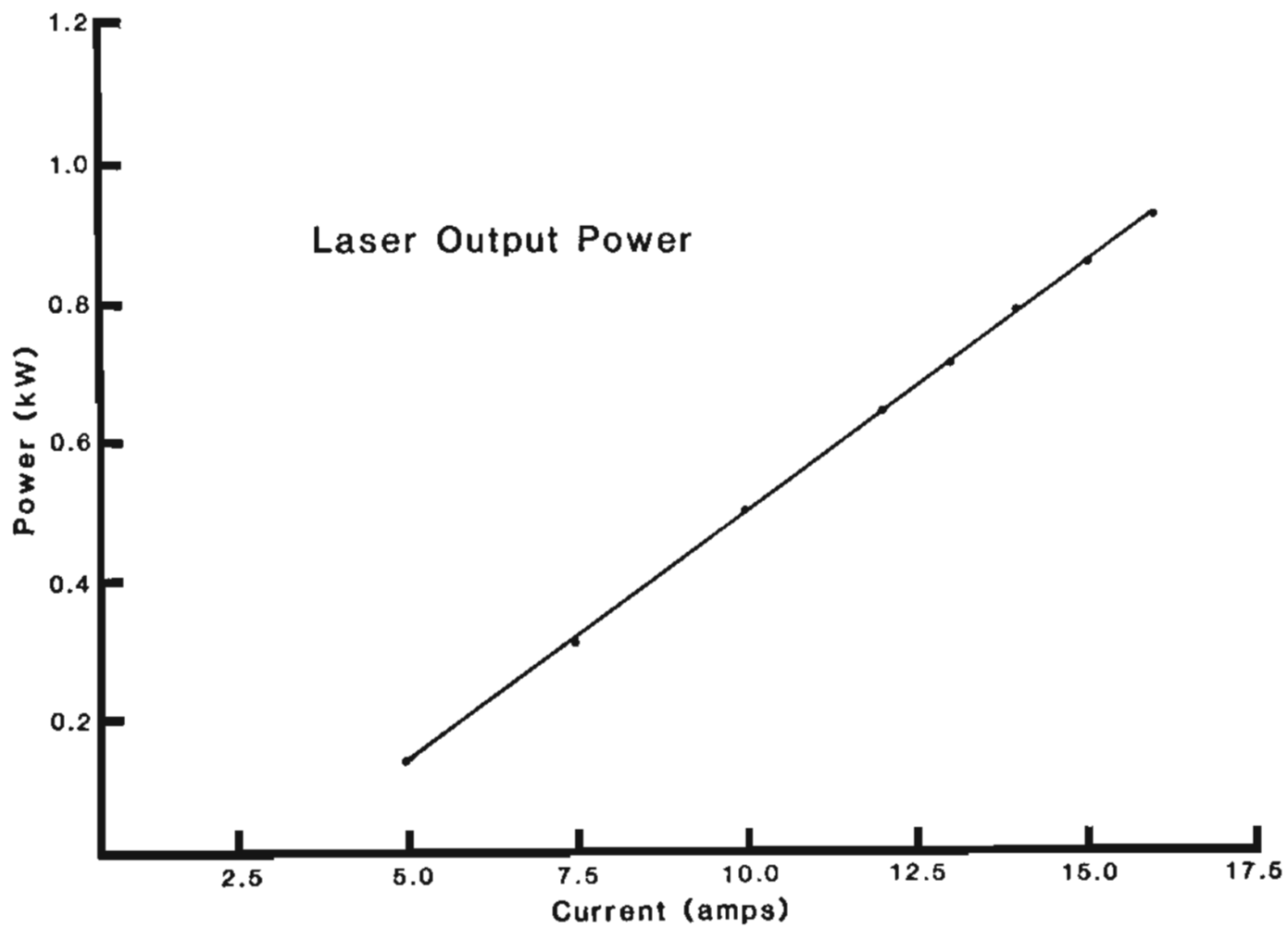
Figure 8. Linear relationship between current and power.

Figure 9. Thick plexiglass sheet outlining unfocussed laser beam characteristics (scale in cm).
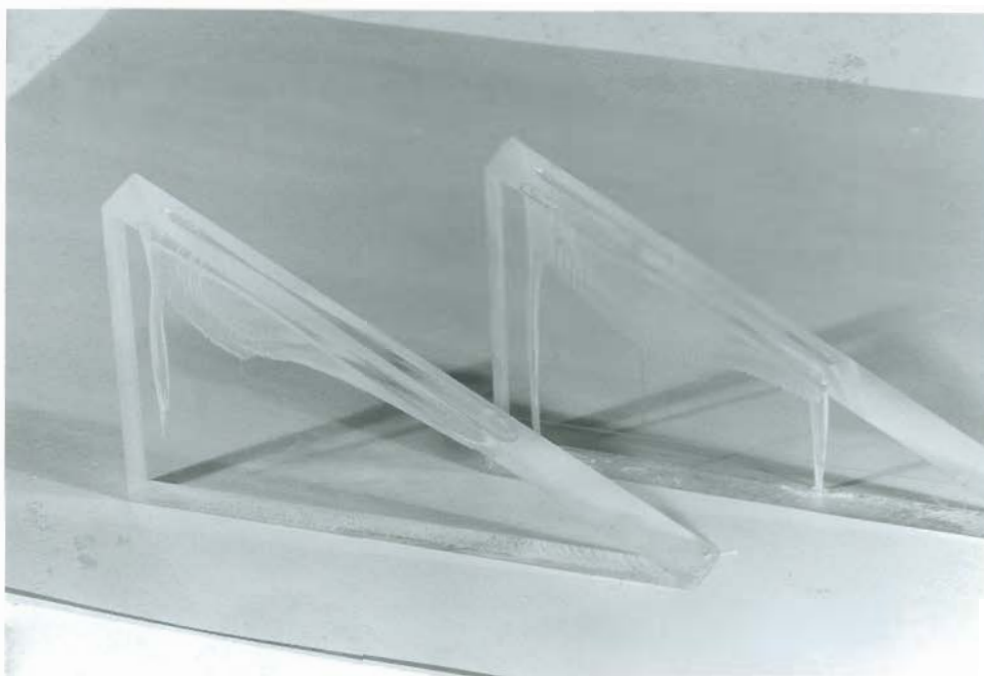
Figure 10. Wedge specimens (30° angle) used for lens focal length determinations.

SPOT SIZE DETERMINATION
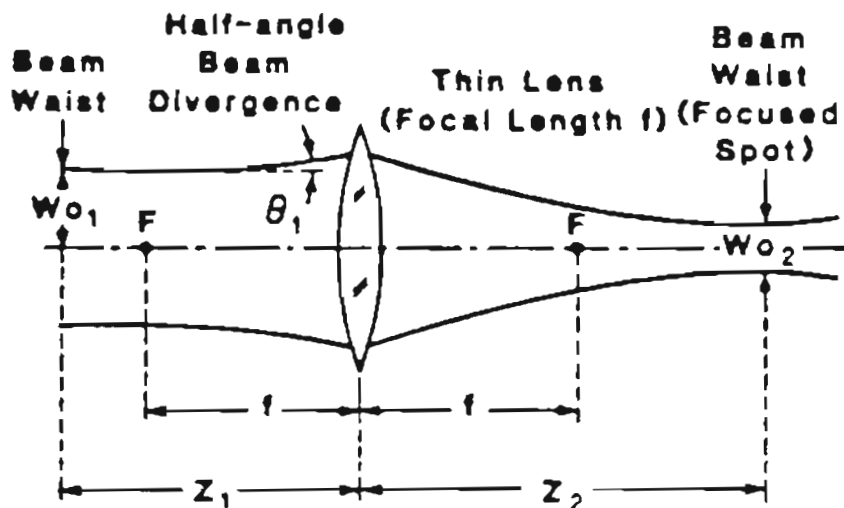
Spot Size At Focal Point (Wo_2)

$$Wo_2 = \frac{\lambda f}{\pi Wo_1}$$

Spot Size Away From Focal Point

The equation relating Wo and $W(Z)$ is:

$$W(Z) = Wo_2 \left[1 + \left(\frac{\lambda Z}{\pi Wo_2{}^2} \right)^2 \right]^{1/2}$$

Figure 11.   Relationships used to calculate focused laser beam spot size.
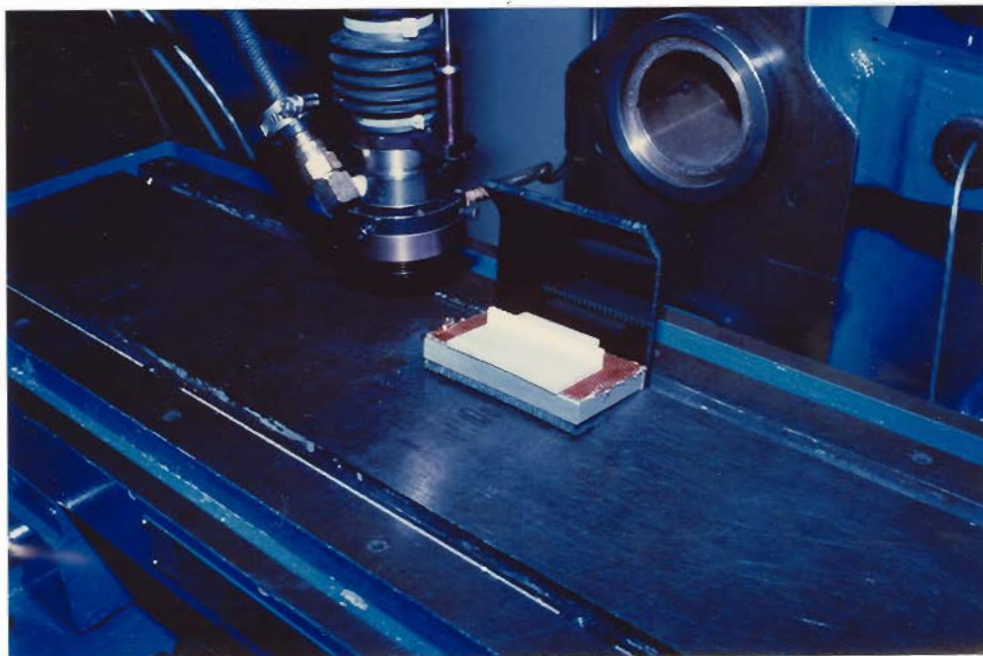
Figure 12. Tilted specimen stage used to protect lens from specular
reflection of laser beam.
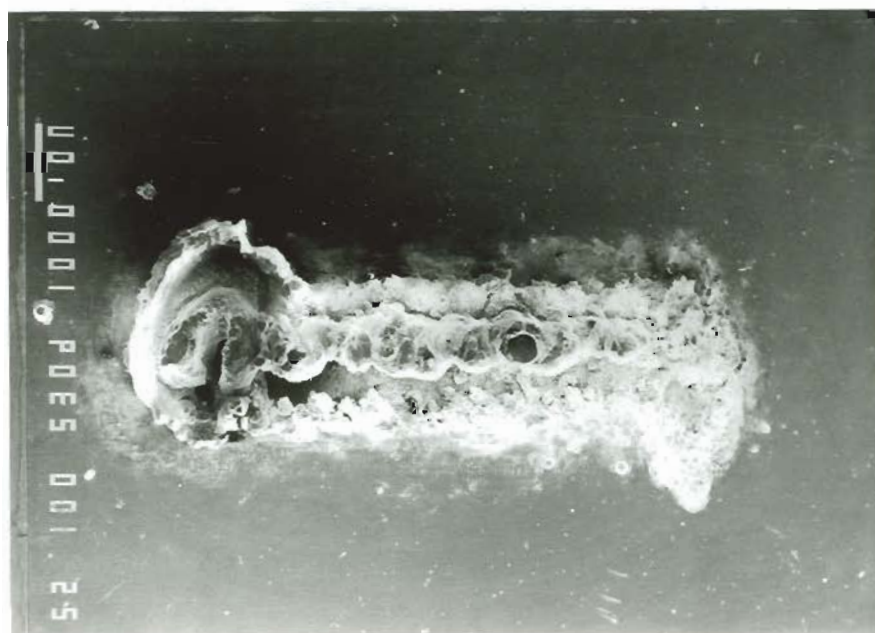
Figure 13. Laser weld made on polished aluminum surface using tilted
stage. (10X).
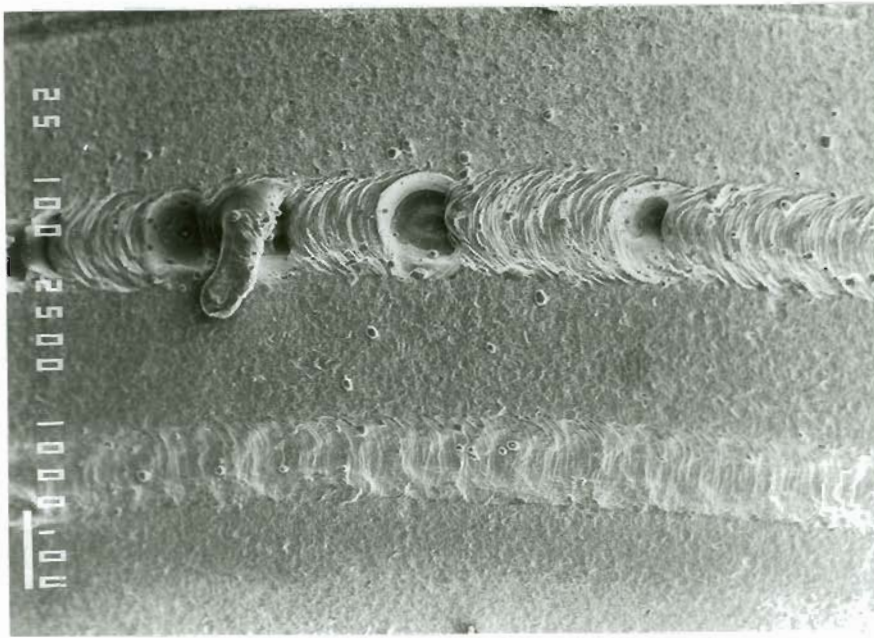
A (10X)
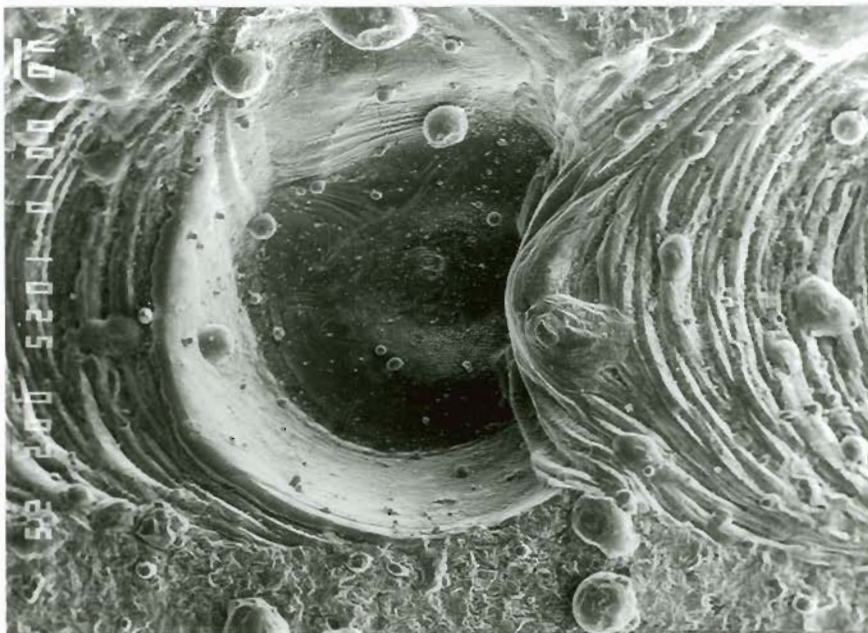
B (50X)

Figure 14. Laser welds made with specimen normal to beam axis demon-
strating both inconsistancy (A) and explosive nature of weld pool (B).
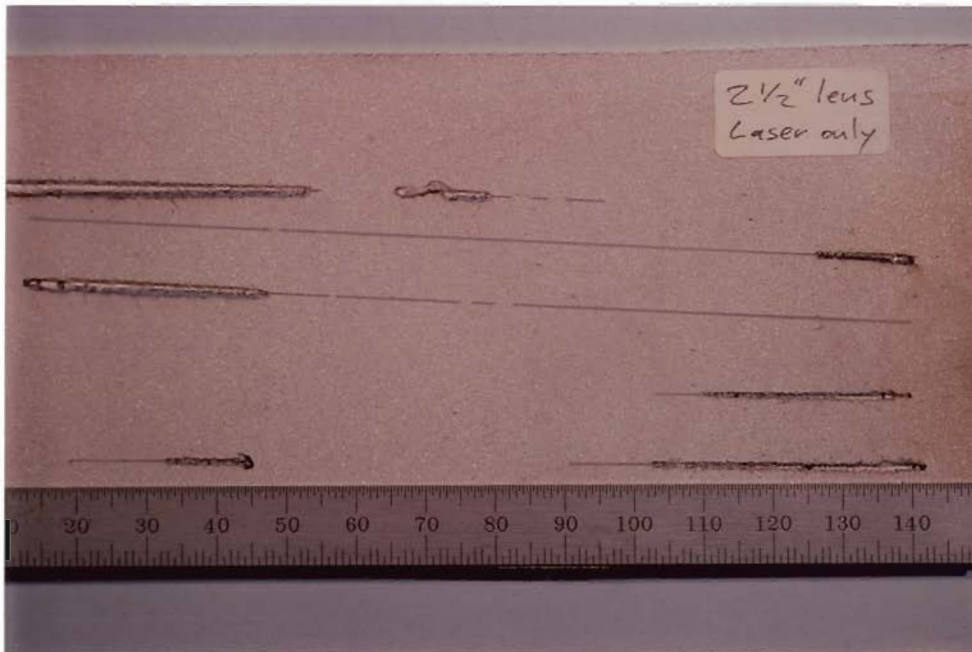
A
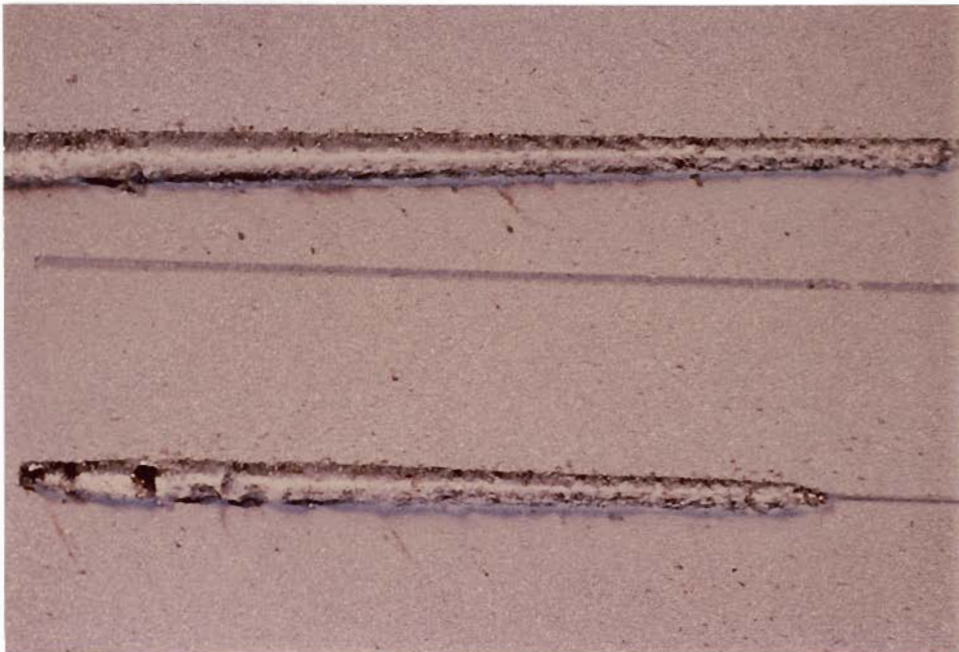
B

Figure 15. Laser welds on aluminum alloy 5052 (A) displaying an
abrupt loss of coupling and (B) same as A, magnified approx. 3.0 times.
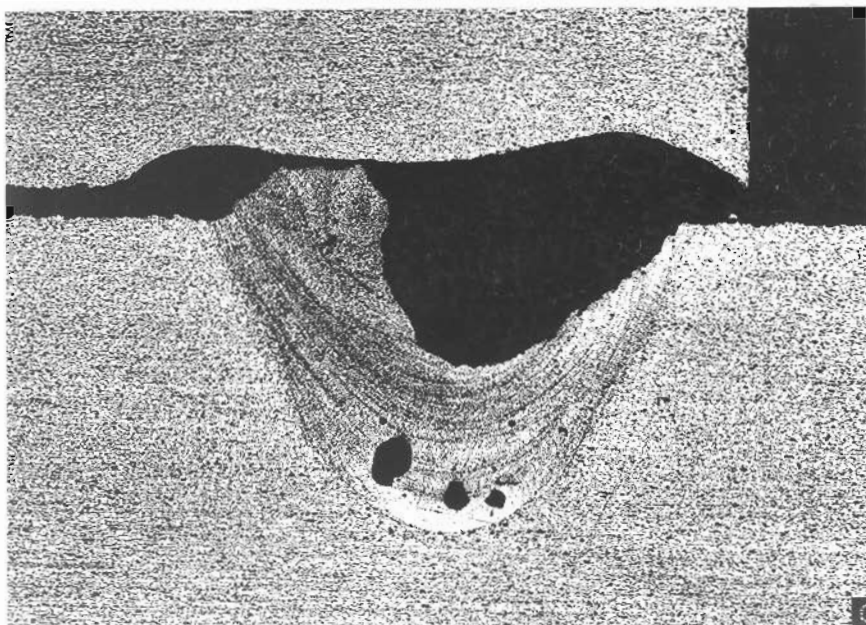
Figure 16.   Cross sectional veiw of weld shown in Fig. 15 (bottom). (30X).
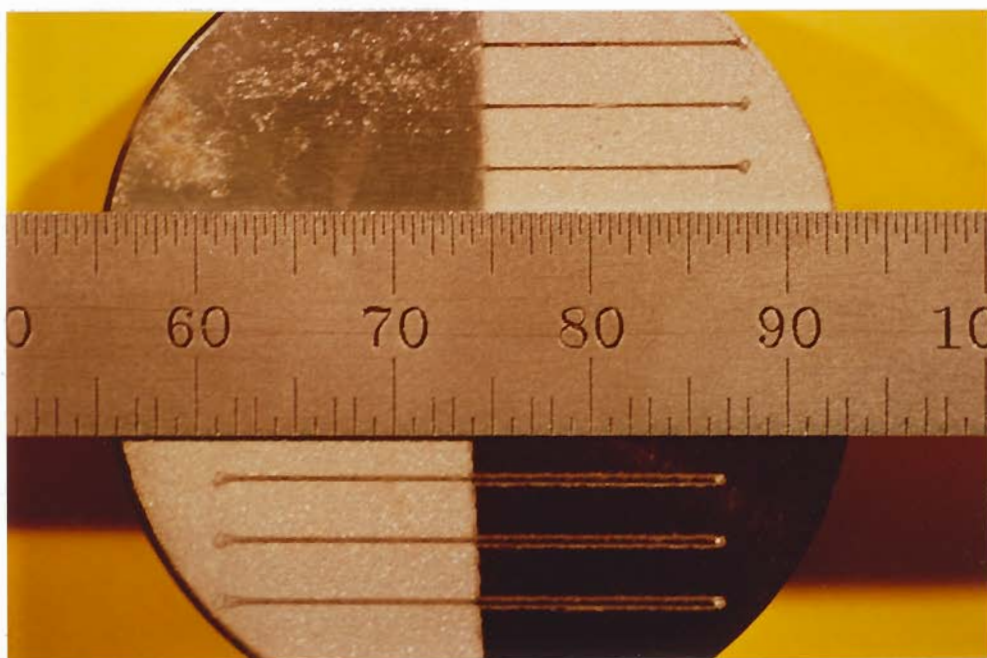
Figure 17.   Aluminum specimen comparing polished, grit blasted and anodized surfaces.
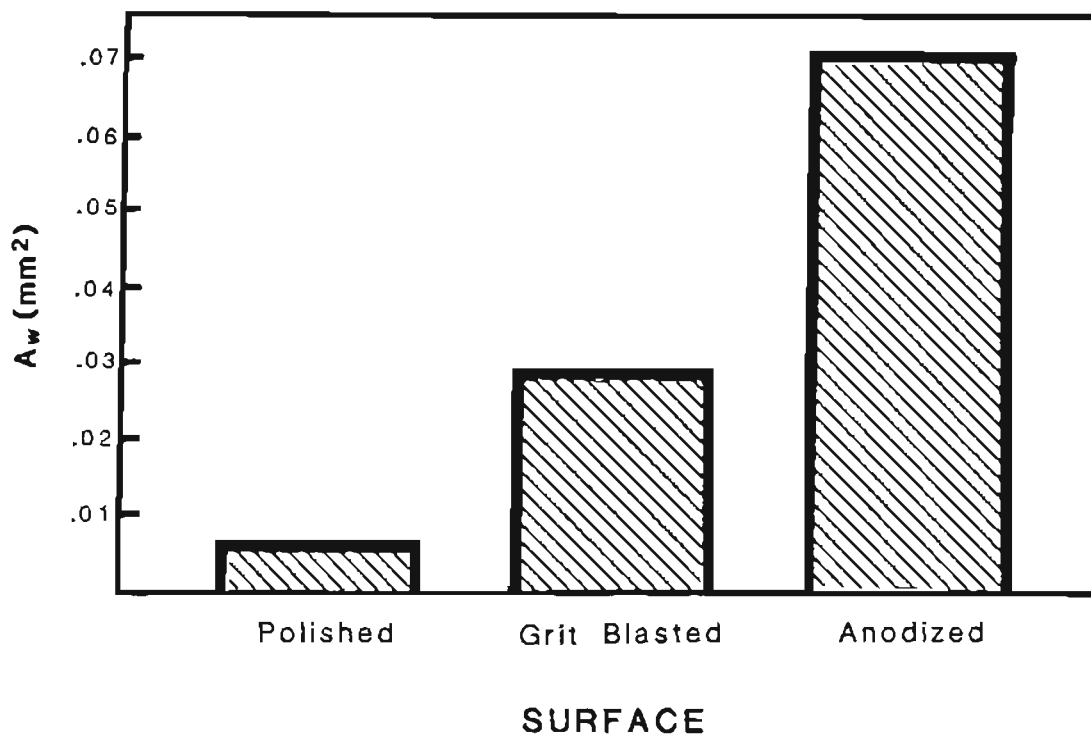
Figure 18. Relative effect of surface preparations on cross sectional area of weld metal deposited by LBW.

Figure 19. Laser "cutting" resulting on 0.8 mm aluminum sheet with 13.01 cm focal length lens.
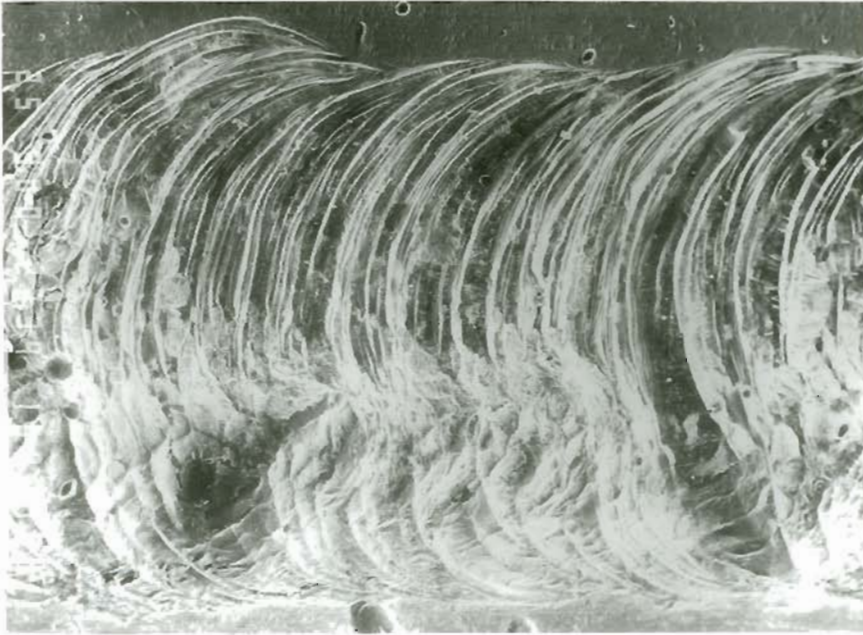
Figure 20. Weld bead surface appearance of weld made on thin aluminum with aluminum backing plate. (30X).
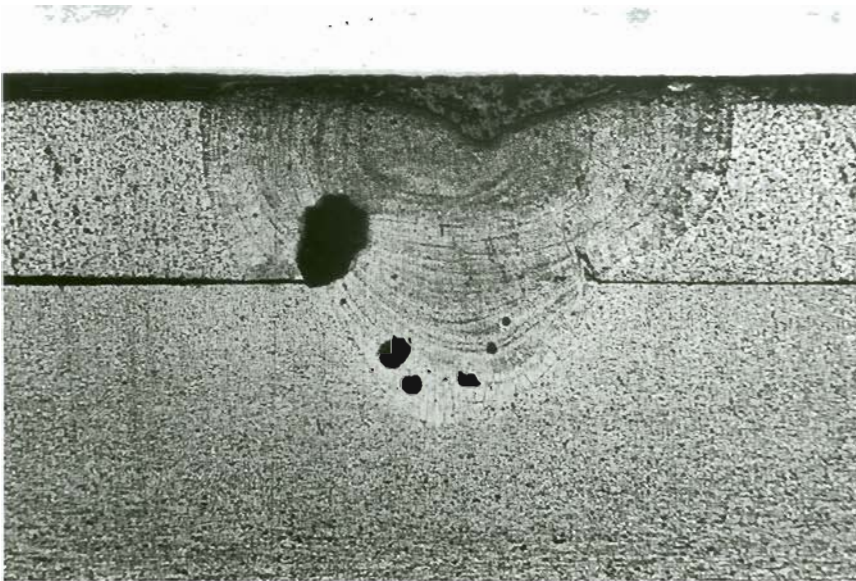
Figure 21. Cross sectional veiw of weld shown in Fig. 20 (note porosity). (30X).
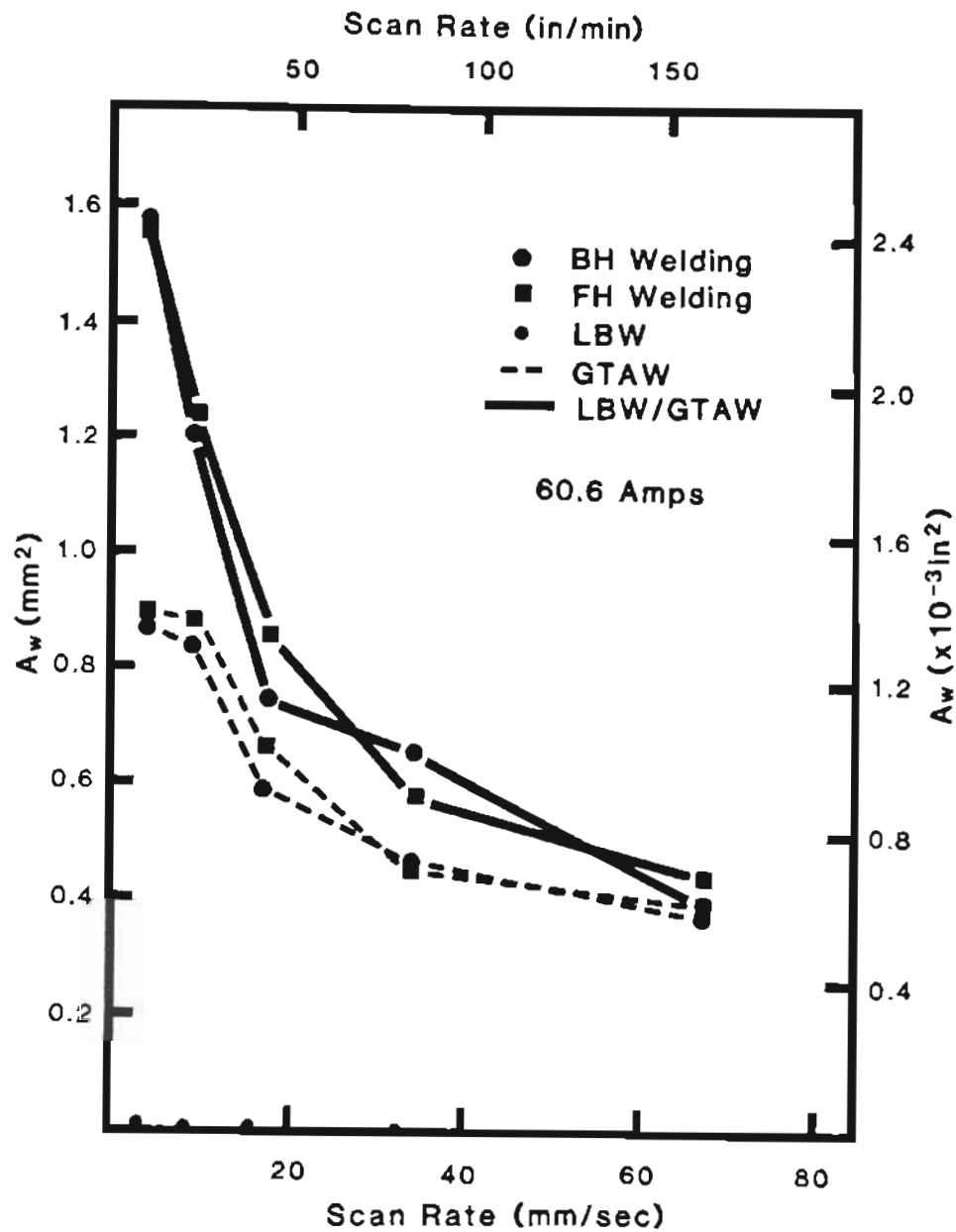
Figure 22. Weld metal cross sectional area in relation to scan rate for 60.6 amp setting.
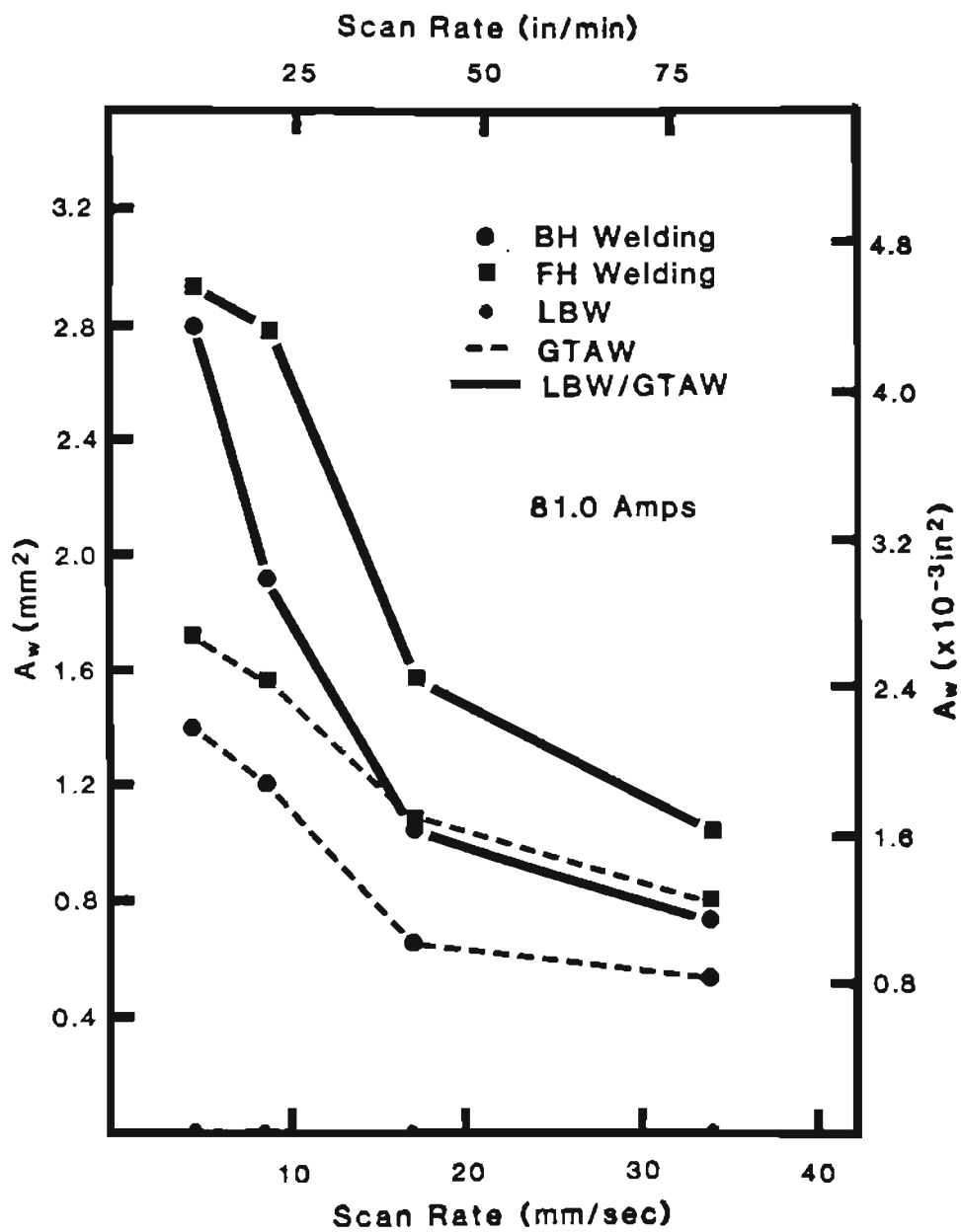
Figure 23. Weld metal cross sectional area versus welding velocity for 81.0 amp setting.
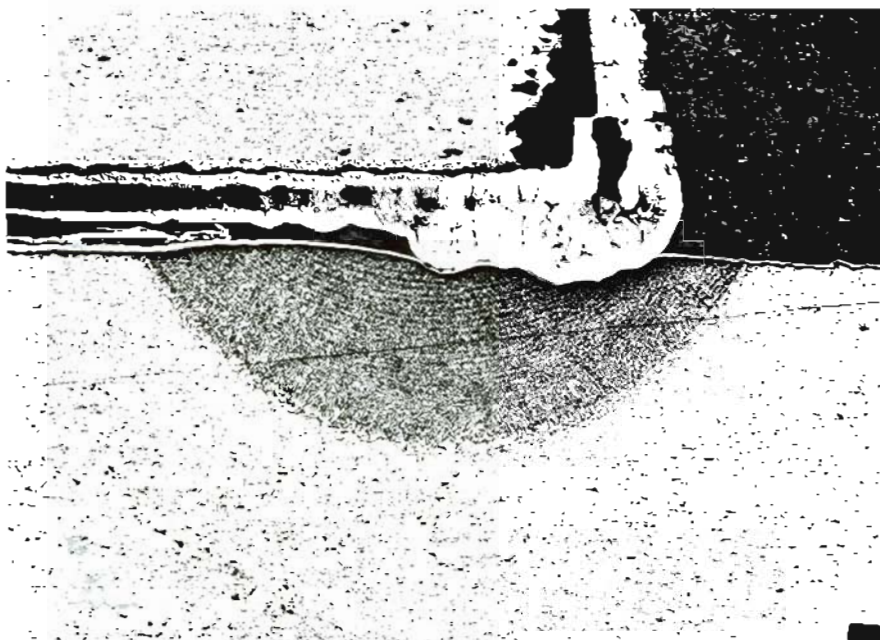
A BH GTAW, 4.2 mm/sec scan rate.

B BH LBW/GTAW, 4.2 mm/sec scan rate.

Figure 24. Comparison of GTAW and LBW/GTAW (GTAW current of 81.0 amps) for backhand (A.&B.) and forehand (C.&D.) welding at a 4.2 mm/sec scan rate. (30X).
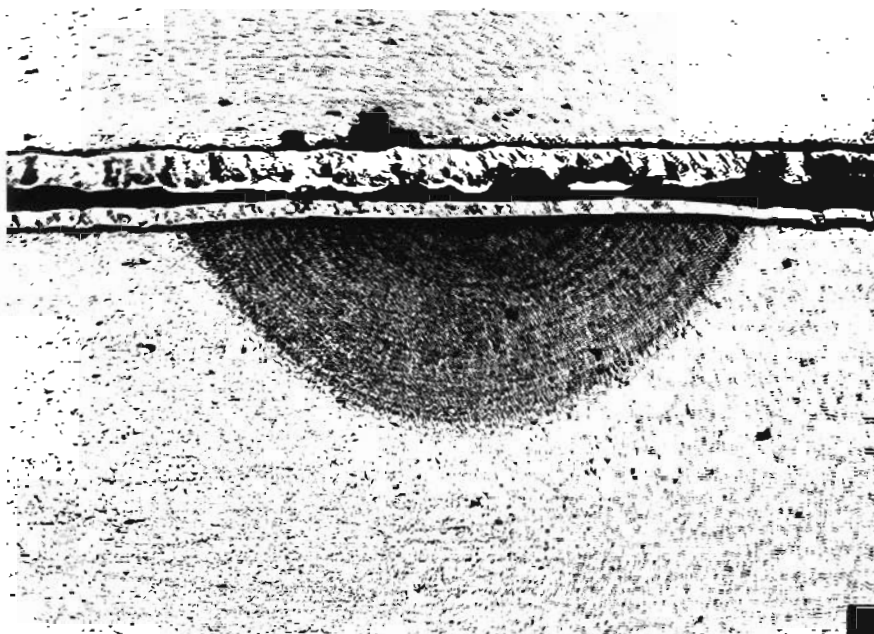
C   FH GTAW, 4.2 mm/sec scan rate.
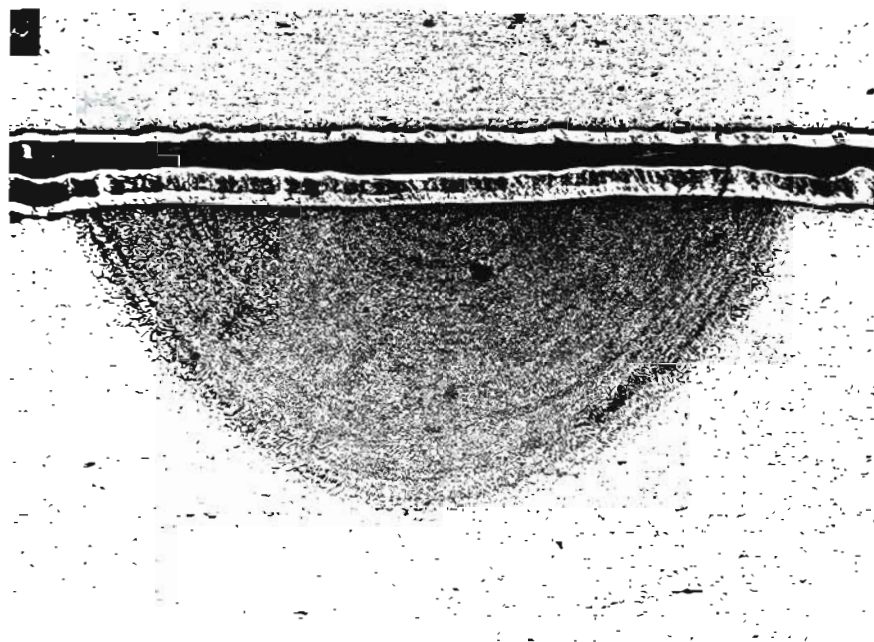
D   FH LBW/GTAW , 4.2 mm/sec scan rate.

Figure 24. (Cont.)
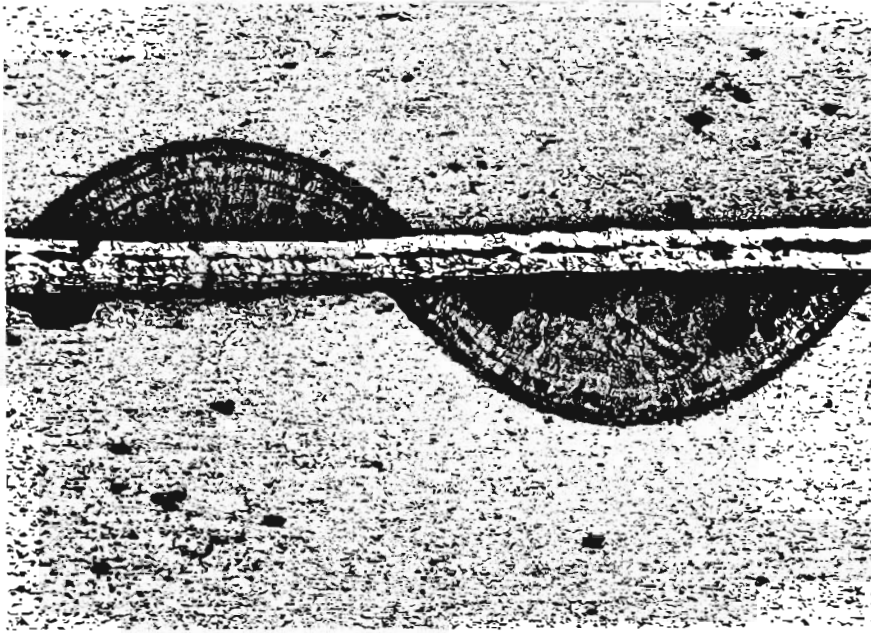
A   Top weld — BH GTAW, Bottom weld — FH LBW/GTAW, 34.0 mm/sec scan rate (Compare appropriately with (B) below).
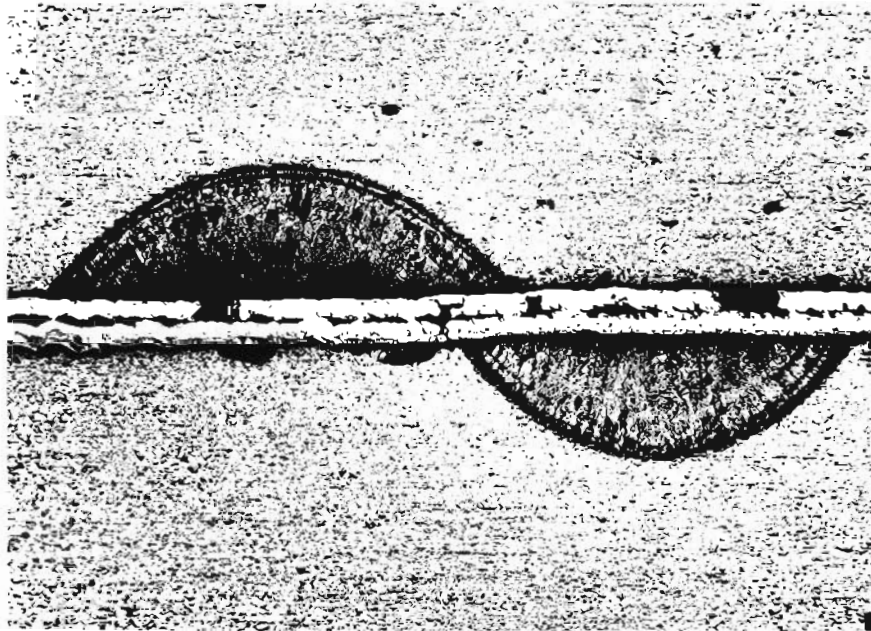
B   Top weld — BH LBW/GTAW, Bottom weld — FH GTAW, 34.0 mm/sec scan rate.

Figure 25.   Comparison of GTAW and LBW/GTAW (GTAW current of 81.0 amps) for backhand and forehand welds. (30X).
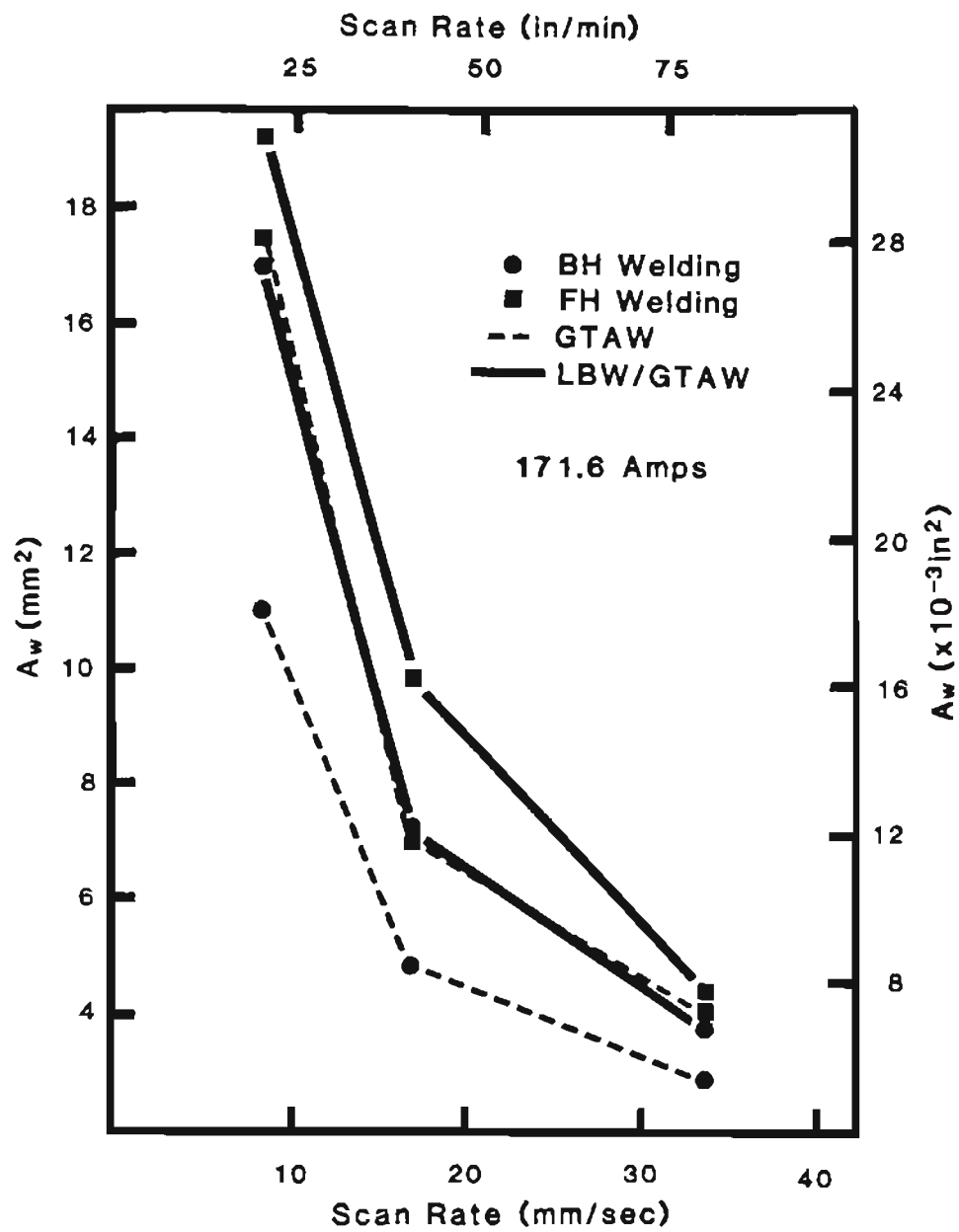
Figure 26. Weld metal cross sectional area versus welding velocity for highest current setting investigated.

Figure 27. Surface appearance of laser weld which began on titanium (left) and ran onto aluminum. (10X).
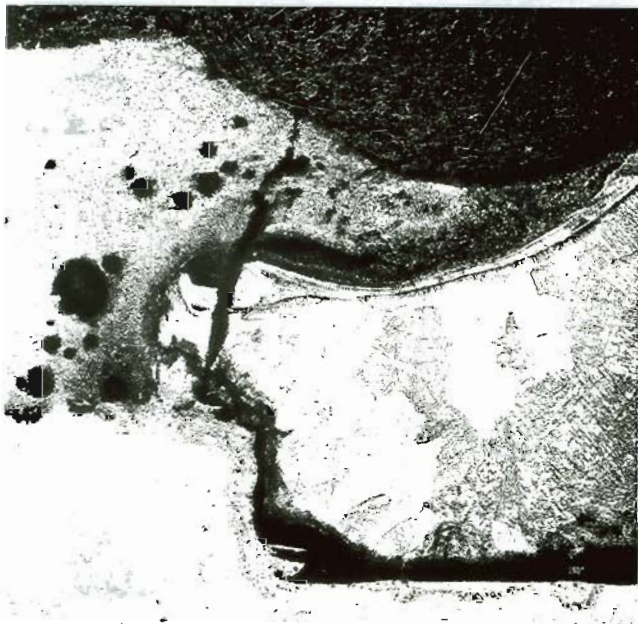
A   Ti-Al junction.

Figure 28. Micrographs of titanium–aluminum weld centerline at (A) interface, (B) titanium side, (C) aluminum side and (D) steady state on aluminum side. (30X).
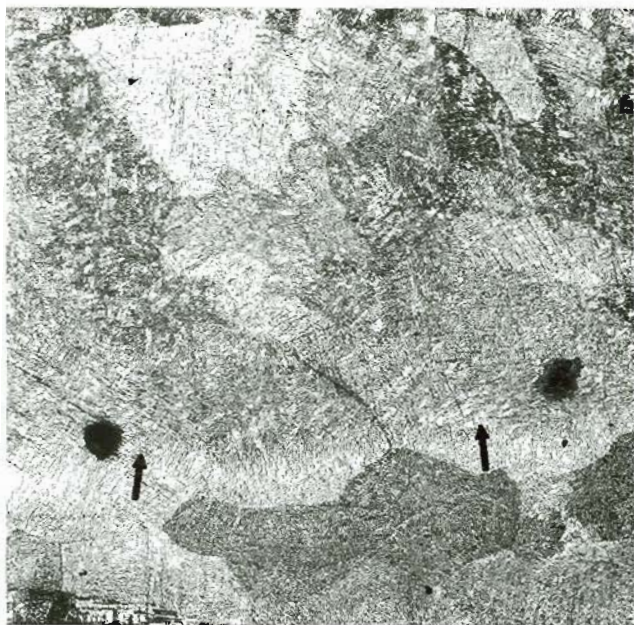
B Ti side (note weld depth at arrows).
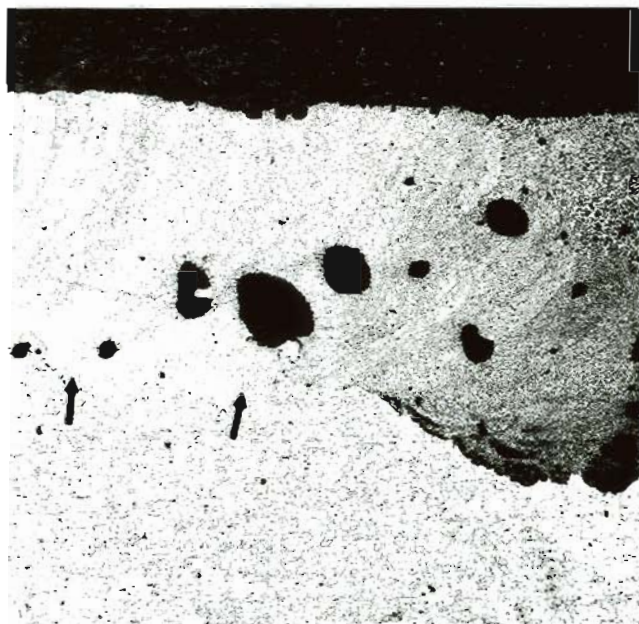
C Al side (note weld depth at arrows and large amount of porosity).

Figure 28. (Cont.)
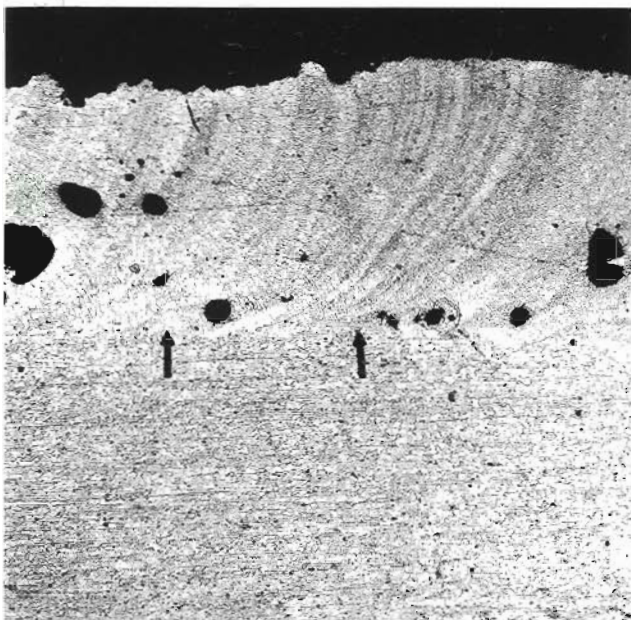
D Steady state in Al (note weld depth at arrows and porosity).

Figure 28. (Cont.)
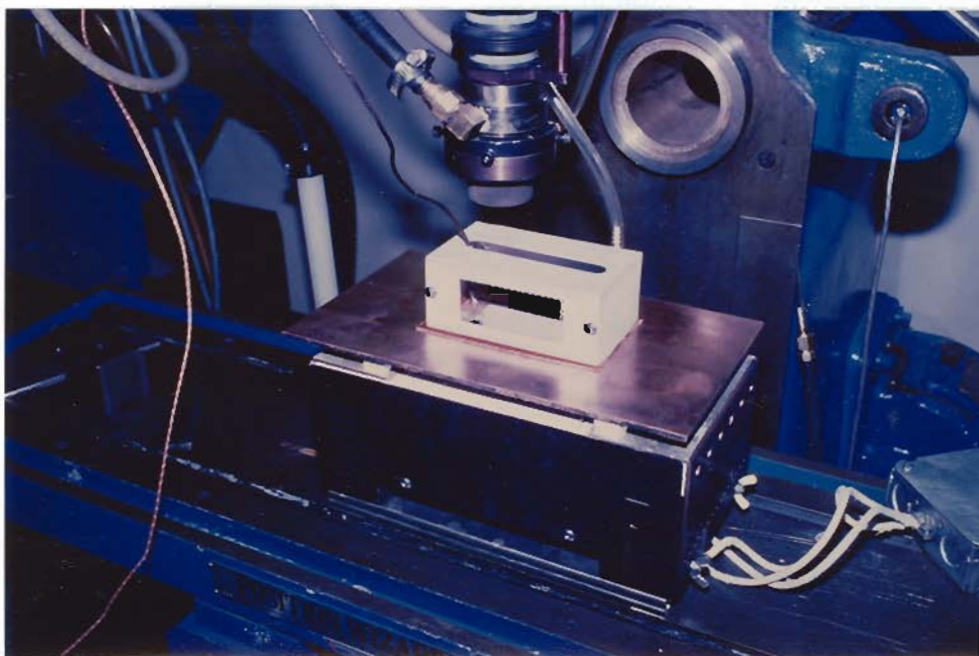
Figure 29. Experimental set-up for weld preheating with enclosed shroud for protection from atmosphere.
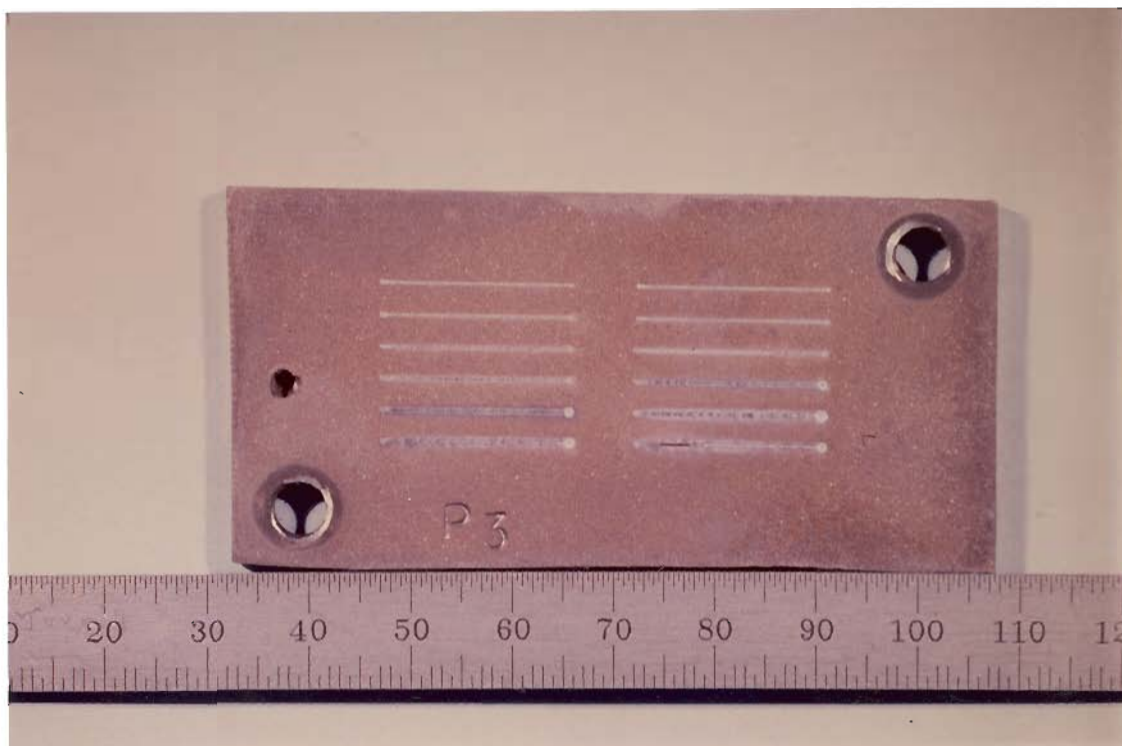
Figure 30. Welds deposited by LBW on preheated aluminum alloy using preheating temperatures of (left, top to bottom) $38^{\circ}C$, $149^{\circ}C$, $260^{\circ}C$, $371^{\circ}C$, $482^{\circ}C$, $577^{\circ}C$, (right, top to bottom) $93^{\circ}C$, $204^{\circ}C$, $316^{\circ}C$, $427^{\circ}C$, $538^{\circ}C$, $577^{\circ}C$.
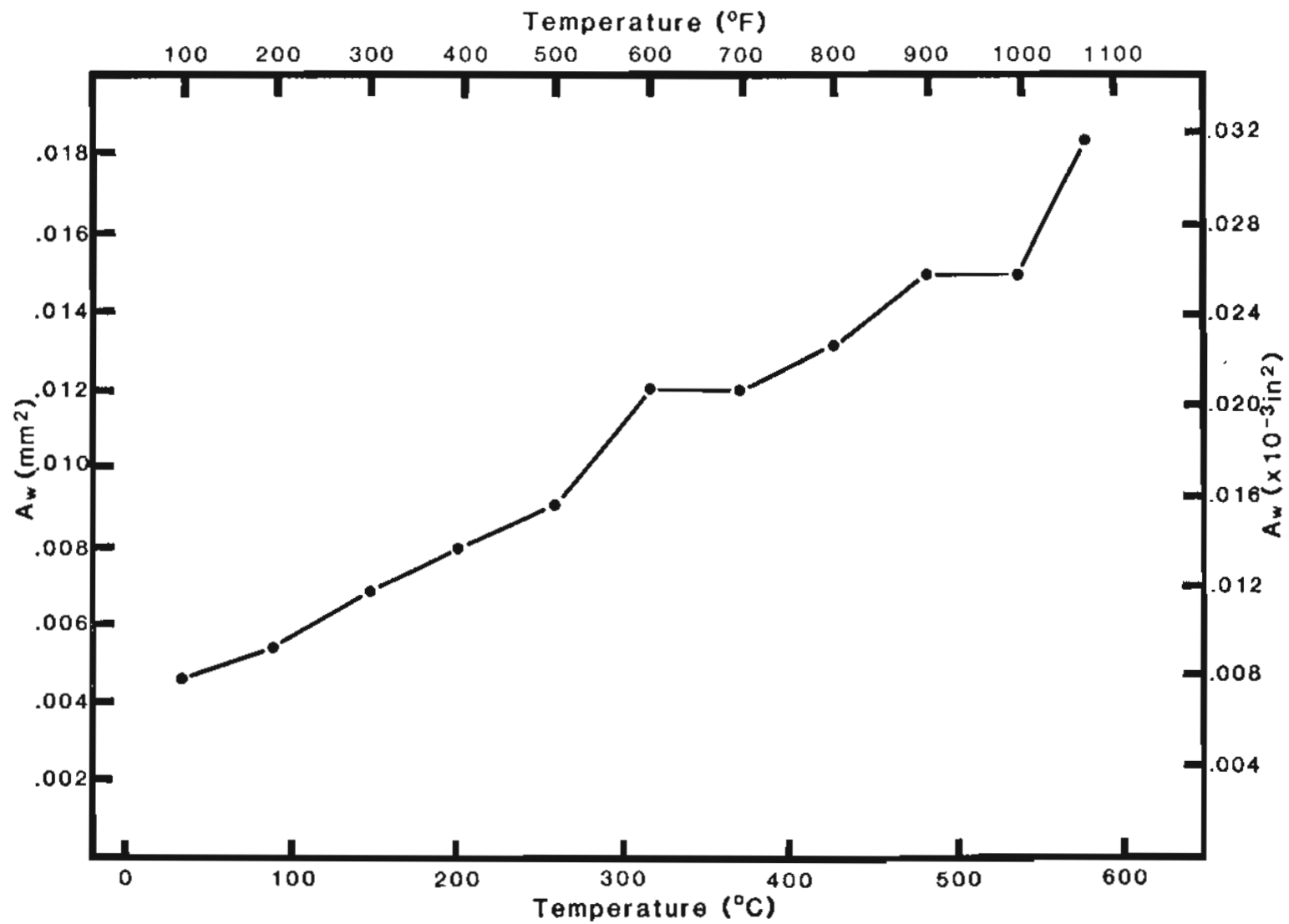
Figure 31.   Effect of preheating on LBW performance for 5052 Al alloy.
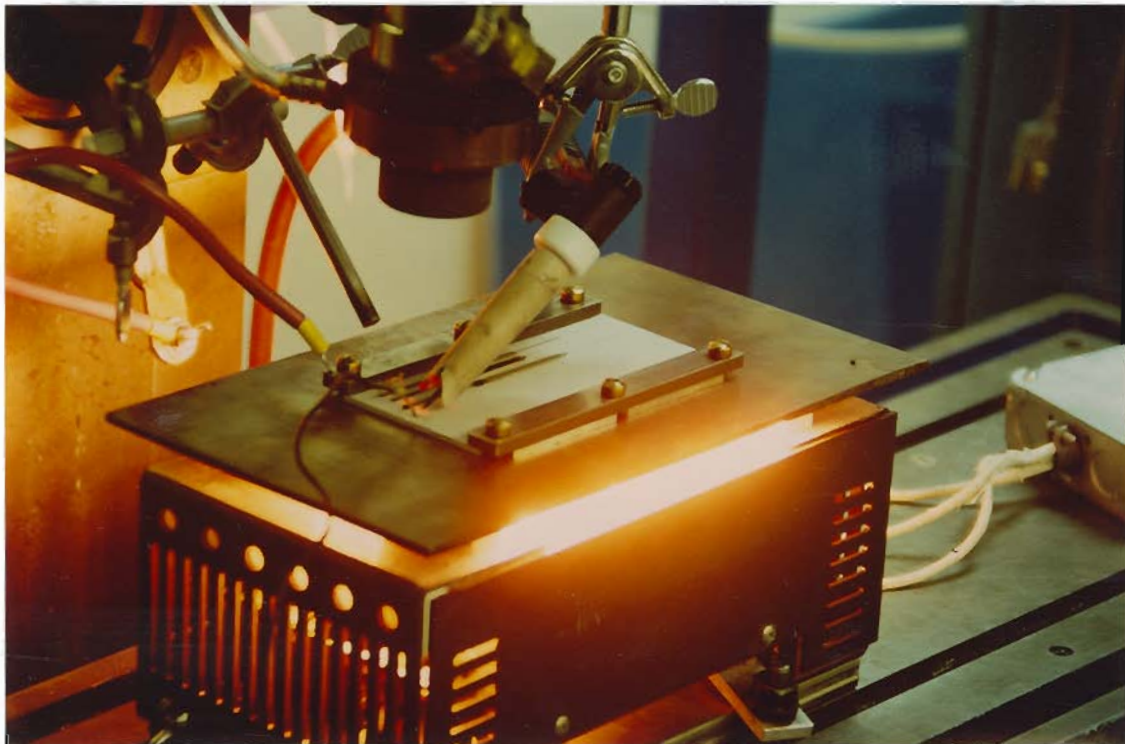
Figure 32.   Preheating set-up without enclosed shroud showing both laser and GTAW torches.
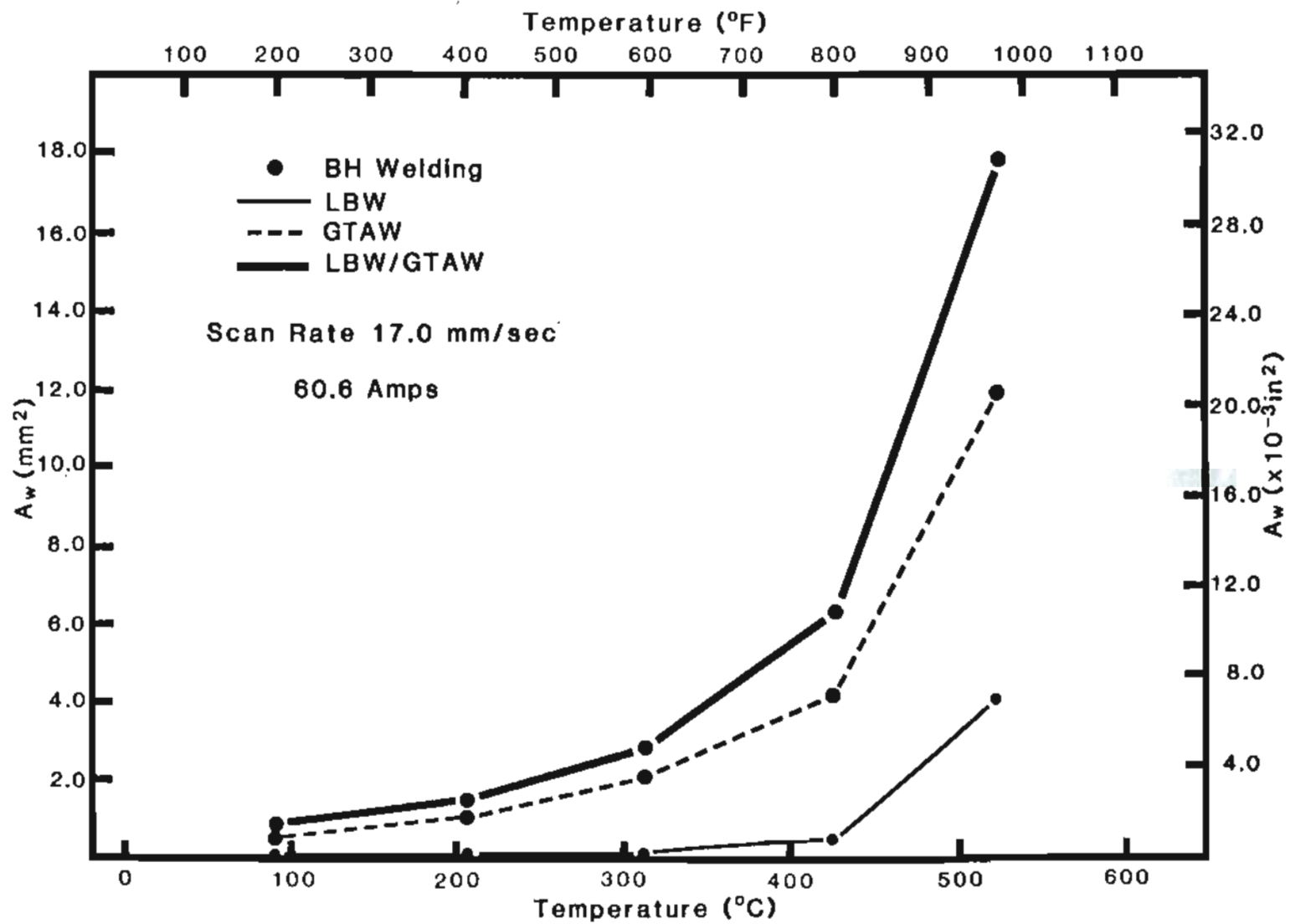
Figure 33. Effect of preheating on welding performance for 5052 Al alloy.
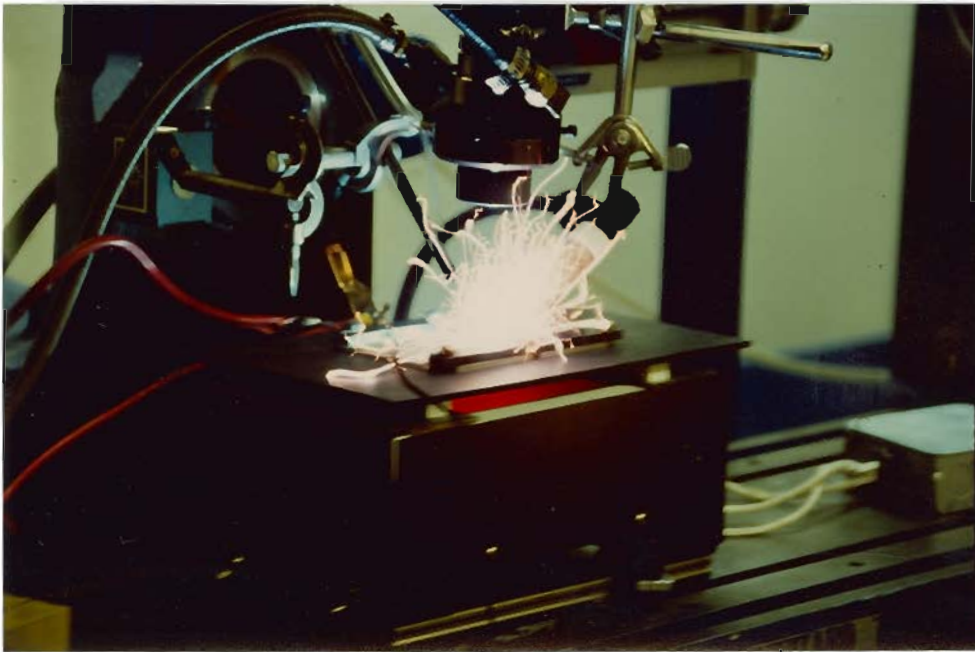
Figure 34. Laser weld in-process preheated to 524°C, with volitilization of magnesium a likely cause of sparking.
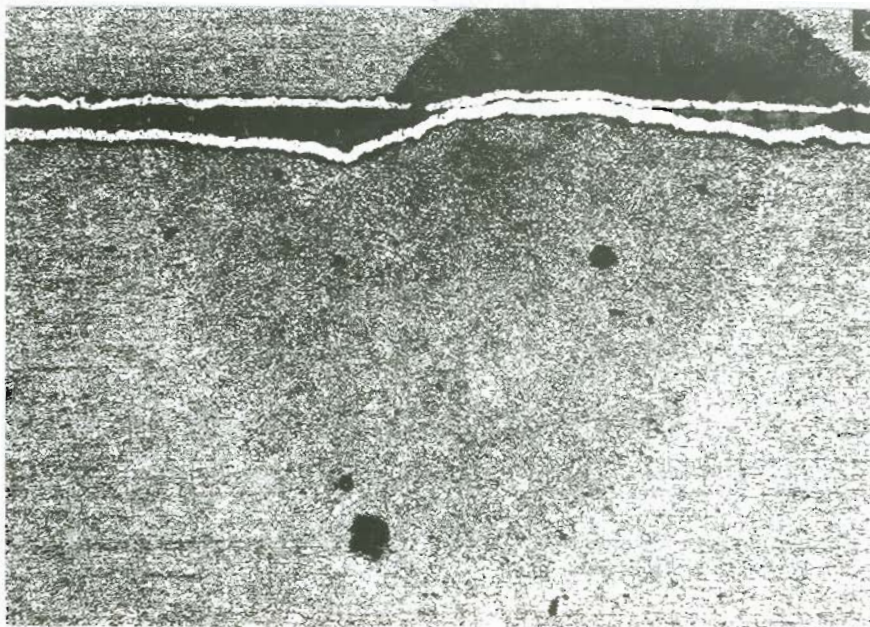
Figure 35. Cross sectional veiw of laser weld made with 524°C preheat showing high aspect ratio. (30X).
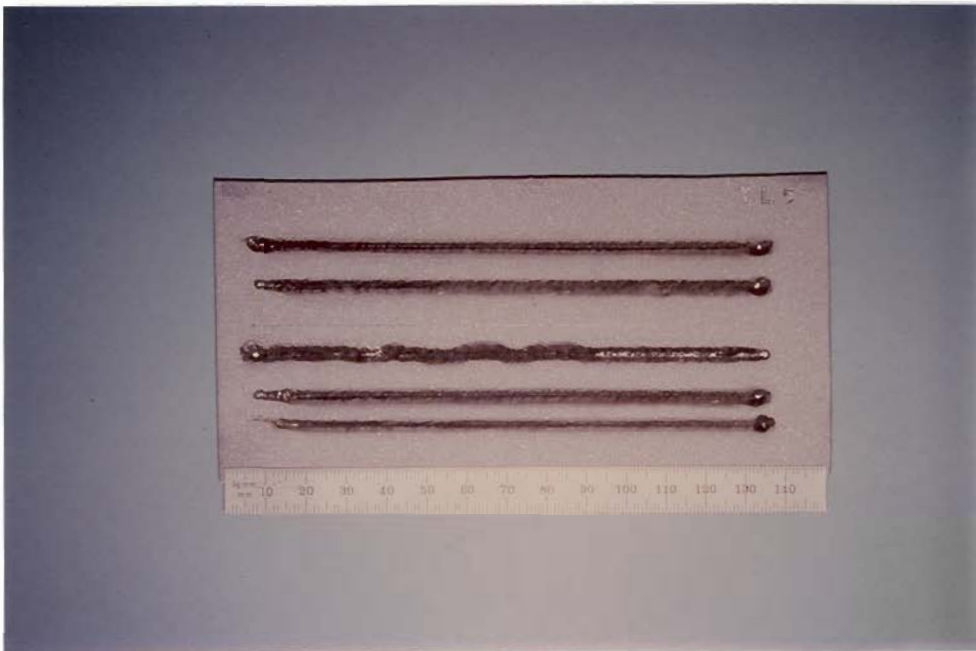
A

B

Figure 36. Difference in soot generation between welds made on (A) 3003 aluminum and (B) 5052 aluminum alloys (LBW welds at arrows, all others LBW/GTAW).
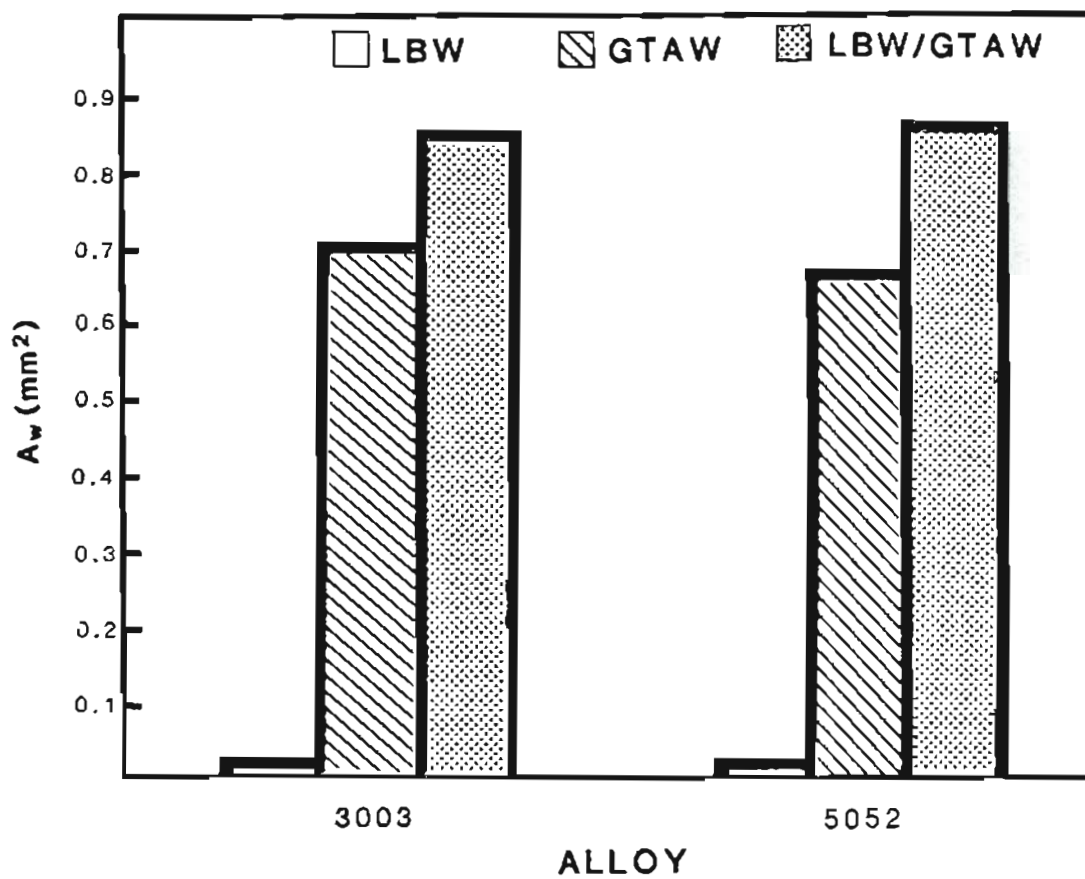
Figure 37. Effect of aluminum alloy type on welding performance.

Figure 38. Mild steel weld bead surfaces of LBW (top), LBW/GTAW (large weld portions in middle two), GTAW (small weld portions in middle two) and higher speed LBW (bottom). (4X).
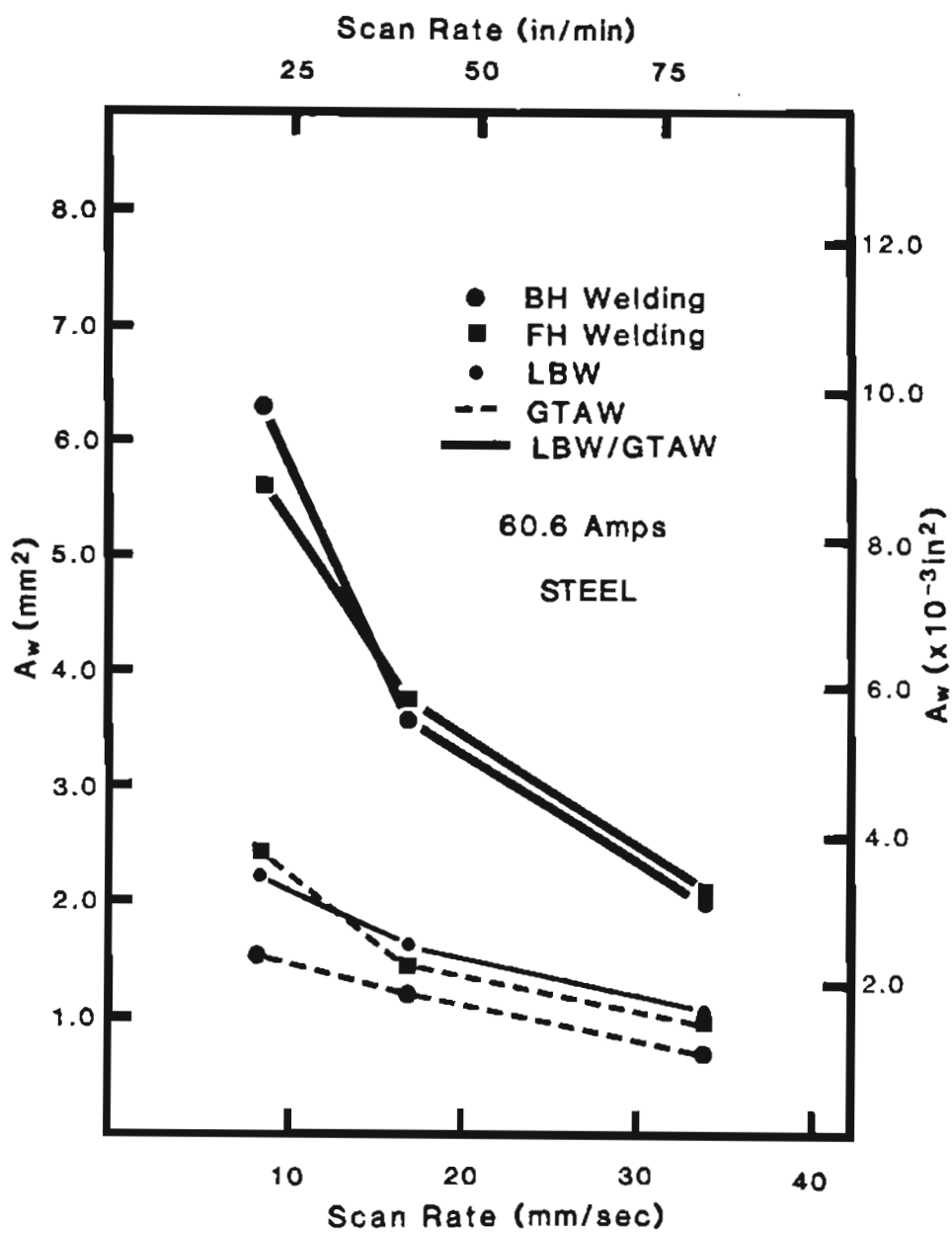
Figure 39. Weld metal cross sectional area in relation to welding velocity for mild steel sample.
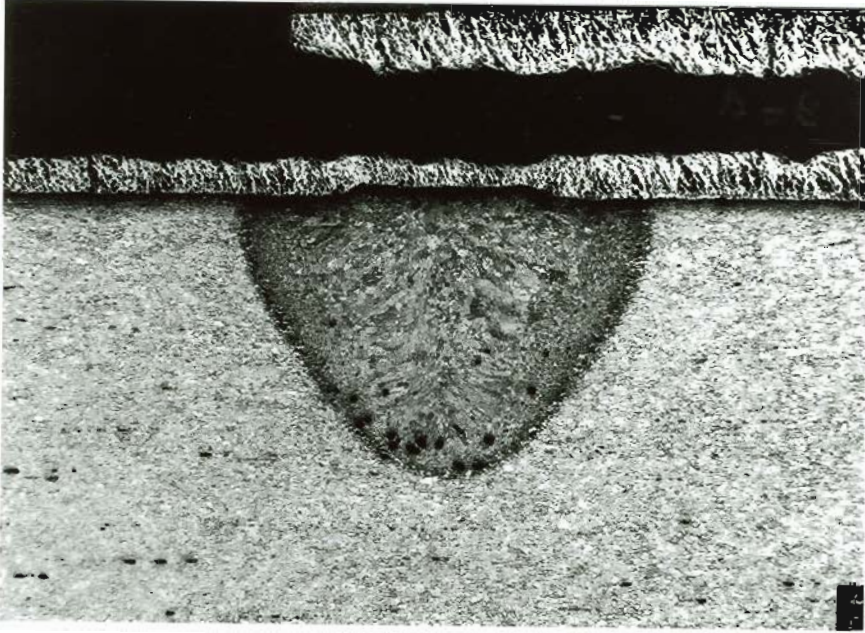
A   Laser beam weld on mild steel at 17 mm/sec. scan rate.
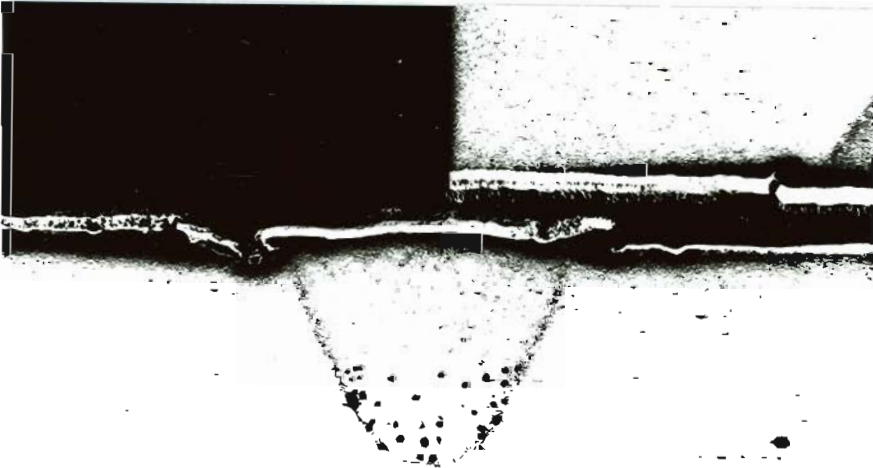
B   Laser beam weld on mild steel at 34 mm/sec. scan rate.

Figure 40. Cross sectional area comparisons of LBW, GTAW and LBW/GTAW welds for BH and FH welding on mild steel at two scan rates. (30X).
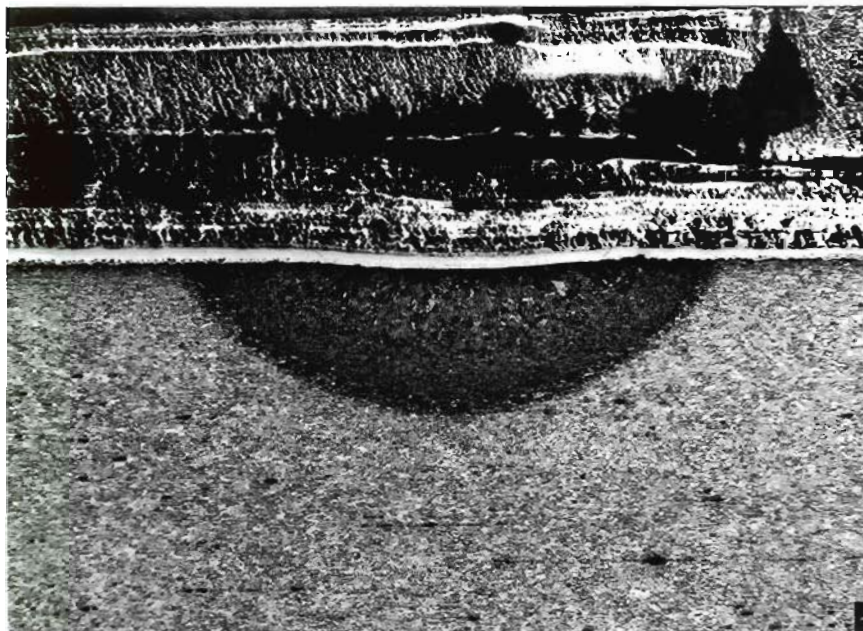
C   BH GTAW weld at 17 mm/sec.

D   BH LBW/GTAW weld at 17 mm/sec.
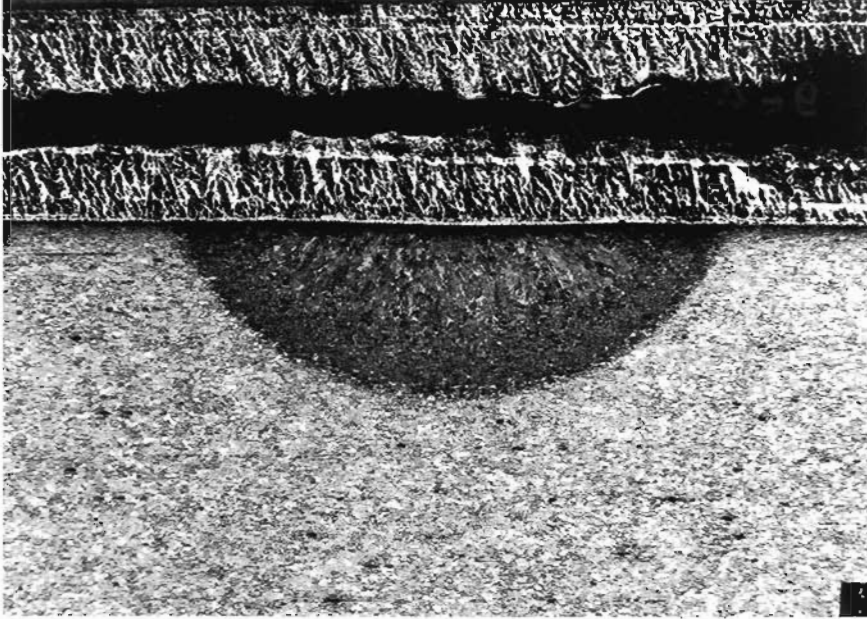
Figure 40.   (Cont.)

E   FH GTAW weld at 17 mm/sec.
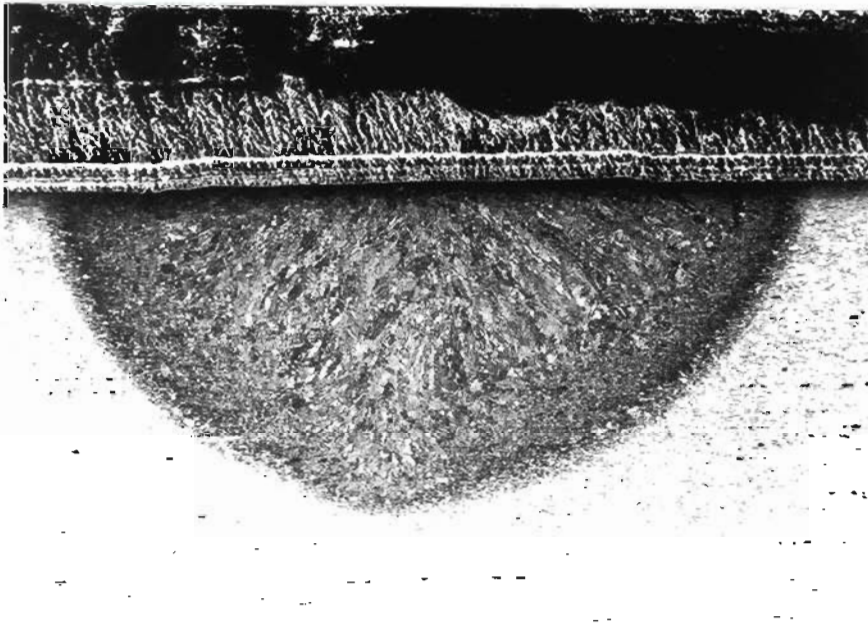
F   FH LBW/GTAW weld at 17 mm/sec.

Figure 40.   (Cont.)

G   BH GTAW weld at 34 mm/sec.

H   BH LBW/GTAW weld at 34 mm/sec.
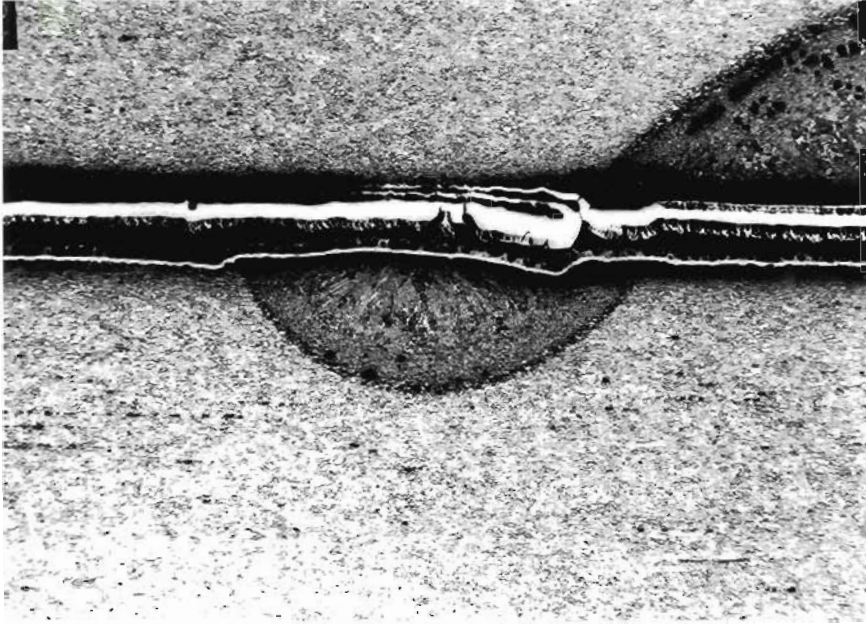
Figure 40.   (Cont.)

I   FH GTAW weld at 34 mm/sec.
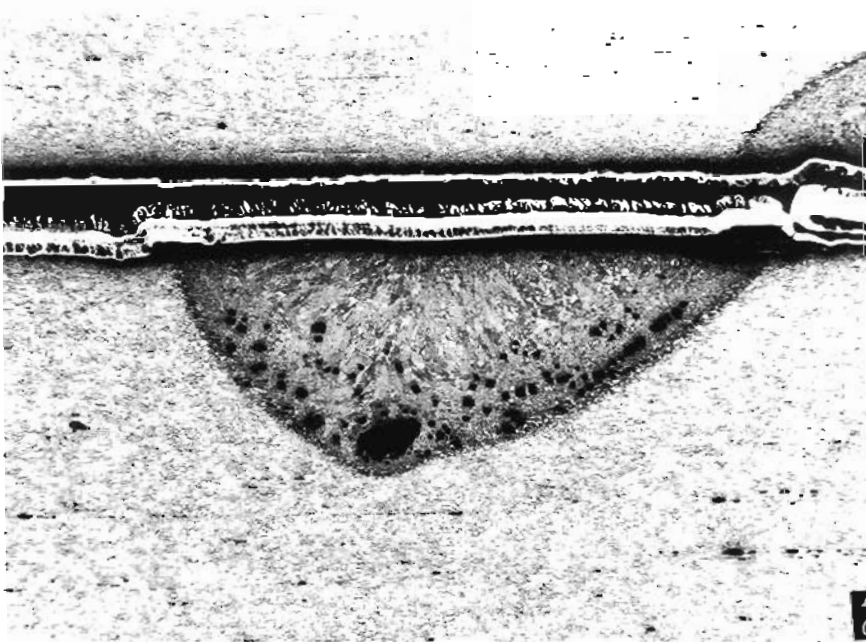
J   FH LBW/GTAW weld at 34 mm/sec.

Figure 40.   (Cont.)
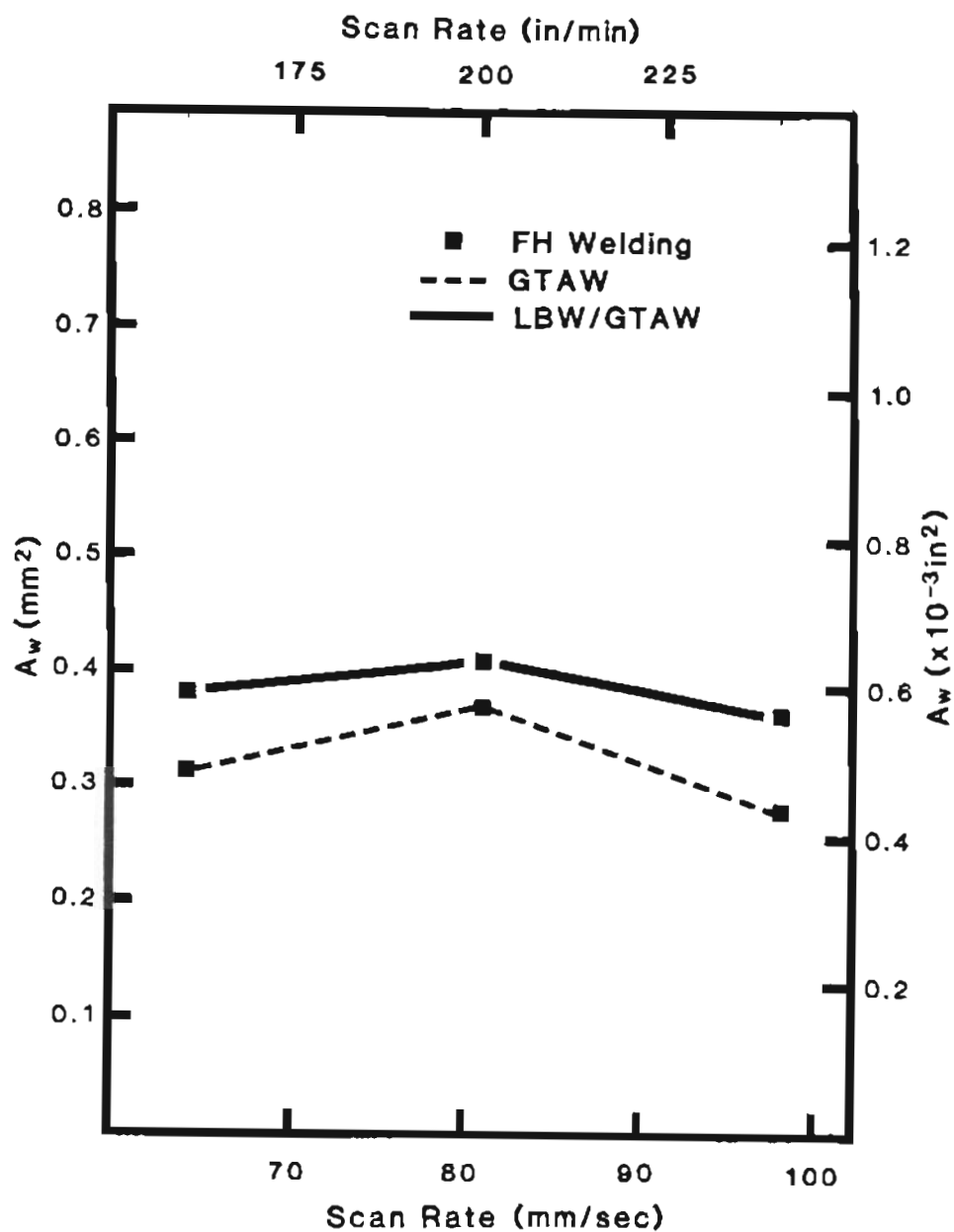
Figure 41. Cross sectional area of aluminum weld metal as a function of higher welding velocities.
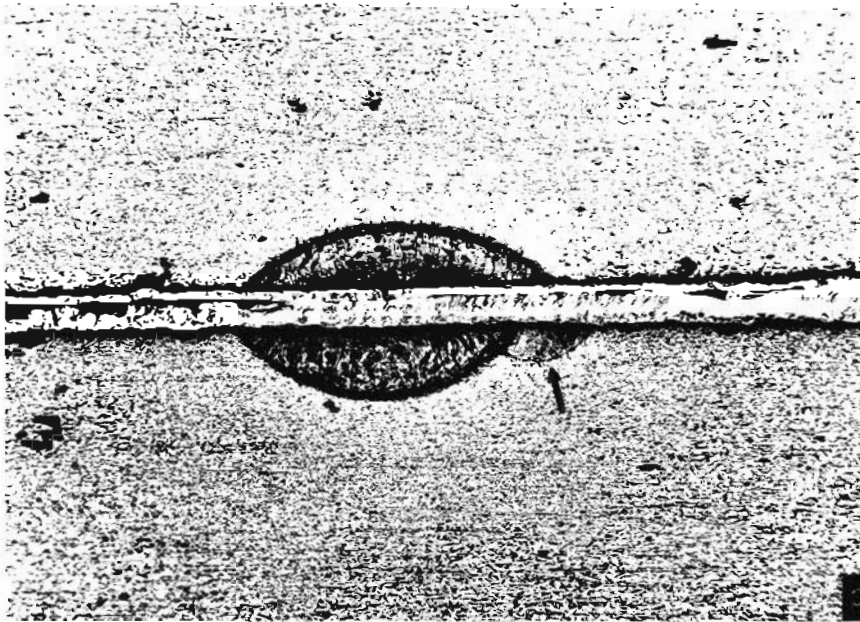
A   Top – FH GTAW at 67.7 mm/sec and Bottom – FH LBW/GTAW at 101.6 mm/sec.
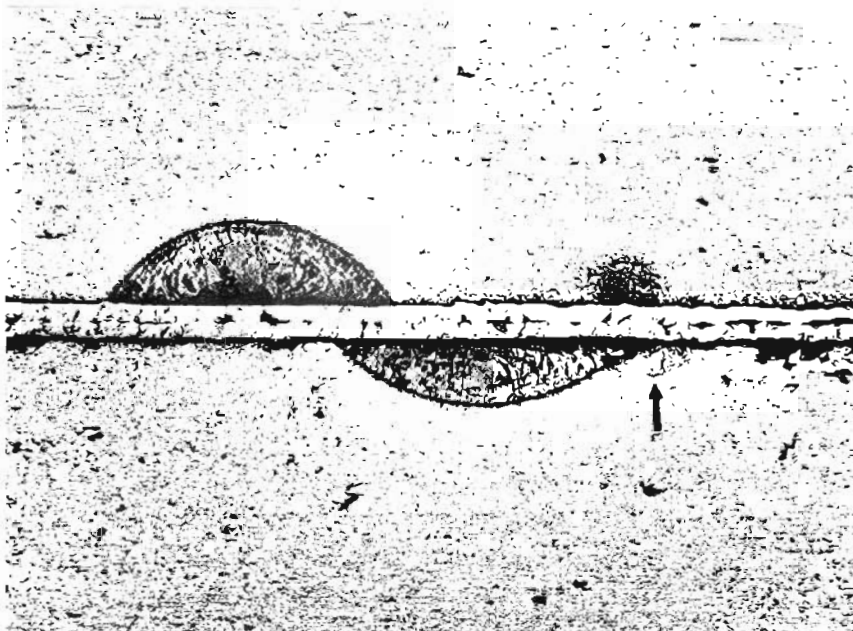
B   Top – FH GTAW at 84.7 mm/sec. and Bottom – FH LBW/GTAW at 84.7 mm/sec.

Figure 42. Cross sectional veiws of welds deposited on 5052 aluminum alloy at high scan rate showing individual welds in LBW/GTAW mode (at arrows). (30X).
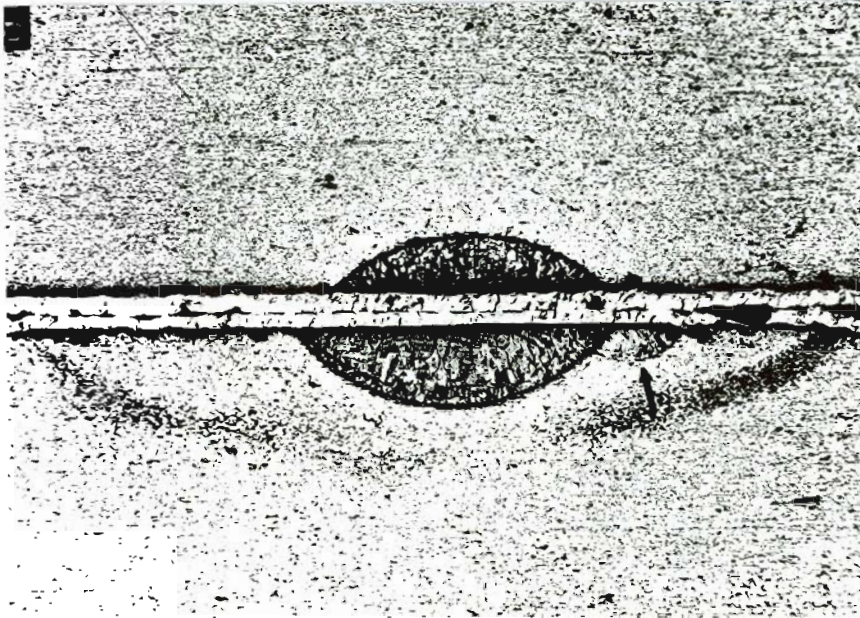
C Top — FH GTAW at 101.6 mm/sec. and Bottom — FH LBW/GTAW at 67.7 mm/sec.

Figure 42. (Cont.)
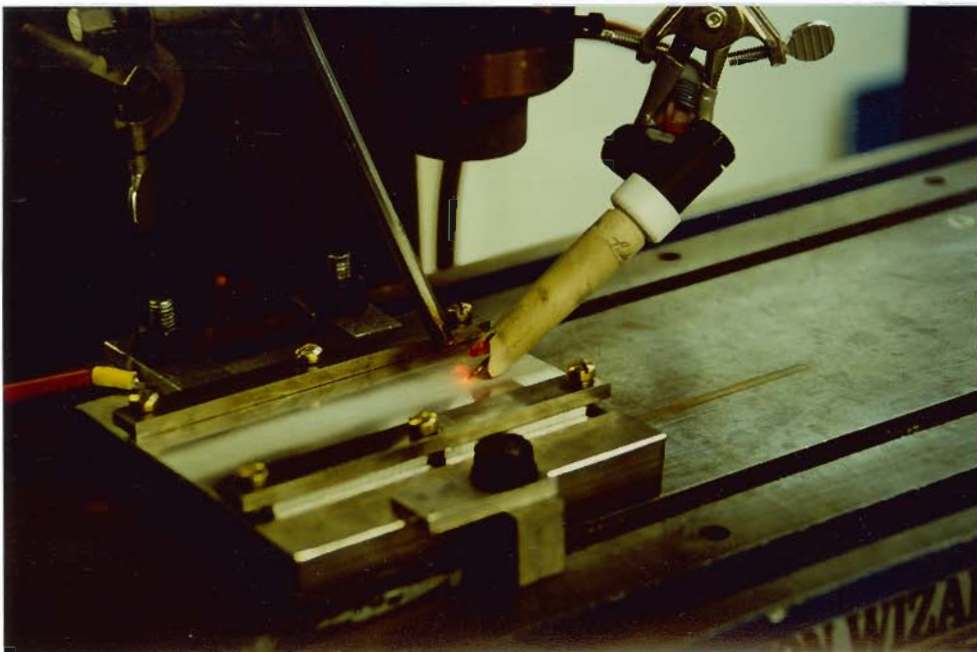
Figure 43. Clamping mechanism used to make square groove autogenous welds in 5052 aluminum alloy.
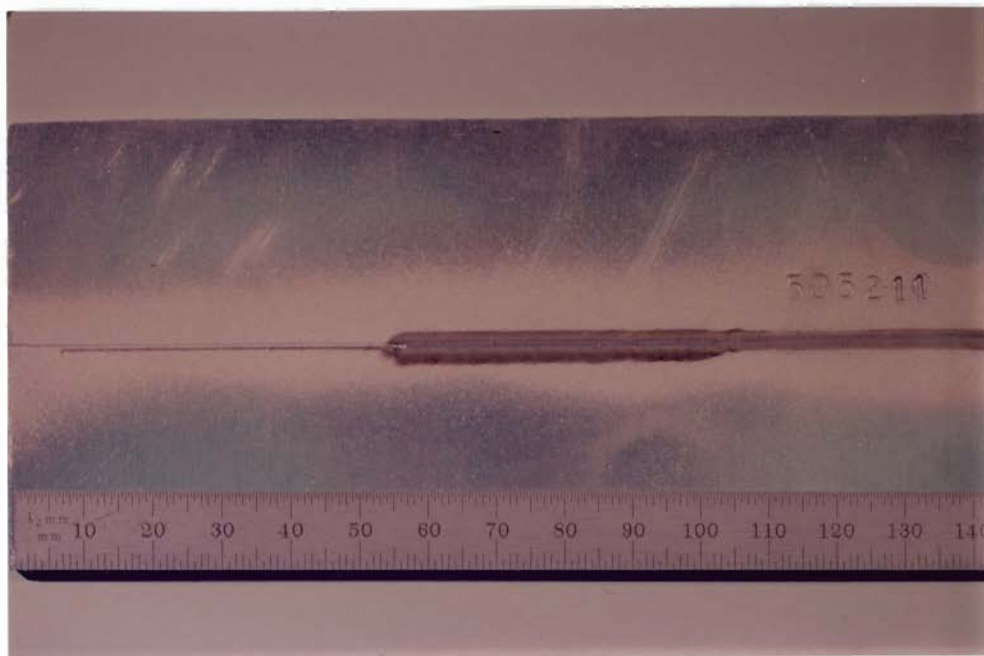
Figure 44. Weld bead surface appearance of joint made with LBW (left), LBW/GTAW (middle) and GTAW (right) on 5052 aluminum alloy at scan rate of 4.2 mm/sec.
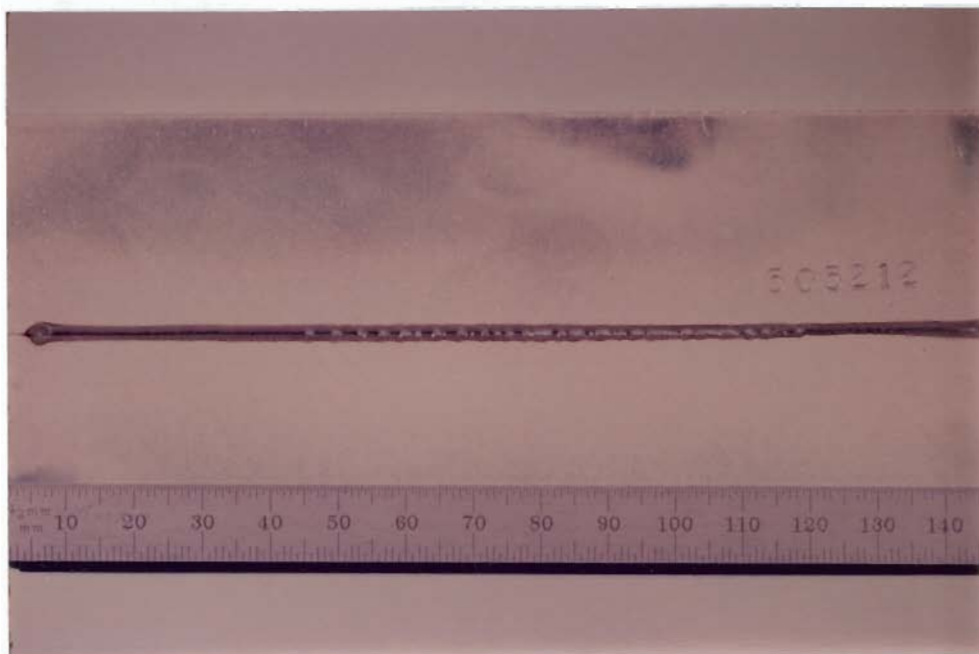
Figure 45. Weld bead surface appearance of joint made on 5052 aluminum alloy by LBW/GTAW (left) and GTAW (right) at scan rate of 84.7 mm/sec.
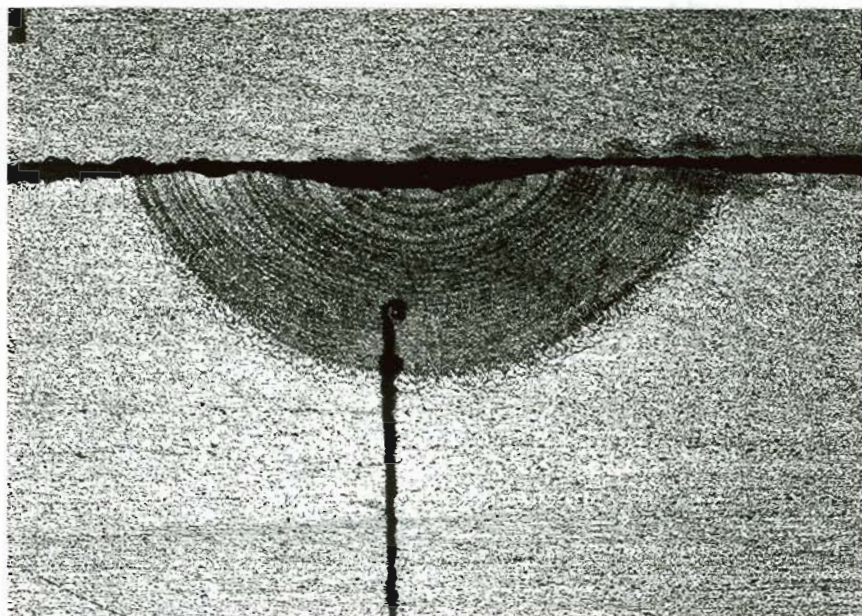
A
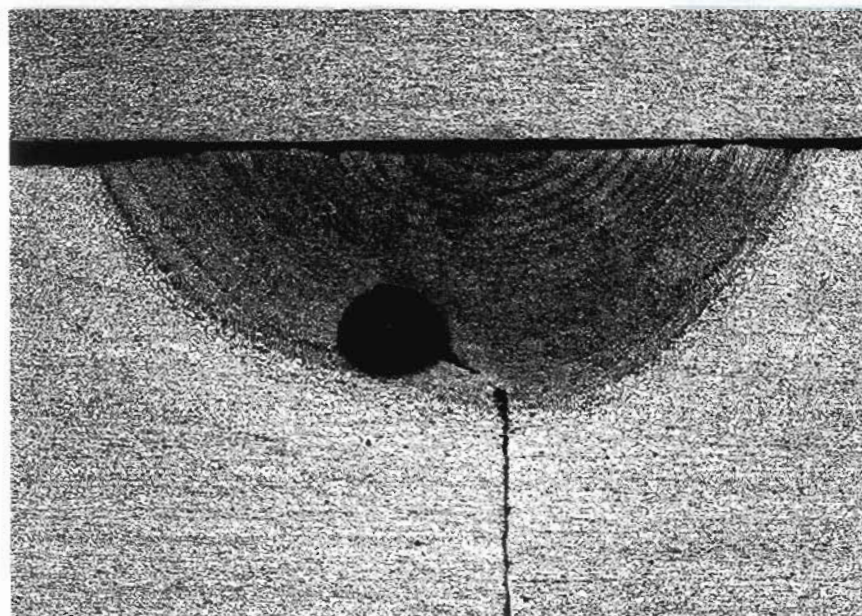
B

Figure 46. Cross sectional micrographs of weld joint made at 4.2 mm/sec. on 5052 aluminum alloy using (A) FH GTAW and (B) FH LBW/GTAW. (30X).
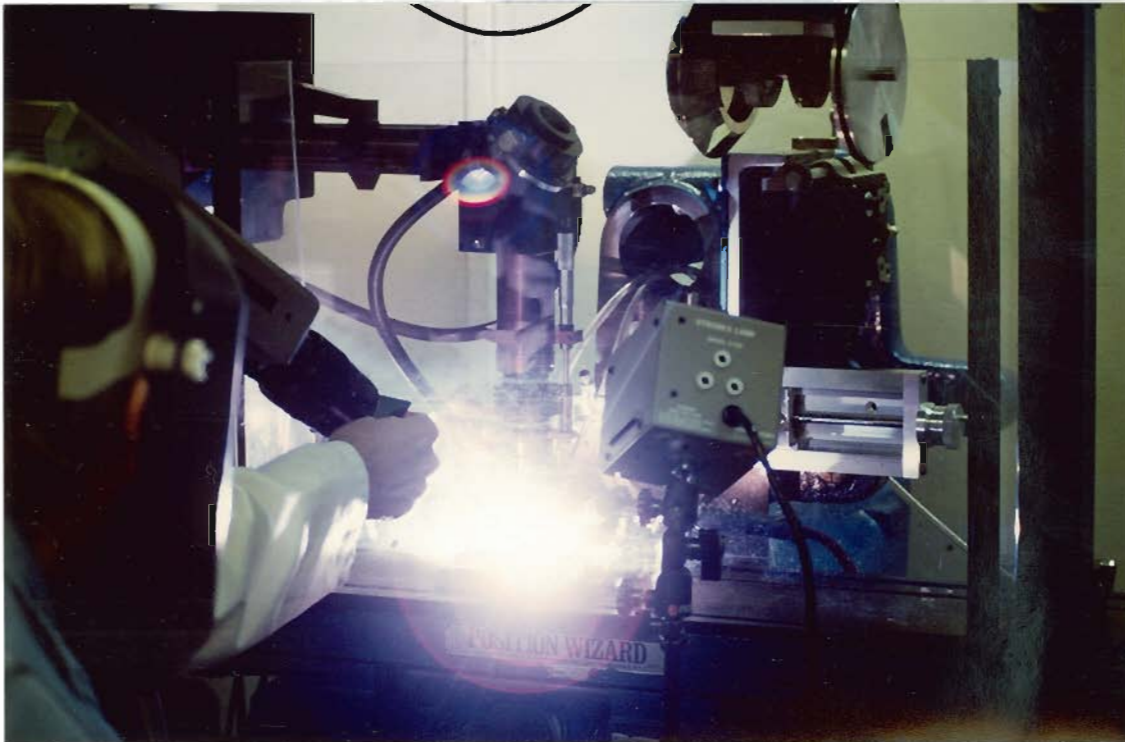
Figure 47. Set-up used for high speed videography of arc-augmented laser welding (GTAW torch at arrow).
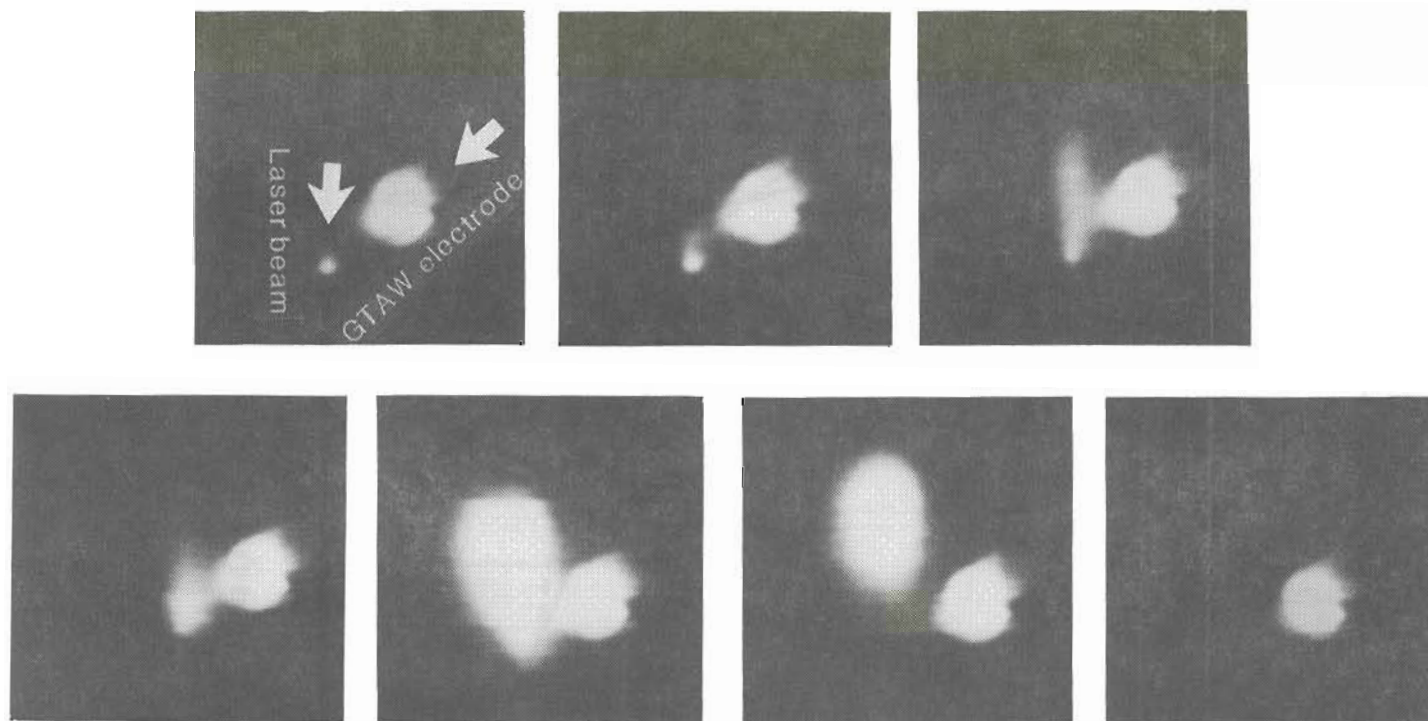
Figure 48. Frame sequence showing arc-rooting phenomena. Note frame #3 (left to right) where laser beam is "outlined", frame #5 where plume is generated and frames #6-7 where plume detaches. Elapsed time between frames = 1 millisec.
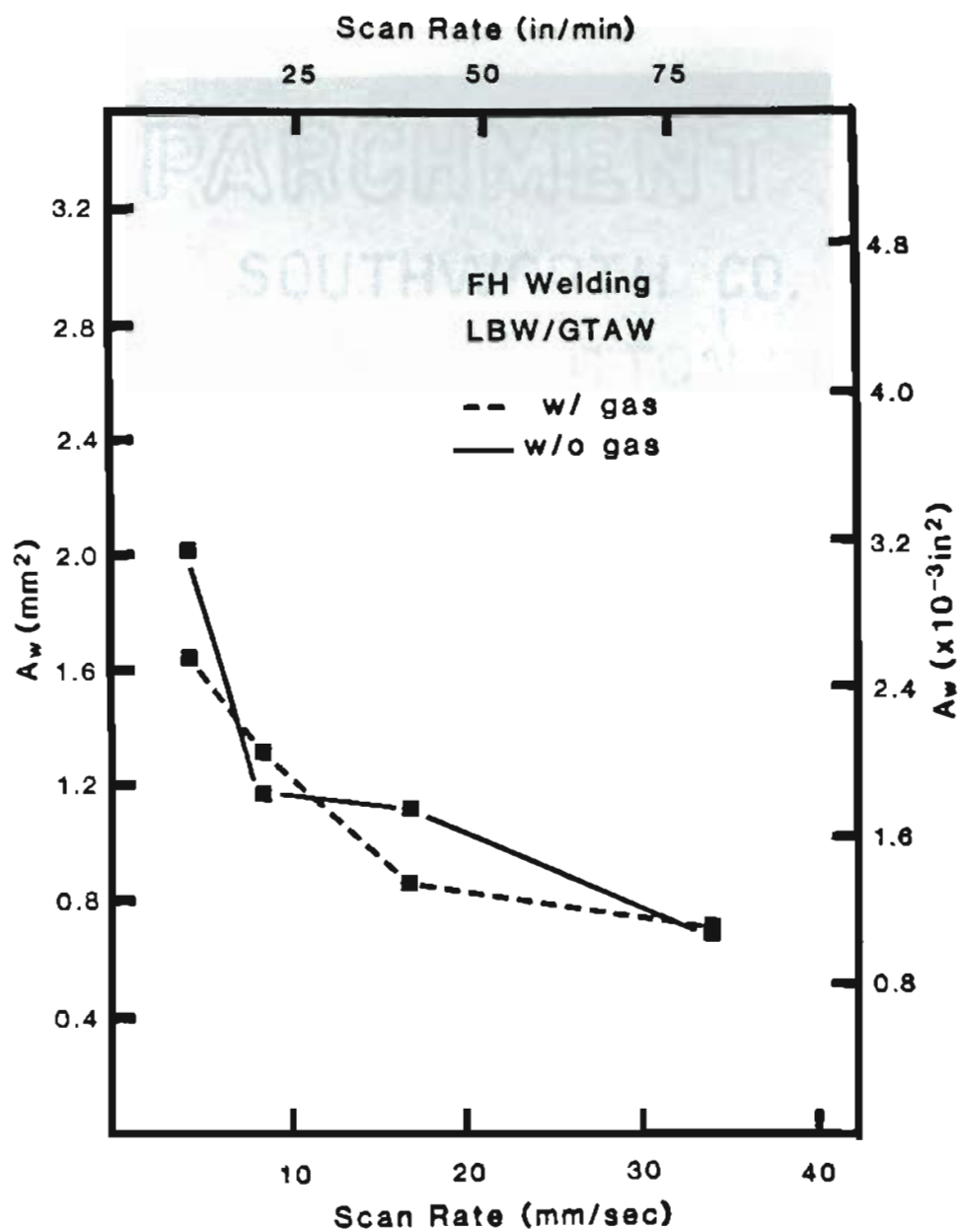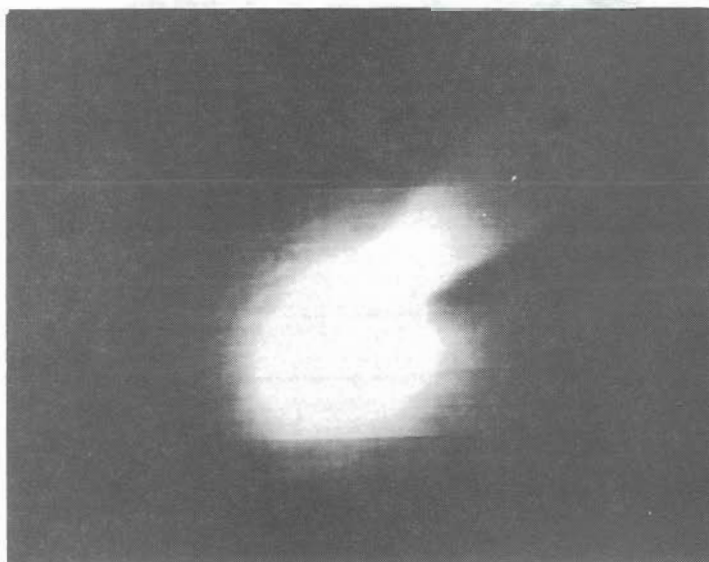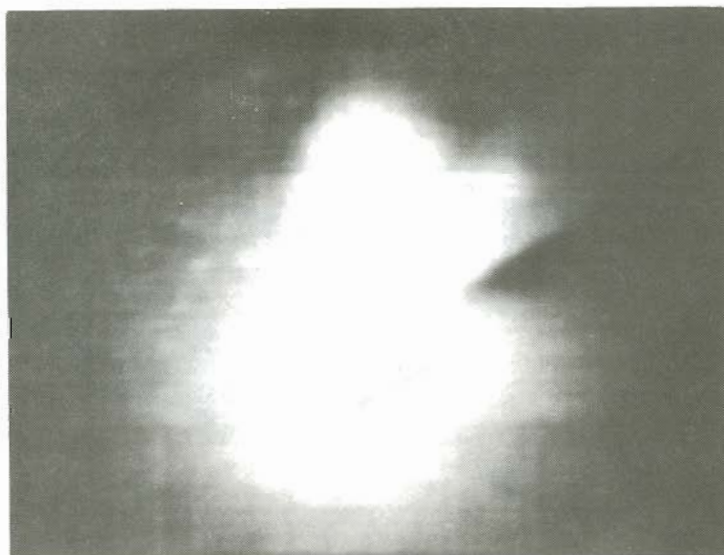
Figure 49. Welding performance due to effect of cross gas jet for plasma dispersal.
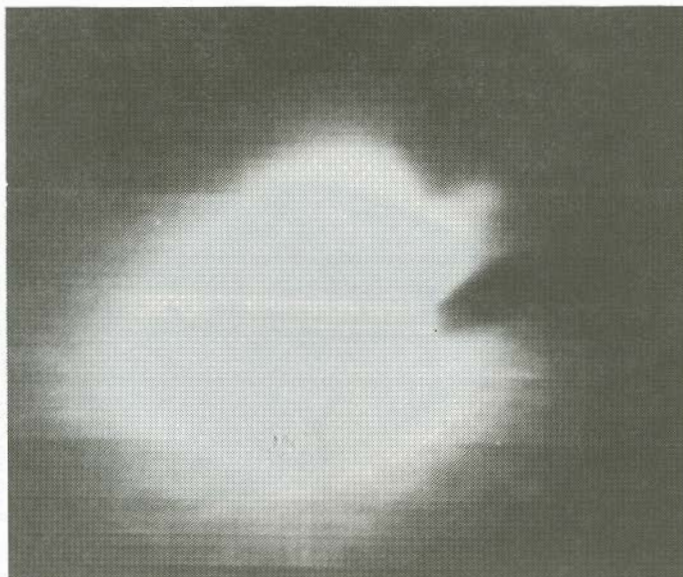
A

B

Figure 50. Comparison of plume shape for (A) FH GTAW, (B) FH LBW/GTAW with gas cross jet and (C) FH LBW/GTAW without gas cross jet.
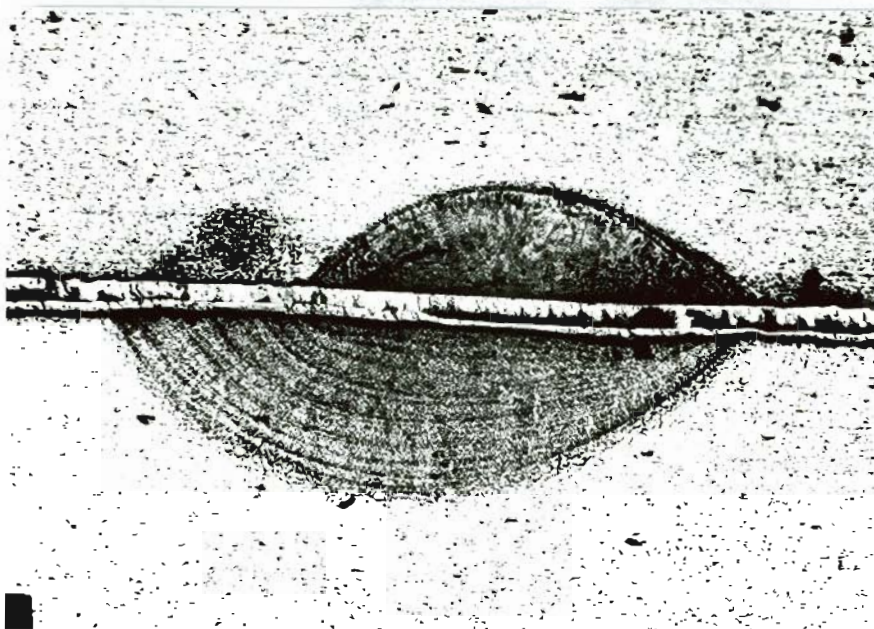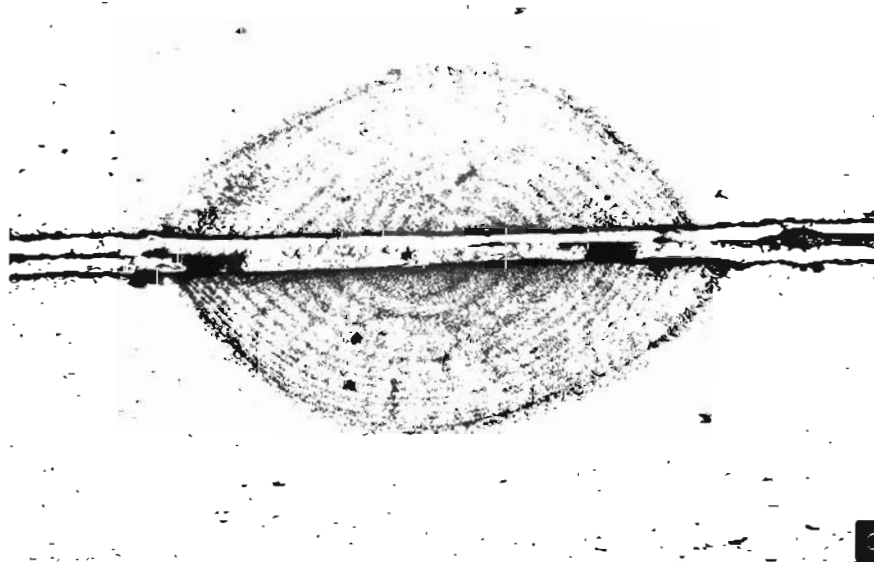
C

Figure 50. (Cont.)

A Top - FH LBW/GTAW, w/gas at 34.0mm/sec. and Bottom - FH LBW/GTAW, w/o gas at 4.2 mm/sec.

Figure 51. Cross sectional micrographs displaying effect of gas cross jet on weld shape (note also solute banding lines). (30X).

B Top — FH LBW/GTAW, w/o gas at 34.0 mm/sec. and Bottom — FH LBW/GTAW, w/gas at 4.2 mm/sec.

C Top — FH LBW/GTAW, w/gas at 8.5 mm/sec. and Bottm — FH LBW/GTAW, w/o gas at 8.5 mm/sec.

Figure 51. (Cont.)

Frame #1   Frame #2
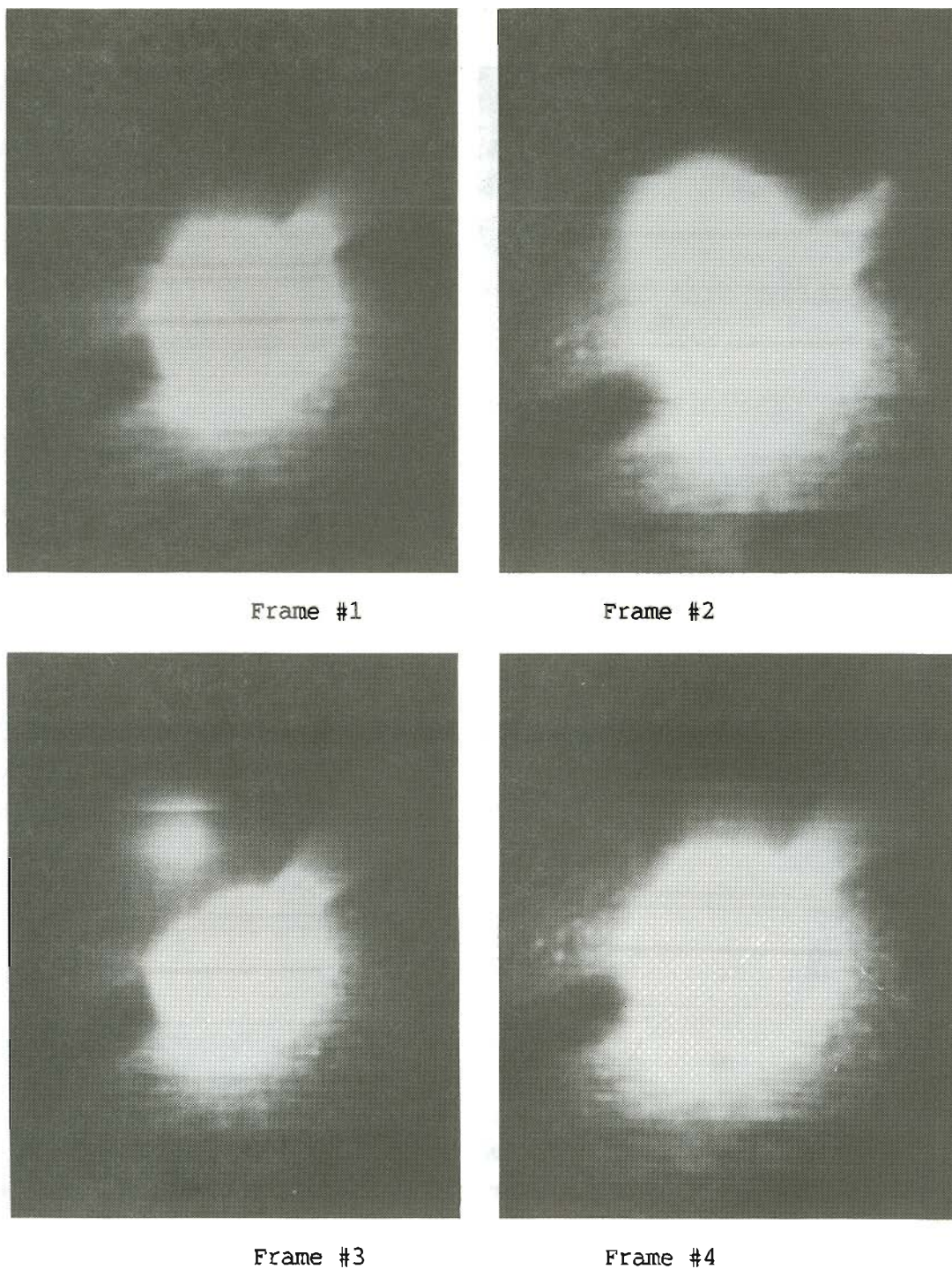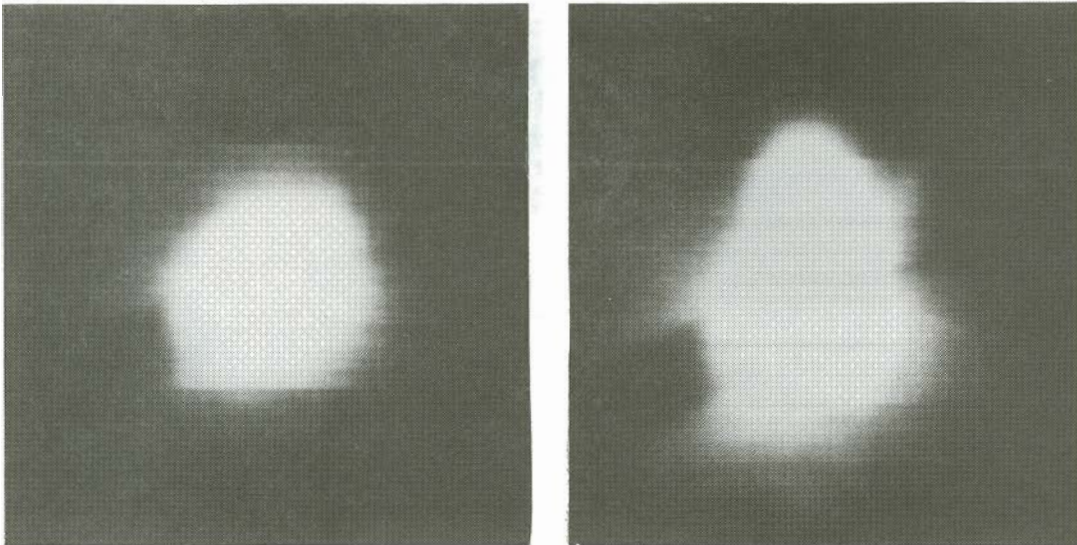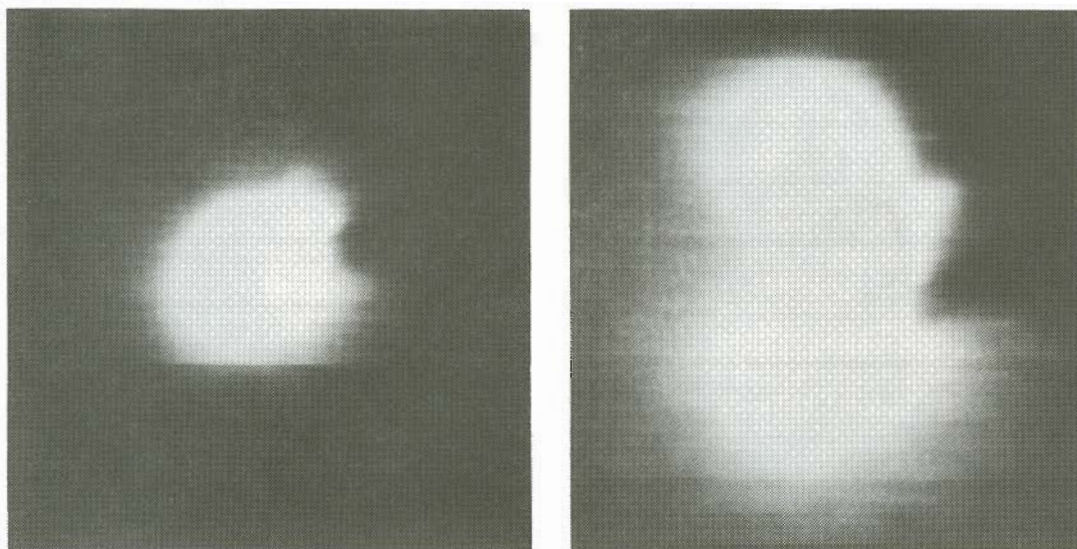
Frame #3   Frame #4

Figure 52. Frame sequence showing generation of plume from combined LBW/GTAW process. Note formation (Frame #2) and subsequent detatchment (Frame #3) of plasma plume. Elapsed time between frames = 1 millisec.

A   BH GTAW (left) and BH LBW/GTAW (right) at 34.0 mm/sec.

B   FH GTAW (left) and FH LBW/GTAW (right) at 34.0 mm/sec.

Figure 53.   Comparison of plume shape for backhand and forehand welding at two different scan rates showing appearance of "pushing" and "pulling" the arc column and arc column extension.
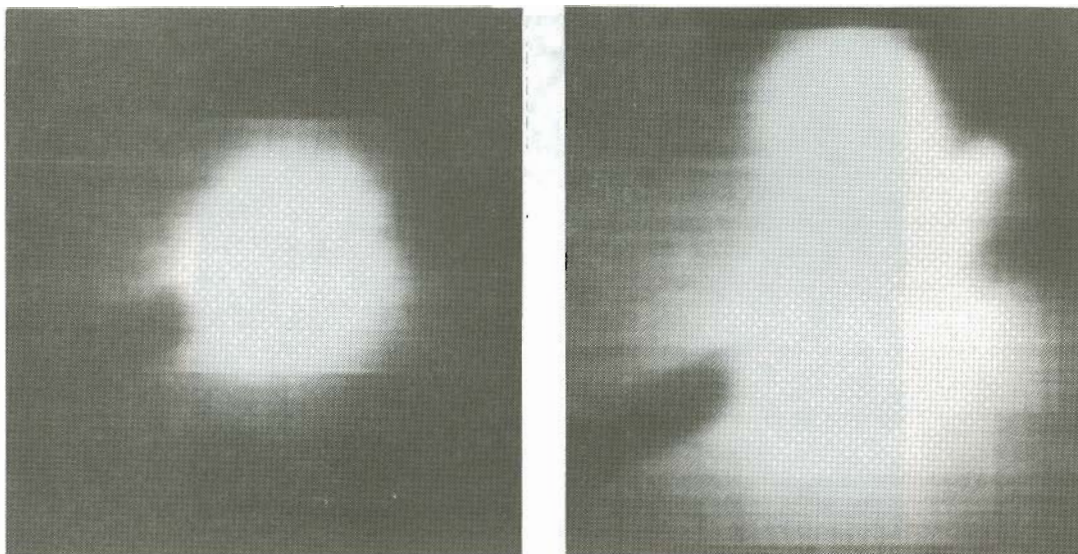
C   BH GTAW (left) and BH LBW/GTAW (right) at 67.7 mm/sec.
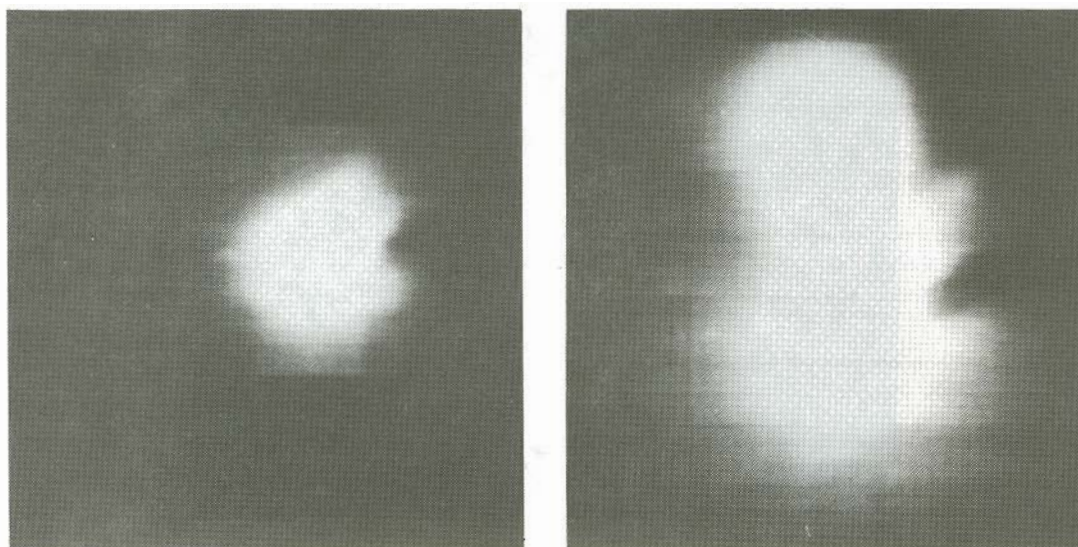
D   FH GTAW (left) and FH LBW/GTAW (right) at 67.7 mm/sec.

Figure 53.   (Cont.)
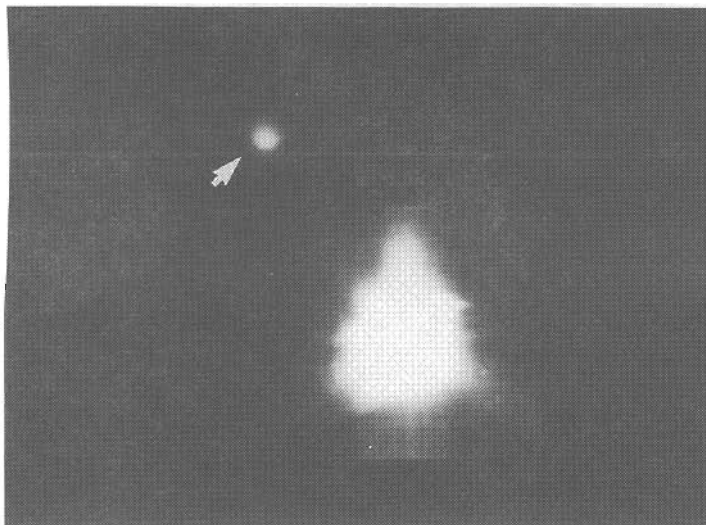
A   LBW on mild steel at 8.5 mm/sec. showing laser induced plasma (spot at arrow is a reflection).
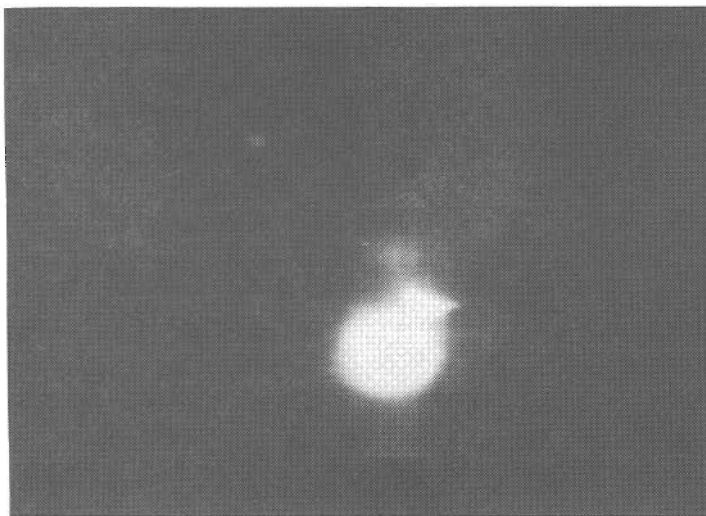
B   LBW induced plasma and glowing GTAW electrode on mild steel.

Figure 54.   Laser induced plasma (LBW only) generated on mild steel sample.
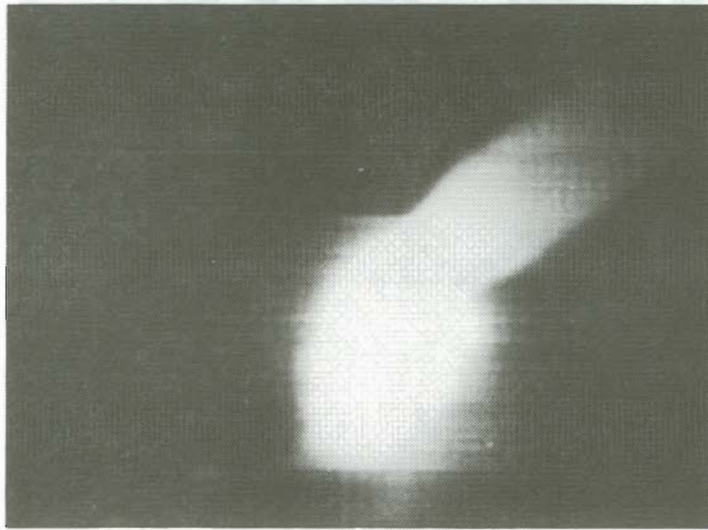
A   BH GTAW on mild steel at 8.5 mm/sec.
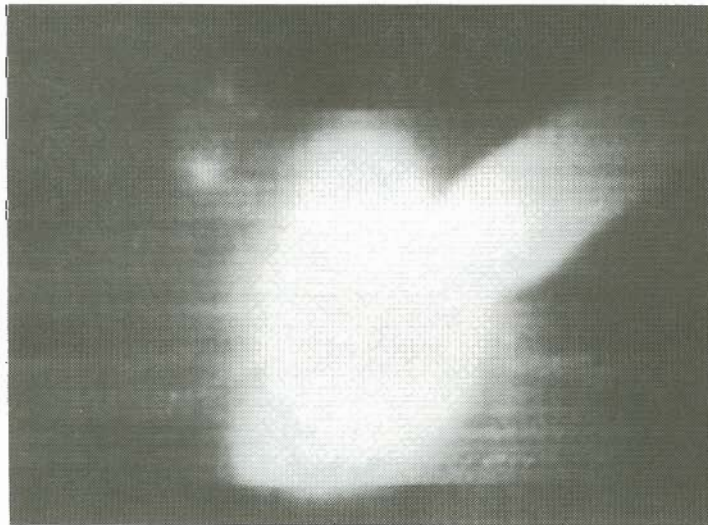
B   BH LBW/GTAW on mild steel at 8.5 mm/sec.

Figure 55.   Contrast between backhand and forehand welding on mild steel in relation to plasma plume generation.
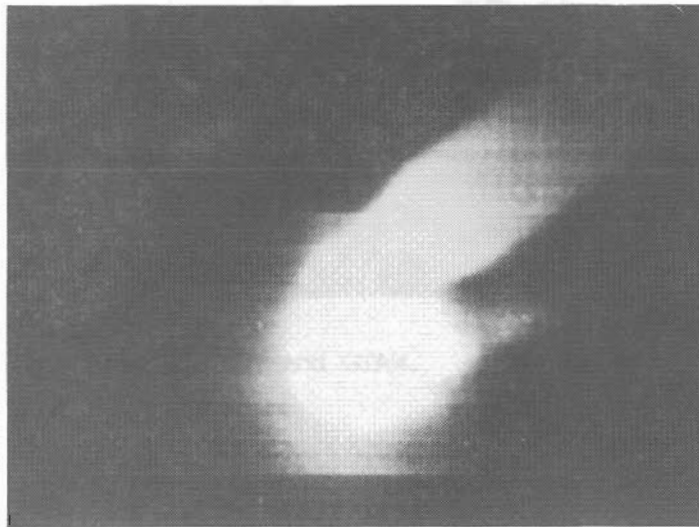
C FH GTAW on mild steel at 8.5 mm/sec.
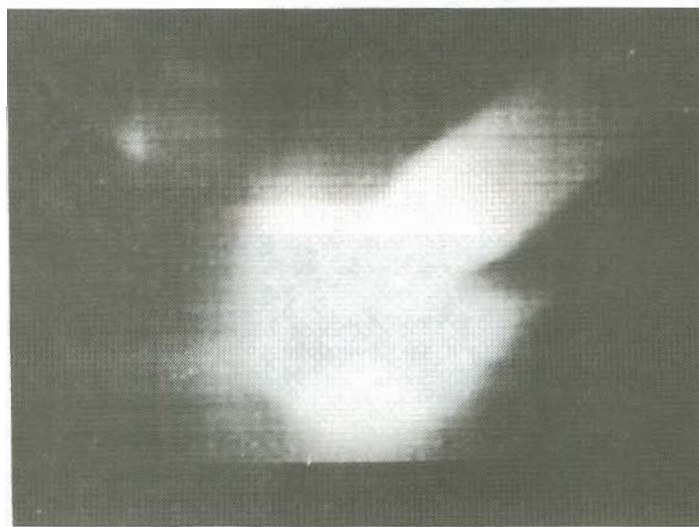
D FH LBW/GTAW on mild steel at 8.5 mm/sec.

Figure 55. (Cont.)
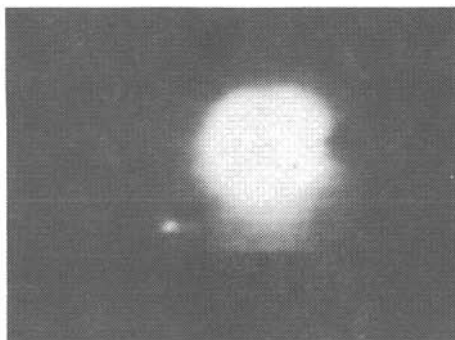
A No interaction between LBW and GTAW.
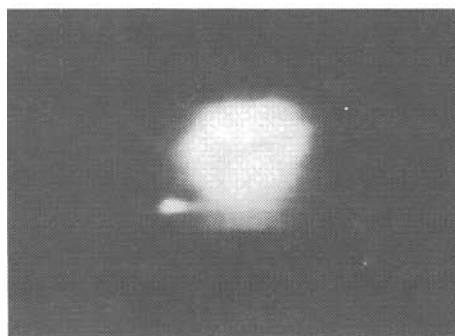
B Stable arcing as GTAW electrode moves closer to LBW zone.
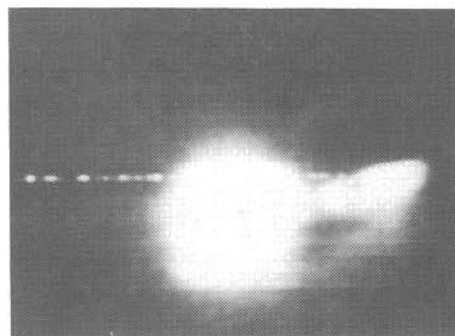
C Unstable arcing producing "double" arc on GTAW electrode.

Figure 56. Moving from no interaction (A) to stable (B) and then unstable arcing (C) from the GTAW electrode.
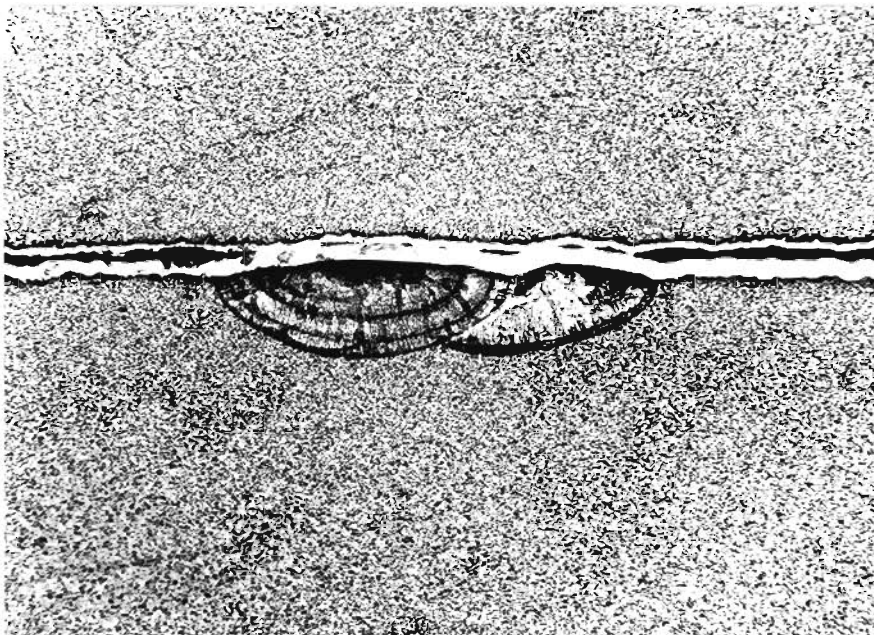
Figure 57. Cross section of "double" weld which resulted from unstable arcing shown in Figure 56. (30X).
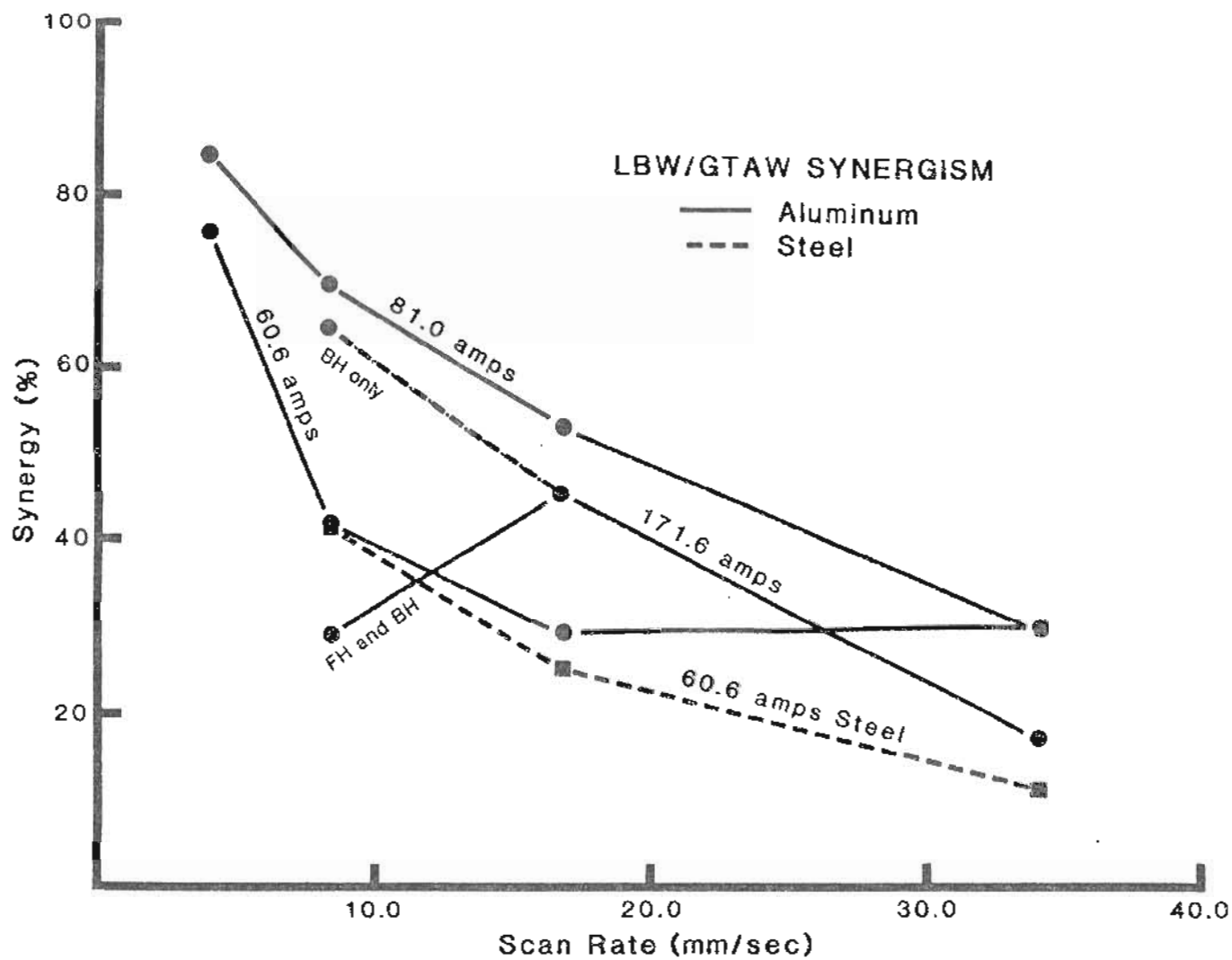
Figure 58. Summary of results from melting efficiency and materials selection showing synergy relative to scan rate (refer to page 21 of text for explanation of synergy calculation).

LASER WELDING PERFORMANCE CORRELATION
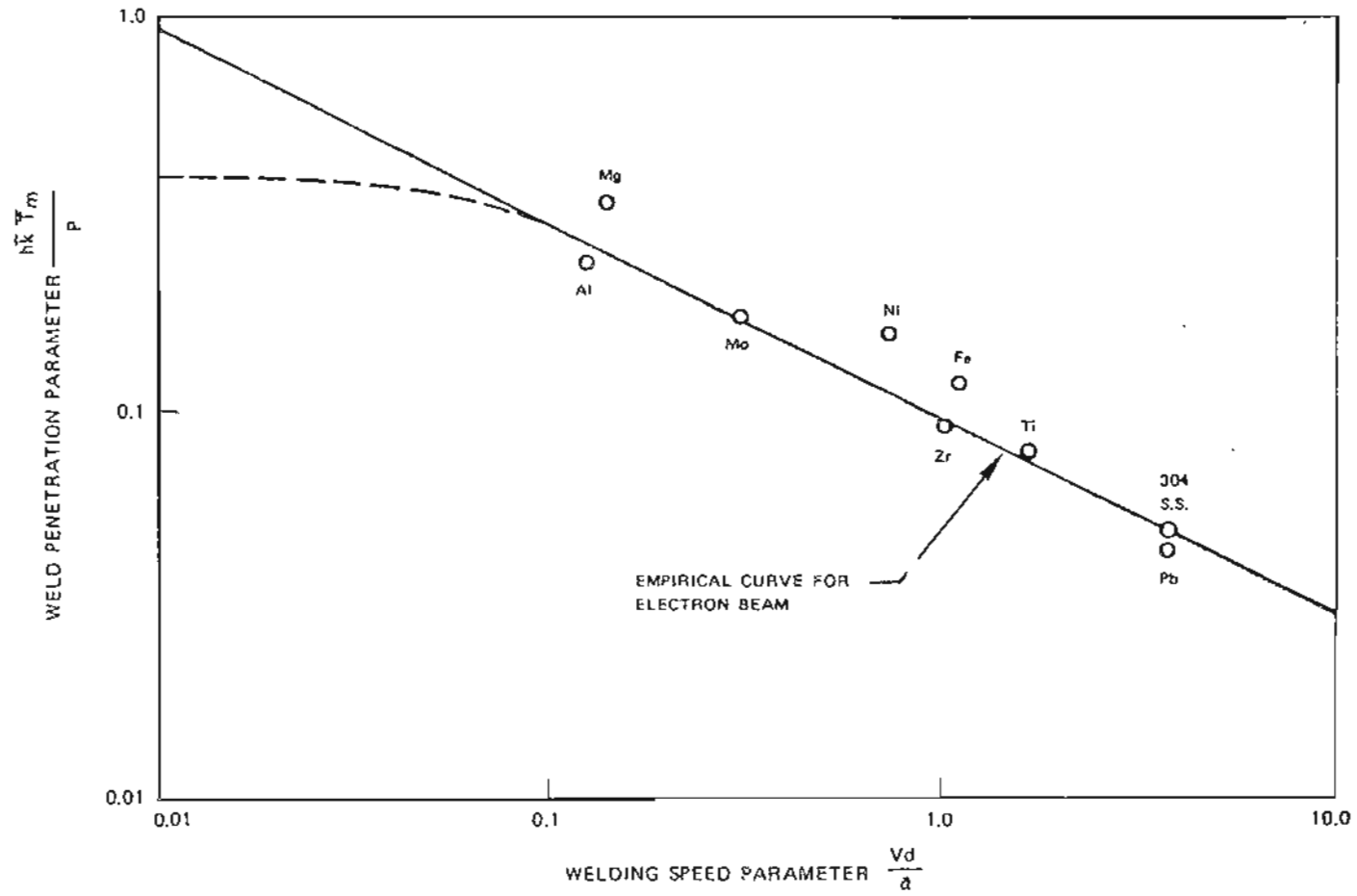
Figure 59. Correlation between thermophysical properties and welding performance for various materials (after Ref. 42).

APPENDIX

Appendix

Table A-1. Summary of welding results including weld width, depth
and width to depth ratio.

| WELD PROCESS	V(mm/sec)	I(amps)	$A_w(mm^2)$	W(mm)	D(mm)	W/D	NOTES
BH GTAW	4.2	60.6	0.87	1.91	0.65	2.93	
BH LBW/GTAW	4.2	60.6	1.58	2.39	0.91	2.64	
FH GTAW	4.2	60.6	0.89	1.89	0.66	2.87	
FH LBW/GTAW	4.2	60.6	1.56	2.50	0.92	2.71	
BH GTAW	8.5	60.6	0.84	1.77	0.63	2.80	
BH LBW/GTAW	8.5	60.6	1.20	2.17	0.78	2.78	
FH GTAW	8.5	60.6	0.88	1.82	0.65	2.80	
FH LBW/GTAW	8.5	60.6	1.22	2.21	0.78	2.83	
BH GTAW	17.0	60.6	0.59	1.58	0.56	2.85	
BH LBW/GTAW	17.0	60.6	0.75	1.83	0.63	2.93	
FH GTAW	17.0	60.6	0.66	1.69	0.56	3.00	
FH LBW/GTAW	17.0	60.6	0.86	1.80	0.68	2.63	
BH GTAW	34.0	60.6	0.47	1.39	0.48	2.91	
BH LBW/GTAW	34.0	60.6	0.66	1.61	0.52	3.08	
FH GTAW	34.0	60.6	0.46	1.44	0.47	3.09	
FH LBW/GTAW	34.0	60.6	0.59	1.88	0.47	4.00	
BH GTAW	67.7	60.6	0.38	1.45	0.34	4.23	
BH LBW/GTAW	67.7	60.6	0.40	1.46	0.39	3.77	
FH GTAW	67.7	60.6	0.40	1.42	0.38	3.77	
FH LBW/GTAW	67.7	60.6	0.44	1.53	0.38	4.06	
BH GTAW	4.2	81.0	1.39	2.45	0.85	2.90	
BH LBW/GTAW	4.2	81.0	2.80	2.92	1.32	2.22	
FH GTAW	4.2	81.0	1.71	2.56	0.95	2.68	
FH LBW/GTAW	4.2	81.0	2.92	3.13	1.33	2.34	
BH GTAW	8.5	81.0	1.20	2.25	0.78	2.89	
BH LBW/GTAW	8.5	81.0	1.92	2.74	0.98	2.78	
FH GTAW	8.5	81.0	1.56	2.63	0.83	3.15	
FH LBW/GTAW	8.5	81.0	2.78	3.29	1.16	2.85	
BH GTAW	17.0	81.0	0.64	1.84	0.51	3.58	
BH LBW/GTAW	17.0	81.0	1.04	2.18	0.68	3.19	
FH GTAW	17.0	81.0	1.06	2.57	0.59	4.39	
FH LBW/GTAW	17.0	81.0	1.56	2.77	0.87	3.20	

Table A-1 (Cont.)

WELD PROCESS	V(mm/sec)	I(amps)	A_w(mm^2)	W(mm)	D(mm)	W/D	NOTES
BH GTAW	34.0	81.0	0.53	1.73	0.43	4.00	
BH LBW/GTAW	34.0	81.0	0.73	1.78	0.56	3.15	
FH GTAW	34.0	81.0	0.79	2.05	0.60	3.43	
FH LBW/GTAW	34.0	81.0	1.03	2.23	0.67	3.33	
BH GTAW	8.5	171.6	11.05	5.41	2.62	2.07	
BH LBW/GTAW	8.5	171.6	16.99	----	----	----	
FH GTAW	8.5	171.6	17.39	----	----	----	
FH LBW/GTAW	8.5	171.6	19.17	----	----	----	
BH GTAW	17.0	171.6	4.81	4.14	1.56	2.65	
BH LBW/GTAW	17.0	171.6	7.30	4.59	2.29	2.00	
FH GTAW	17.0	171.6	7.05	5.51	1.91	2.89	
FH LBW/GTAW	17.0	171.6	9.90	5.88	2.33	2.52	
BH GTAW	34.0	171.6	2.91	3.42	1.23	2.79	
BH LBW/GTAW	34.0	171.6	3.81	3.81	1.71	2.23	
FH GTAW	34.0	171.6	4.08	4.04	1.50	2.69	
FH LBW/GTAW	34.0	171.6	4.37	4.14	1.31	3.16	
FH LBW/GTAW	4.2	60.6	1.64	2.95	0.82	3.58	w/gas
FH LBW/GTAW	4.2	60.6	2.16	2.81	1.06	2.67	w/o gas
FH LBW/GTAW	8.5	60.6	1.32	2.44	0.77	3.17	w/gas
FH LBW/GTAW	8.5	60.6	1.18	2.34	0.74	3.18	w/o gas
FH LBW/GTAW	17.0	60.6	0.85	1.62	0.68	2.39	w/gas
FH LBW/GTAW	17.0	60.6	1.13	1.88	0.79	2.37	w/o gas
FH LBW/GTAW	34.0	60.6	0.70	1.91	0.52	3.67	w/gas
FH LBW/GTAW	34.0	60.6	0.68	1.93	0.51	3.75	w/o gas
FH GTAW	67.7	60.6	0.31	1.32	0.31	4.29	
FH LBW/GTAW	67.7	60.6	0.38	1.75	0.34	5.13	
FH GTAW	84.7	60.6	0.37	1.32	0.40	3.33	
FH LBW/GTAW	84.7	60.6	0.41	1.71	0.35	4.88	
FH GTAW	101.6	60.6	0.28	1.29	0.27	4.83	
FH LBW/GTAW	101.6	60.6	0.36	1.60	0.35	4.63	
BH GTAW	17.0	60.6	0.51	1.73	0.39	4.44	93°C
BH LBW/GTAW	17.0	60.6	0.85	2.43	0.52	4.67	93°C
BH GTAW	17.0	60.6	0.99	2.29	0.62	3.71	204°C
BH LBW/GTAW	17.0	60.6	1.23	2.49	0.76	3.28	204°C
BH GTAW	17.0	60.6	2.07	3.08	0.91	3.38	316°C
BH LBW/GTAW	17.0	60.6	2.84	3.51	0.93	3.77	316°C
BH GTAW	17.0	60.6	4.14	3.55	1.69	2.10	427°C
BH LBW/GTAW	17.0	60.6	6.39	4.66	1.97	2.37	427°C
BH GTAW	17.0	60.6	11.88	----	----	----	524°C
BH LBW/GTAW	17.0	60.6	17.78	----	----	----	524°C
BH LBW	17.0	----	4.16	3.04	2.01	1.51	524°C

Table A-1 (Cont.)

WELD PROCESS	V(mm/sec)	I(amps)	$A_w(mm^2)$	W(mm)	D(mm)	W/D	NOTES
BH GTAW	8.5	60.6	1.55	2.86	0.71	4.05	steel
BH LBW/GTAW	8.5	60.6	6.33	4.68	1.92	2.44	steel
BH LBW	8.5	————	2.23	2.55	1.31	1.94	steel
FH GTAW	8.5	60.6	2.43	3.23	1.09	2.95	steel
FH LBW/GTAW	8.5	60.6	5.59	4.27	1.81	2.36	steel
BH GTAW	17.0	60.6	1.21	2.44	0.70	3.50	steel
BH LBW/GTAW	17.0	60.6	3.62	3.39	1.44	2.36	steel
BH LBW	17.0	———	1.63	1.92	1.26	1.52	steel
FH GTAW	17.0	60.6	1.44	2.48	0.78	3.17	steel
FH LBW/GTAW	17.0	60.6	3.75	3.48	1.52	2.29	steel
BH GTAW	34.0	60.6	0.69	2.12	0.47	4.50	steel
BH LBW/GTAW	34.0	60.6	1.99	2.77	1.13	2.46	steel
BH LBW	34.0	————	1.04	1.36	1.18	1.16	steel
FH GTAW	34.0	60.6	0.95	2.07	0.66	3.14	steel
FH LBW/GTAW	34.0	60.6	2.12·	2.98	1.12	2.67	steel